UNIVERSITA' DEGLI STUDI DI VERONA

Department of Biotechnology

Graduate School of Natural Science and Engineering

Doctoral Program in Biotechnology

Cycle XXXII

Chemical modification- and interaction-induced conformational transitions of the protein Tau

S.S.D. CHIM/06

Coordinator: Prof. Matteo Ballottari

Tutor: Prof. Michael Assfalg

PhD Student: Carlo Giorgio Barracchia

INDEX

ACRONYM

1D Mono-dimensional
2D Bi-dimensional
AD Alzheimer's Disease
AFM Atomic Force Microscopy
ARA Arachidonic Acid
Aβ Amyloid-β
C-terminal carboxy-terminal
CD Circular Dichroism
CMC Critical Micellar Concentration
CNS Central Nervous System
Cys Cysteine
DEST Dark State Exchange Saturation Transfer
DHA Docosahexaenoic Acid
DLS Dynamic Light Scattering
DSS 4,4-dimethyl-4-silapentane-1-sulfonic acid
DTT dithiothreitol
FA Fatty Acid
GHz Gigahertz
Gly Glycine
HSQC Heteronuclear single-quantum coherence
IPTG Isopropyl-β-D-1-thiogalactopyranoside
kDa kiloDalton
L Liter
LB Luria broth
Lys Lysine
M Molar
MAP Microtubule-Associated Protein
MAPT Microtubule Associated Protein Tau (Human gene)
mg milligram
MHz Megahertz
min minute
mL milliliter
mm millimeter
mM millimolar
mol mole
MTBD MT-binding domain
MTs Microtubules
N-terminal amino-terminal
NFTs Neurofibrillary Tangles
NMR Nuclear Magnetic Resonance
NP Nanoparticle
OLA Oleic Acid
P/FA Protein/Fatty Acid ratio
PD Parkinson's Disease
PHFs paired helical filaments
ppm Chemical shift in parts per million
PUFA Poly Unsatured Fatty Acid
R_2 Transverse relaxation rate
R_h Radius of hydration
SDS-PAGE Sodium Dodecyl Sulfate Polyacrylamide Gel Electrophoresis
SFs Straight Filaments
TCEP tris(2-carboxyethyl)phosphine hydrochloride
ThT Thioflavin-T
Ub Ubiquitin
UPS Ubiquitin-Proteasome System
α-syn α-Synuclein
µg microgram
µL microliter
µM micromolar

Abstract

The aggregation of the neuronal Tau protein and the formation of neurofibrillary tangles is one of the major hallmarks of Alzheimer's disease (AD) and other tauopathies. The processes underlying this structural transition are still unknown. Recent evidence indicated that, *in vivo*, Tau in paired helical filaments purified from AD brains is characterized by several post-translational modifications including polyubiquitination. Due to the role of ubiquitination in the clearance of misfolded proteins by proteasomal degradation, dysfunction of the ubiquitin-proteasome system was proposed to be one of the key mechanisms of neurodegeneration. In this context, we aim to define the effect of ubiquitination on the structural propensities of Tau, on its aggregation pathway to fibrils, and on its clearance.

In latest years, it is becoming evident that the physiological role of Tau extends beyond its ability to modulate microtubule dynamics. Thanks to the identification of numerous binding partners, including signaling molecules, cytoskeletal elements, and lipids, its involvement in diverse activities has been suggested. Anionic cofactors such as lipids were proposed to play a major role in shifting conformational equilibria towards either aggregation-resistant or pro-aggregating structures. Lipids are abundant in the cellular environment and accessible to cytosolic Tau, and interactions between lipid membranes and Tau have been proposed to play a role in the protein's physiological function. However, their influence on the conformational dynamics of Tau remains poorly characterized. Beyond plausible interactions under normal conditions, lipid-promoted Tau aggregation is of great interest due to its role in the process of neurodegeneration. It is known that the levels of free cytosolic fatty acids can be increased in pathology. In this context, we aim to investigate the equilibrium binding of Tau4RD to anionic lipid vesicles and fatty acids. Particularly, we are interested in identifying the polypeptide regions involved in the interactions and detecting conformational transitions experienced by Tau in the presence of lipid molecules.

Recently, nanoparticles have attracted increasing interest as aggregation modulators and were found to either accelerate or inhibit fibrillogenesis, depending on their properties (size, charge, hydrophobicity, material), environment (pH, ionic strength, temperature), NP/protein molar ratios. However, despite intense investigation, our understanding of how amyloidogenic proteins interact with NPs remains limited. Solution NMR experiments have been increasingly used to describe the interaction of proteins with NPs at the individual residue level. Indeed, recent efforts demonstrated that several NMR observables, such as chemical shifts, signal intensities, amide exchange rates, and relaxation parameters, together with newly designed saturation transfer experiments, could be successfully employed to characterize the orientation, structure and dynamics of proteins adsorbing onto NP surfaces. In this context, we aim to describe the interaction pattern of the NP-Protein hybrid assemblies at the individual residue level by solution NMR spectroscopy. The collected data should serve to figure out which conformations of the model proteins are prevalent at the NPs surface and to describe the relationship between particle features and conformational preference.

In summary, the activity of this thesis project concerns the investigation of conformational properties of protein Tau induced by ubiquitination and by interactions with lipids and nanoparticles.

1 Introduction

1.1 Neurodegenerative Diseases

Neurogenerative diseases are a very common disorder among elderly people. In recent decades, are becoming more prevalent, although the mechanism that leads to progressive dysfunction and death of nerve cells in different parts of the human brain is still unknown[1]. These age-dependent disorders are becoming one of the most serious health and socioeconomic problems as a result of increased life expectancy. Indeed, in recent years, the elderly population has increased[2,3] and according to recent estimates, more than 45 million people worldwide are living with dementia and this number will increase to more than 130 million people by 2050 (Figure 1)[4,5].

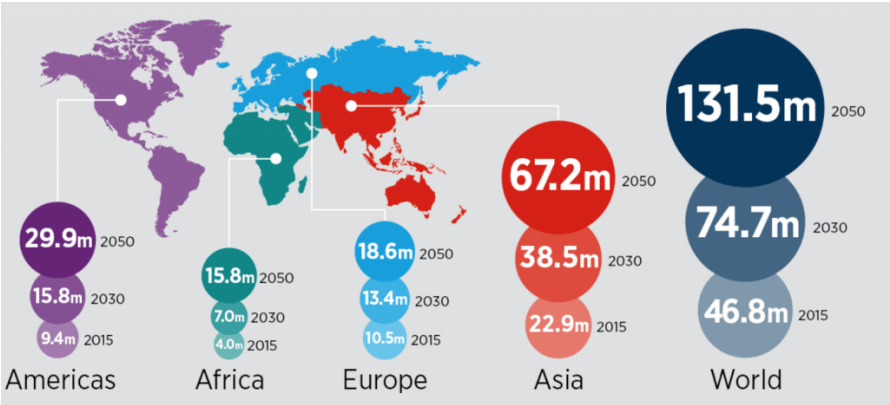

Figure 1: The chart shows the number of elderly people suffering from dementia and expected growth in the future. Data refer to: 2016-2050(estimates)Source: Alzheimer's Disease International (ADI).

Over the past decades, research on neurodegenerative diseases has grown: according to a PubMed research powered by the Nation Library of Medicine for the keyword "*neurodegenerative disease*", more than 65.000 citations for the past ten years have been found, including over 20.000 citations each on Alzheimer disease and about 10.000 citations for Parkinson disease. This clearly shows that the remarkable advances in understanding the genetic basis of neurodegenerative diseases have been a major driving force in all fields of research on these disorders by opening many new lines of investigation. It is, therefore, necessary to continue to develop

new ways of advancing new therapeutic strategies in order to drastically reduce the mortality of these disorders in the elderly population [6,7].

Which are the hallmarks of these diseases? According to the common lines of investigation, apparently there is a common pathogenesis that characterizes the neurodegenerative disorders: Alzheimer's disease (AD), Parkinson's Disease (PD) and others, are marked by the aggregation and deposition of misfolded proteins, which cause destabilization of neuroplasticity followed by neuronal cell loss, resulting in specific clinical impairments [8]. Almost all major neurodegenerative disorders are characterized by the insidious accumulation of insoluble filamentous aggregates of normally soluble proteins in the Central Nervous System (CNS) [8], as reported in Table 1.

Diseases	Microscopic Lesion	Location	Aggregated protein
Alzheimer's disease	Amyloid plaque	Extracellular	Amyloid-β (Aβ)
	Neurofibrillary tangle (NFTs)	Intracytoplasmic (neurons)	Tau
	Lewy bodies	Intracytoplasmic (neurons)	α-synuclein
Amyotrophic lateral sclerosis	Hyaline inclusions	Intracytoplasmic (neurons)	Superoxide dismutase-1 (SOD1)
Cortical basal degeneration/progressive supranuclear palsy	Tau positive inclusion	Intracytoplasmic (neurons, oligodendroglia and astrocytes)	Tau
Dementia with Lewy bodies	Lewy bodies	Intracytoplasmic (neurons)	α-synuclein
Huntington disease	Neuronal inclusions	Intranuclear (neurons)	Huntington (containing polyglutamine repeat expansion)
Multiple system atrophy	Glia cytoplasmic	Intracytoplasmic (oligodendroglia)	α-synuclein
Parkinson's disease	Lewy bodies	Intracytoplasmic (neurons)	α-synuclein
Pick's disease	Pick bodies	Intracytoplasmic (neurons)	Tau
Prion diseases	Prion plaques	Extracellular	Protease-resistant prion protein (PrP)

Table 1: Neurodegenerative diseases characterized by the deposition of aggregated proteins. (Adapted from Skovronsky et al, 2006) [8].

1.1.1 **Alzheimer disease**

Alzheimer's disease (AD) is the most common and prevalent neurodegenerative disorder, being more prevalent than Lewy body dementia (LBD) and frontotemporal dementia (FTD), however, despite intense efforts, it has remained an insufficiently understood disorder. This type of dementia usually starts slowly, affecting first the parts of the brain responsible for memory, thinking and language and, as all neurodegenerative diseases, it is characterized by a progressive and slow loss of cognitive functions, directly connected to severe dementia [9]. Moreover is marked by a decline in memory and cognitive deficits such as problems with language, visuospatial skills, impaired judgment, and decision-making [10,11]. Over time, these symptoms worsen to the point where patients do not recognize close relatives and have problems with basic daily activities. In addition to memory impairment, sufferers affected by this disease develop other symptoms, such as changes in mood and personality, changes in reasoning skills.

Among all elderly population afflicted with neurodegenerative disorders, more than half suffer from AD [12], and it has been estimated that the number of people worldwide affected by this pathology, today ~15 million, will triple by the year 2050 [13]. More than 95% of AD cases are diagnosed late because the main risk factor is determined by advanced age. Other risk factors include, as examples, cardiovascular diseases [14], inflammation [15], and traumatic brain injury.

Alzheimer's Disease was described for the first time a century ago, in a brief report of 1907 by Alois Alzheimer: a deceased patient presented the pathological hallmarks – plagues and tangles – of the neurodegenerative disease that later came to be known with his name [16]. In the last two decades, the mechanisms underlying this pathology have come to be understood, starting from the discovery of the Aβ protein as part of the plaques and the hyperphosphorylated Tau, as the main part of the NFTs [9,17,18]. Although only the possible or probable AD can be diagnosed clinically routinely and the certain diagnosis of AD can be made only post-mortem, the scientific community is still fighting to better understand this devastating disease.

Neuropathologically, AD is characterized by the extracellular deposition of amyloid plaques containing the aggregated amyloid precursor protein (APP) peptide fragment Aβ and the intracellular neurofibrillary tangles (NFTs) composed of

hyper-phosphorylated Tau protein in paired helical or straight filaments (PHFs, SFs) [19] (Figure 2). Amyloid deposits and NFTs are associated with normal aging; however, these lesions are also the two main neuropathological lesions described in patients with AD [20]. Patients with AD show an extensive loss of nerve cells in the brain, resulting in a dramatic reduction of the brain mass and consequent cognitive decline. Moreover, as reported, these changes in the brain can also lead to loss of synaptic contacts and changes in neuronal morphology [21].

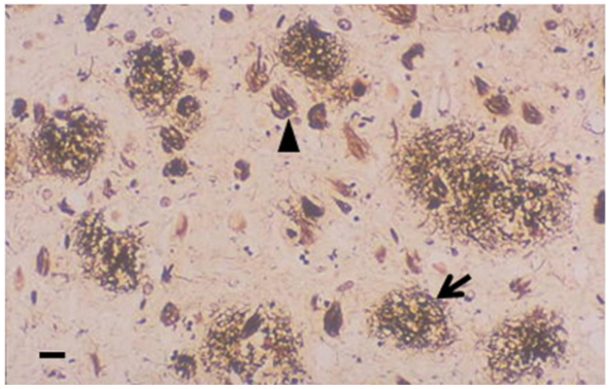

Figure 2**:** The hallmarks of Alzheimer's disease. Senile plaques of Aβ (arrow) and NFTs of phosphorylated Tau protein (arrowhead) detected by silver staining of a section of the brain cortex (Adapted from Allsop et al., 2014) [22].

The increase in the production and aggregation of Aβ, which leads to the accumulation of its toxic species, could be understood with the hypothesis of the amyloid cascade. According to this interpretation, the aggregation of Aβ is directly connected to the outset of Tau pathology in AD, known as Tauopathy. Although the key role of Aβ is well understood in the familial form of Alzheimer's (due to dominant autosomal mutations in the precursor genes of this protein) [23], it is unclear how Tauopathies might be dependent on Aβ aggregation. However, it is clear that AD is directly linked to neuronal death due to Tau oligomerization/aggregation. Furthermore, it is important to note that some changes in the expression or alternative splicing of the MAPT gene are associated with AD risk although there is no known mutation in this gene linked to AD. Despite this, it is known that Tau is essential for the toxic effect of Aβ [24]. Some evidence indicates an interaction between the aggregation of Tau and Aβ, both in vitro and in vivo. As demonstrated in a mouse model of AD, the pathology of Aβ can facilitate the pathology of Tau by

accelerating Tau fibrillization. Therefore this event may lead to a reduction of the density of dendritic spines and cognitive impairment [25].

1.1.2 AD pathogenesis and the UPS

In the last few years, some studies provided evidence that the ubiquitin-proteasome system (UPS) plays a critical role in many neurodegenerative diseases, including AD [26], showing a stronger correlation with this disease [27].

The UPS and the autophagy-lysosome system are two major pathways that degrade intracellular proteins (Figure 3) in non-pathological conditions. UPS is implicated in different cellular processes, like protein trafficking, antigen presentation, and protein degradation [28].

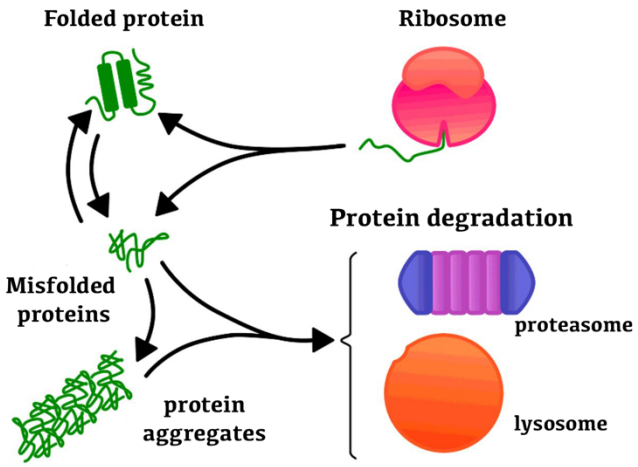

Figure 3: Scheme of cellular pathways of protein degradation (Adapted from Jackson M.P. et al., 2016)[29].

Moreover, UPS is the major cellular mechanism that regulates intracellular protein levels. UPS plays an important role in eliminating damaged, misfolded and mutant proteins [30].

UPS substrates are directly connected with Ubiquitin, a highly conserved protein. It binds covalently to the damaged protein, targeting it to the proteasome, where it will be degraded by proteolysis [28,31].

Dysfunction in the UPS may initiate or facilitate the aggregation of Tau, however, there is a direct interconnection between abnormal UPS activity and PHF formation. In fact, impaired proteasome function might be the consequence of AD, instead of the cause of Tauopathies [27].

1.1.3 The Ubiquitination Machinery

Ubiquitin (Ub) is an 8.5 kDa regulatory protein found in almost all tissue in many eukaryotic organisms, it contains a 76 residue highly conserved, in a wide variety of eukaryotic organisms [32]. Regarding its role in protein degradation, Ub is usually linked to the target proteins through isopeptide bonds between the C-terminal Gly residues of Ub and the ε-amino groups of lysine (Lys) residues in proteins. These bonds could be done by single modification (monoubiquitination) or by one Ub at multiple site of the same target (multi-monoubiquitination). Furthermore, it can be done by the formation of Ub chains (polyubiquitination) (Figure 4) [33].

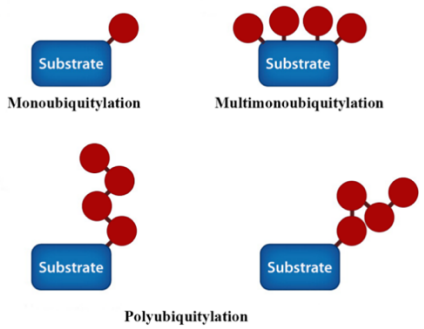

Figure 4: Scheme of different ubiquitinated substrates (Adapted by Komander et al, 2012) [33].

Ubiquitin is characterized by seven potential lysine residues (K6, K11, K27, K29, K33, K48 and K63) (Figure 5) that participate in chain linkage formation [34].

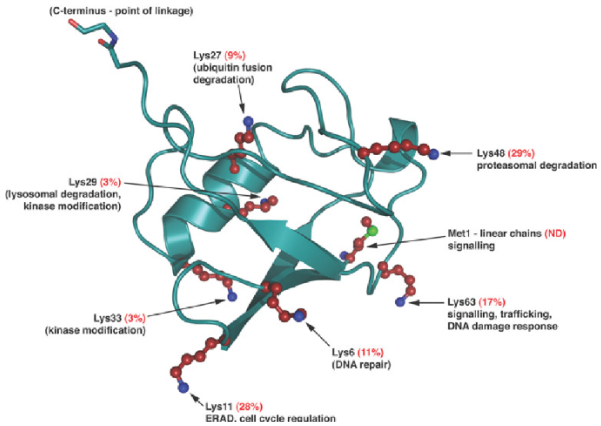

Figure 5: Ubiquitin and its seven lysine residues (Adapted by Komander et al, 2009) [35].

Thus, in the chains, the different Ub-Ub linkages form distinct conformations and consequently the fate of ubiquitinated substrate depends on the length and linkages

type of the chains, but also depends on the set of downstream interacting proteins that "*interpret*" the diverse Ub signals. As examples, substrates modified with K48-linked poly-Ub are usually targeted for degradation by the 26S proteasome [36]. Whereas K63-linked poly-Ub play a non-degradative role and have been implicated in DNA damage tolerance, NF-kB activation and other pathways implicated in receptor endocytosis and sorting [37].

The natural ubiquitination process is based , in vivo, on a complex machinery, based on multi-enzymes cascade involving E1 (Ub-activating), E2 (Ub-conjugating), E3 (Ub-protein ligase) enzymes (Figure 6) [38].

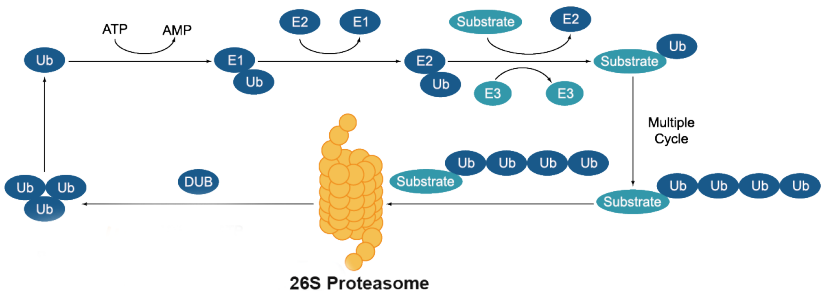

Figure 6: Scheme of the Ubiquitin System

In an ATP-dependent first step, a ubiquitin-activating enzyme, **E1**, activates Ub at its C-terminal residue, with the release of AMP. The Ub activation by E1 enzyme is a crucial event that constitutes an important and unique starting point of the UPS. The Ub-activated is then transferred to an active site Cys residue of a ubiquitin-carrier protein, **E2**. The Ub C-terminus is attached to the E2 catalytic cysteine residue via thioester linkage catalyzing the transfer of the activated Ub to an intermediate. Finally, an **E3** ligase acts as an adaptor that binds both substrate and Ub-E2, allowing an efficient transfer of Ub from the E2 to the substrate, by hardly understood mechanisms.

The human genome encodes for different forms of these enzymes: two E1 enzymes, 37 E2 enzymes, and over 600 E3 ligases, and many other enzymes for stretching chains and de-ubiquitinases enzymes. This wide enzymatic variety indicates that the ubiquitination process is extremely specific and regulates many substrates proteins.

1.2 Tau protein

In eukaryotic cells, the cytoskeleton is a functional network involved in a diverse range of cellular activities, such as mitosis, meiosis, motility, morphogenesis and intracellular trafficking. The core components of this network are the microtubules (MTs), intracellular structures composed of a heterodimer of alpha and beta tubulin proteins. MTs are highly dynamic and exhibit a non-equilibrium behavior termed dynamic instability, in which MTs undergo rapid stochastic transitions between growth and shortening, as a result of the association and/or dissociation of tubulin dimers at its extremities [39]. The stability and dynamics of the assembly of MTs are promoted by proteins which are known as Microtubule-Associated Proteins (MAPs) [20]. Among these MAPs, Tau is a major protein that participates in the association-dissociation of the MTs, conferring dynamics and polymerization to the system [40] (Figure 7).

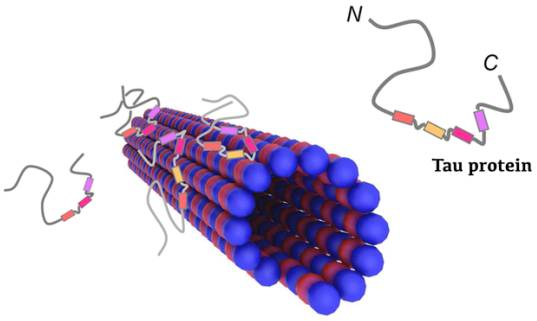

Figure 7: Cartoon showing MT decorated with adsorbed Tau (Adapted from Choi et al., 2009) [42].

Tau is described as a highly soluble, natively unfolded and extremely heat-stable protein. It is predominantly expressed in the neurons (preferentially localized to the axons), where it plays a critical role in tubulin assembly and stabilization of microtubules, thereby promoting the normal function of neurons [20].

In the human, Tau is encoded by the MAPT gene, located on the long arm of chromosome 17 [43]. There are mainly six Tau isoforms in the brain, showing differences in their primary structure due to the presence or absence of some specific exons [44] (Figure 8).

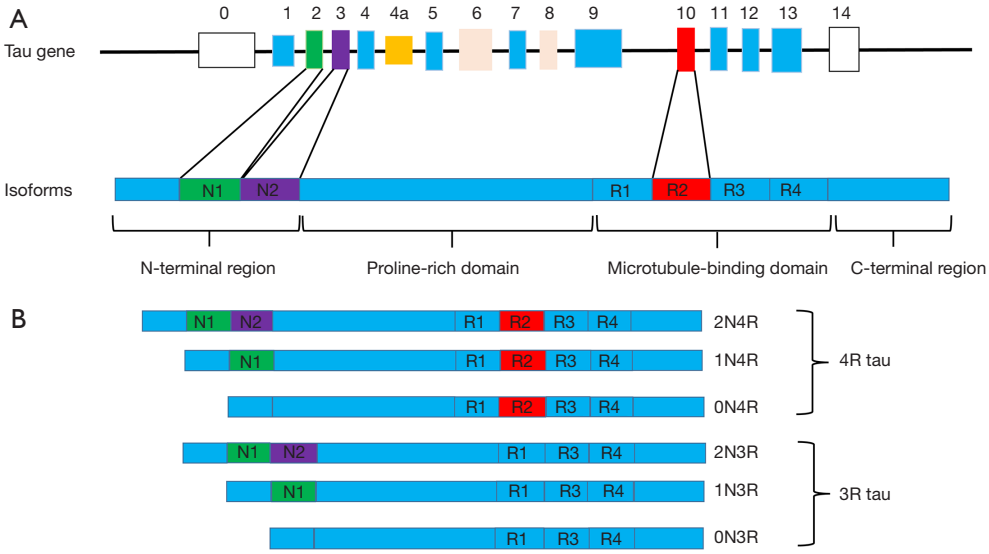

Figure 8 (A) Schematic representation of the human Tau gene and (B) six isoforms in the human brain. (Adapted from Gao et al., 2018) [45].

1.2.1 Structure and Function of Tau Protein

The primary structure of Tau protein consists of an N-terminal acidic portion followed by a proline rich region and the C-terminal tail, which is the basic part of the protein (Figure 9) [46,47]. In other words, Tau can be described as a dipole with two domains of opposite charge, which can be modulated by post-translational modification [47].

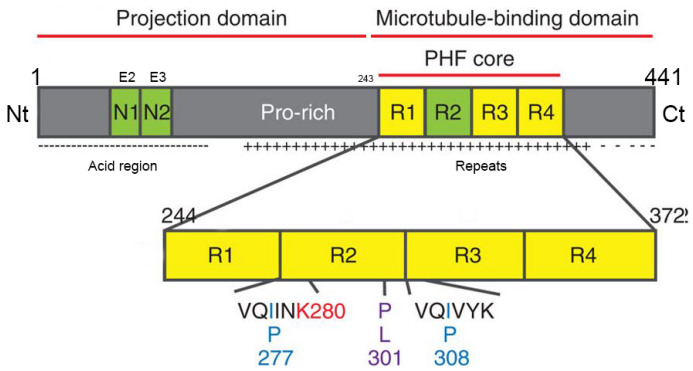

Figure 9: Schematic representation of the functional domains of the full-length Tau sequence (Adapted from Shammas et al., 2015) [48].

The N-terminal part is known as "**Projection Domain**" (amino acids 1-243), since it projects from the microtubule surface, where it may interact with other cytoskeletal elements and plasma membrane [49] (Figure 9). In certain types of axon, the N-

terminal region of Tau plays a crucial role in their stabilization and organization, because the projection domain determines the spacing between MT in axon and may increase axonal diameter [50]. The C-terminal part is known as "**Microtubule Binding Domain** (**MTBD**)" (amino acids 244-369), characterized by four repeated domains (R1-R4) with which Tau protein binds and stabilizes MT. These repeats consist of stretches of a highly conserved 18-residue segment that are imperfectly repeated in the protein, separated by flanking regions [51,52]. Within the R1-R2 and R2-R3 two hexapeptide motifs were identified, which are crucial for Tau change in conformation and induce microtubules. These two motifs are the most potent part to induce microtubule polymerization, but also have a high β-sheet-forming propensity [48], and are further characterized as drivers of the abnormal self-assembly of Tau [5].

Tau is a heat resistant protein and limited affected by acid treatment without loss of its function, as the common MAPs [41]. This property is probably due to the low content of secondary structure which is deduced from data collected with various biophysics techniques, like CD, FTIR, and NMR, which exclude the existence of stable secondary structure elements [53–55](Figure 10). Consequently, this low content of secondary structure [56], combined to its highly flexible conformation, classify Tau as a "natively unfolded" protein [57].

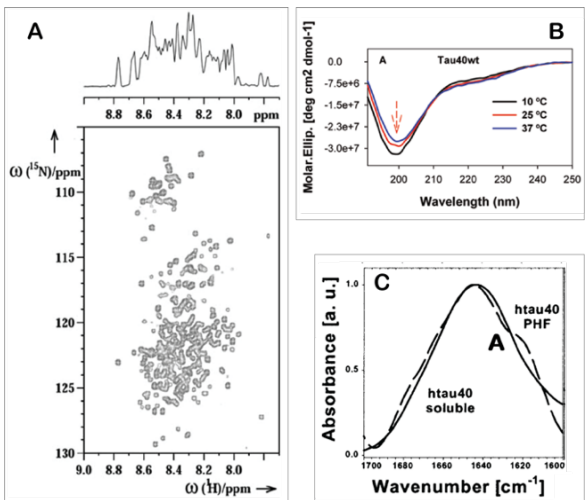

Figure 10: The naturally unfolded nature of Tau protein. **A**. 1H-15N HSQC Spectrum of typical unfolded protein with poor signal dispersion and with the protons signals occupying only 1ppm. **B**.CD Spectrum, shows a dip at 200 nm corresponding to random coil. **C**. FTIR Spectrum, the peak at ~ 1645 cm-1 indicates the random coil typical structure. (Adapted from (**A**)Lippens el at, 2006; (**B**) Gorantla et al, 2017; (**C**) von Bergen et al, 200158–60)

Consequently, it has not yet been possible to obtain a structural analysis using crystallography. Therefore, nuclear magnetic resonance spectroscopy (NMR) has been proposed as a method that could allow a description of Tau conformations and dynamics with high resolution [61]. Combining NMR with a wide range of experimental techniques, like FRET, EPR, SAXS, as well as computational studies, can be provide a consistent description of the three-dimensional structure [54,55,62]. Moreover, measurements of gyration and hydrodynamic radii pointed to an average structure slightly more compact than that expected for a polypeptide in complete random coil conformation [54,62]. Combining these analyses, in 2006 was proposed an original folded form for this protein in the unbound state in solution, known as "*paper clip*" fold. In this original folded form, the C-terminus folds over the MTB region, while the N-terminus folds back over the C-terminus, bringing both termini in close proximity [55] (Figure 11). Particularly, in the MTB region, the conserved hexapeptide at the beginning of the Tau repeats R2 and R3 converts the protein into this particular conformation [63].

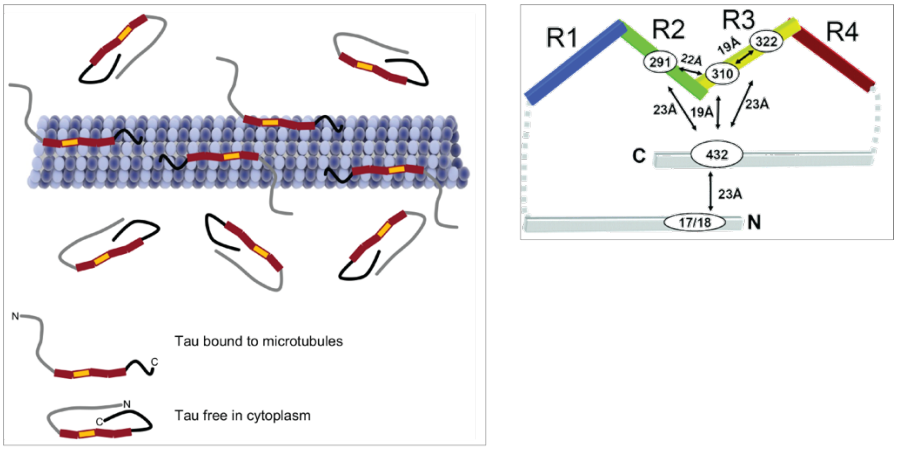

Figure 11:"*Paper-Clip*" model of soluble Tau (Adapted from Guo et al., 2017 and Jeganathan et al., 2006) [64,65].

Although efforts have focused on the characterization of the structure of this protein, its intrinsically disordered nature [53], combined with its multiple post-translational modifications [66], and the occurrence of six isoforms [67], makes it is difficult to define precisely its function.

1.2.2 Conformational Rearrangements of Tau Protein

The dynamic structure of Tau is influenced by the presence of chemical modifications and conformational rearrangements upon interaction with binding partners [63,68–70].This leads to the most prominent conformational transition of Tau, that is the formation of supramolecular structures in a self-assembly process, that eventually leads to the accumulation of insoluble deposits of Tau aggregates [71,72]. Moreover, it also appears that this aggregation could be nucleated by the two hexapeptide motifs probably due to the propensity of these residues to form β structure[73]. Remarkably, unmodified Tau is highly soluble and has very little tendency to aggregate in solution, and does not show any evidence of adopting stable secondary or tertiary structure [41]. It is possible that the formation of the "paper-clip" structure contributes to preventing protein self-assembly [55].
By contrast, truncated forms of Tau do not acquire this conformation and are more prone to aggregation [74].

Although point mutations that reinforce β-propensity and specific chemical modifications were reported to accelerate fibrillization of Tau in vitro, the inducers of Tau aggregation in neurons and the structure of the aggregation-competent intermediate(s) remain currently unknown [75].
According to recent evidence, it is becoming clear that the physiological role of Tau goes beyond its ability to modulate microtubule dynamics [76,77]. Indeed, the identification of different and numerous binding partners (such as signaling molecules, cytoskeletal elements and lipids) suggest its involvement in diverse activities [76]. Anionic cofactors such as proteins, nucleic acids, and lipids were proposed to play a major role in shifting conformational equilibria towards either aggregation-resistant or pro-aggregating structures [75]. *In vitro*, sulfated glycosaminoglycans promote Tau aggregation through a charge compensation mechanism [78] and similar effects are elicited by nucleic acids [79] and acidic lipids [80].

1.2.2.1 Tau Aggregation

One of the most significant features of a living system is the ability of the molecular structure to self-assemble [81], indeed, the spontaneous aggregation of proteins to form a large structure is one of the elements that characterize and

distinguish both normal and aberrant biology [48]. The pathological formation of insoluble aggregates via self-assembly of soluble proteins into oligomeric structures lays at the root of a number of human diseases, including neurodegenerative disorders such as AD and PD [82]. Formation of these insoluble aggregates includes different proteins and there may be different and multiple causes of their abnormal aggregation, such as post-translation modifications. In other cases, the formation of these insoluble aggregates is due to the unfolded nature of the soluble protein, exposing their surface for unfavorable interactions. These interactions are often localized around specific regions prone to forming β-structure, which leads to highly stable aggregates that are not easily removed by the proteasome system [82].
Consequently, there is a general interest in preventing or retarding and identify the causes of the aggregation process, to understand the onset of these diseases.

Tau is an unfolded, highly soluble protein which, as mentioned in the previous paragraph, plays a critical role in MTs assembly, stabilization and promoting normal function of neurons. In many neurodegenerative disorders, including AD, Tau can undergo several post-translational modifications that determine the loss of the capacity to bind MTs, impairing the organization of the cytoskeleton in the axonal process. This abnormal behavior is promoted by conformational changes and misfolding in the normal structure of Tau [47,83], which leads to its aberrant aggregation into fibrillary structures inside the neurons of demented individuals. Experimental evidence shows that Tau undergoes conformational changes in which the conversion of monomer to dimer is followed by the formation of toxic oligomers [84–88]. Afterwards the oligomers aggregates form the Paired Helical Filaments (**PHFs**), leading to the formation of Neurofibrillary Tangles (**NFTs**) [89] (Figure 12), the major pathological hallmarks of AD, abundant in the brains of AD patient. This event can influence the stability of MTs and other processes related to Tau protein [47,90].

In vitro, a good model to understand the pathological Tau fibrillization has been developed, using polyanionic cofactors [91]. These molecules, such as heparin, accelerate Tau fibrillization producing filamentous structures that are structurally similar to those found in AD [92]. The molecular basis of this process is still unknown

but is probably attributable to an electrostatic interaction that causes structural and conformation changes of Tau protein that induce fibrillization [92,93].

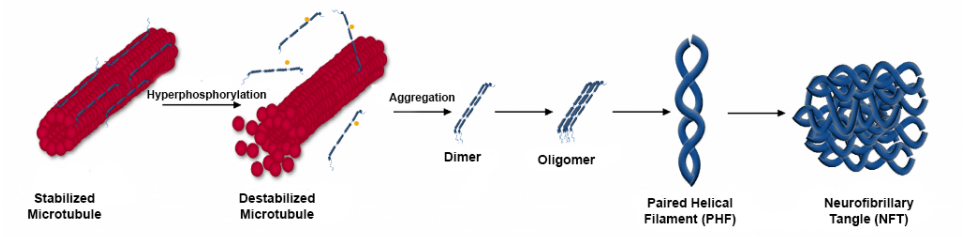

Figure 12: Scheme of Tau dissociations from MITs, leading to their destabilization. It then aggregates into oligomer, PHFs and, ultimately, NTFs. (Adapter from P. Thomson, 2018) [94].

1.2.2.2 Post-translational modification of Tau

The mechanisms responsible for the non-functional activities of Tau protein are still unknown. To counter the onset of these toxic oligomers (because they have a high affinity to unmodified Tau molecules), cells try to hide them, triggering some protective processes such as phosphorylation. Unfortunately, in AD these protective process fails, leading to an increase in the amount of Tau molecules released available for the aggregation [95]. These hypotheses are still under debate because the formation of this toxic PHF-core is unknown and it is likely due to a combination of different events in neurons, such as oxidative stress or abnormal post-translational modifications and protein degradation.

Several studies propose as main cause of this failure, the abnormal post-translational modifications [96,97]. Tau, indeed, is subjected to a wide range of post-translational modification that are identified in Tauopathies, like hyperphosphorylation, truncation glycosylation, glycation, nitration, and ubiquitination (Figure 13). Therefore, many different Tau binding partners can be regulatory components of post-translational modifications, such as protein kinase and phosphatase. Moreover, Tau is also a substrate for the ubiquitin–proteasome system (UPS) and for chaperone-mediated autophagy [98].

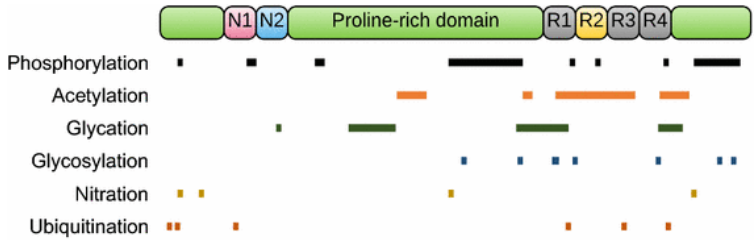

Figure 13: Illustration of the main post-translational modifications identified on Tau. The colored bars show the approximate sites of each modification on the largest human 2N4R Tau (Adapted from Guo et al, 2017) [5].

Ubiquitination of Tau

Ubiquitination is an enzymatic process that involves the binding of a ubiquitin molecule to a target protein. This process is sometimes described as the molecular "*kiss of death*" for a protein, as the substrate usually becomes inactivated and is tagged for degradation by the proteasome [99]. Ubiquitin-Proteasome-System (UPS) plays a crucial role in the regulation of intracellular proteins, removing mutant, damaged and misfolded protein. Recent evidence has shown that dysfunctions in the UPS are directly connected to Tau degradation/aggregation and neurodegeneration in AD [26,30].

The first clue for the pathological link between UPS and Tau was first identified in the frequent co-localization of ubiquitin (Ub) in PHFs and NFTs. Ubiquitinated Tau occurs in both mono-Ub and poly-Ub forms [100]. Recent mass spectroscopy analysis on PHFs [60] observed also polyUb chains with Lys6-, Lys11-, Lys63-linkage [101–103], although the significance and fate of the Ub-Tau complex, particularly in relation to proteasomal degradation or autophagic clearance, remain unclear [27]. This analysis has identified that ubiquitination marks Tau at specific Lys (K) residues: K254, K311 and K353, all located on MBD [101].

Among these, the canonical degradation signal formed by Lys48-linked polyubiquitin chains was identified, suggesting that the ubiquitination of Tau could be involved in early molecular events at the onset of the Alzheimer's diseases (Figure 14**).** Notably, K311 belongs to one of the Tau hexapeptide motifs (VQIVYK), R3, proposed to be core nucleation sites for the formation of amyloid fibrils.

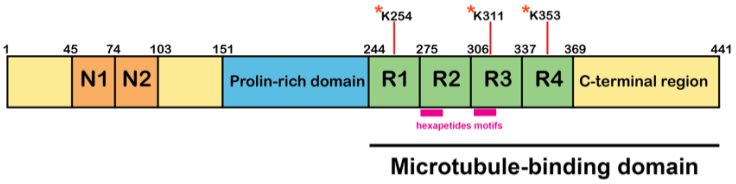

Figure 14: Cartoon of the ubiquitination site (red *) of Tau, located on MBD.

A further clue between Ub-dependent protein degradation and Tau turnover comes from the identification of the Tau-E3 ligase. This ligase is the carboxyl terminus of the Hsc70–interacting protein (CHIP)–Hsc70 complex, with UbcH5B as the E2 enzyme [104,105]. CHIP was found to be able to ubiquitylate unfolded proteins [106] before removal by 26S proteasome. This evidence supports the notion that UPS could be a major system responsible for the clearance of soluble Tau.

To gain a molecular understanding of the influence of Ub on the aggregation propensity of Tau, it is crucial to have access to diverse ubiquitinated Tau products. Enzyme-based reaction protocols have been developed to produce ubiquitinated proteins suitable for biophysical characterization [107]. Enzymatic strategies exploit the coordinated action of the cascade of enzymes (E1, E2 and E3) that are responsible for protein ubiquitination *in vivo*. This approach can potentially yield great amounts of ubiquitinated samples, conjugated by native isopeptide bonds. Although the main limitation is that specific E2 and E3 enzymes need to be known. Synthetic and semi-synthetic chemical approaches have proven a powerful alternative to enzymatic strategies, while presenting limitations and drawbacks on their own [108,109]. Despite the availability of several ubiquitin ligation methods, in vitro ubiquitination of Tau has not been reported so far.

1.2.3 **Tau/lipids in health and disease**

Membrane lipids may be closely associated with protein aggregates formation and amyloidogenesis *in vitro* and *in vivo* [110].

The brain contains a high concentration and variety of lipids, especially fatty acids (FAs), second only to adipose tissue, where they play a critical role in neuronal membrane fluidity and permeability, serve as energy reservoirs and function as second messengers signaling [111]. Among all lipids, polyunsaturated fatty acids (PUFAs) affect the aggregation of some misfolded proteins that have been

implicated in neurodegenerative disorder [110,112,113]. All the long-chain FAs were found to enhance protein aggregation to some extent. Especially unsaturated FAs demonstrated greater stimulation of filamentous aggregates formation [113].

The first reports on the implication of fatty acids (FAs) on protein aggregation, described that FAs stimulated the assembly of both Aβ peptides and Tau filaments *in vitro* [80,110]. Especially, Tau-membrane interaction is the focus of numerous studies [114–116]. Indeed, it has been suggested that Tau in AD brains may exhibit abnormal interactions with the neuronal cell membrane. This interactions could play a role in the protein's physiological function [116,117], however the influence membranes on the conformational dynamics of Tau remains poorly characterized.

Beyond plausible interactions under normal conditions, lipid-promoted Tau aggregation is of great interest due to its role in the process of neurodegeneration. Indeed, lipids are abundant in the cellular environment and therefore easily accessible to cytosolic Tau. Above all, under the pathological condition in which an increase in the amount of the levels of free cytosolic FAs were observed. Indeed, it has been reported that elevated concentrations of saturated fatty acids are able to cross the blood brain barrier, constituting a significant risk factor for AD [119].

Brain neurons are particularly rich in polyunsaturated fatty acids, such as arachidonic (ARA) and docosahexaenoic (DHA) acids, which are liberated into the cytosol by the action of phospholipases [120]. Tau could participate in the formation of co-aggregates with lipids, in analogy with the formation of such assemblies by α-synuclein, another disordered amyloidogenic polypeptide implicated in neurodegeneration [121,122]. This hypothesis is supported by the observation of Tau filaments associated with lipid membranes[123] and by the discovery of fatty acids in NFTs [124].

The importance of lipid-protein co-assembly in the onset and progress of amyloid diseases has been pointed out recently [114]. The association of intrinsically disordered polypeptides with free lipids, micelles, and vesicles is predicted to dramatically affect the structures and physico-chemical properties of these biomolecules and to modulate their interactions with other molecular partners and cells.

Thorough investigations of lipid-protein co-assembly are necessary to deepen our understanding of both the healthy and aberrant action of amyloid

proteins. Results obtained from these investigations could prove the basis for the development of therapeutic strategies against devastating neurodegenerative diseases.

1.3 Nanoparticles

In recent years, there has been a drastic increase in research, technological development in the field of nanotechnology [125]. One of the fundamental components of nanotechnology are nanoparticles (NPs), which are widely used in molecular diagnostics and biotechnology, with many applications in in-vivo imaging, drug delivery systems, biosensors and many others [126–128].

Nanoparticles are a wide class of materials that includes particulate substrates with a dimension less than 100 nm at least [129,130]. NPs exhibit unique properties at nanoscale such as physical, chemical and biological, compared to their respective particles at larger scales. Although NPs may differ largely in terms of dimension, shape, size and their material [131], they are produced with a general architecture as follows [132] (Figure 15):

- A surface layer which can be functionalized with a variety of small molecules, metal ions, surfactants, and polymers, depending on the desired physicochemical and bioactivity of the designed particles.
- A shell layer, which is chemically different material from the core
- The core, which is essentially the central portion of the NPs and usually refers to the NPs itself. Its composition is highly varied, including metals, ceramic, organic polymers, lipids, etc.

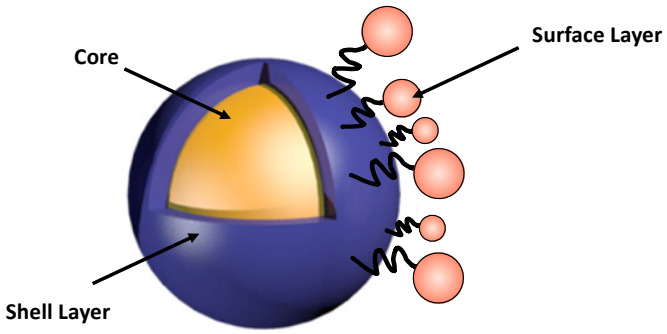

Figure 15: Nanoparticles Structure Scheme

The rapid development of novel nanoparticulate materials for application in many areas of bioscience necessitates an improved characterization of the nano-bio interface [126] and, in particular, understand how NPs interact with biological systems

represents a key point for the identification of the biocompatibility or bio-adverse interaction [133].

The complexity, the heterogeneity and the presence of different biomolecules make the biological environment a unique environment to study the behavior of the NPs immersed in it. In this medium, in fact, NPs can interact with different biomolecules, such as nucleic acids, lipids, proteins [134], in particular the latter are most relevant because they profoundly influence NPs biodistribution and bioreactivity. According to evidences, proteins may display preferential orientations with respect to the NP surface, mediated by specific noncovalent chemical interactions.

1.3.1 Nobel Metal Nanoparticles: Gold NP

For centuries noble metal nanoparticles, such as gold and silver, have been used in several fields. In the last decades, these NPs have attracted intense scientific and technical interest due to their unusual optical, electronic, and thermal properties. Mostly, also for the facile synthesis and surface bioconjugation and feasibility in clinical diagnostics and therapeutics.

Gold-NPs (AuNPs), in particular, represent an attractive delivery vector in biomedicine due to their low toxicity and unique electronic and chemical properties [135], and are among the most abundant in scientific literature. Typically, the size of this AuNPs is in the range from 5 nm to 400 nm (Figure 16). Their synthesis process is very simple and generally is done according to the classic reduction method with an appropriate modification [136]. Briefly, a sodium citrate solution is added to boiling $HAuCl_4$ solution and the reaction solution is allowed to mix under reflux.

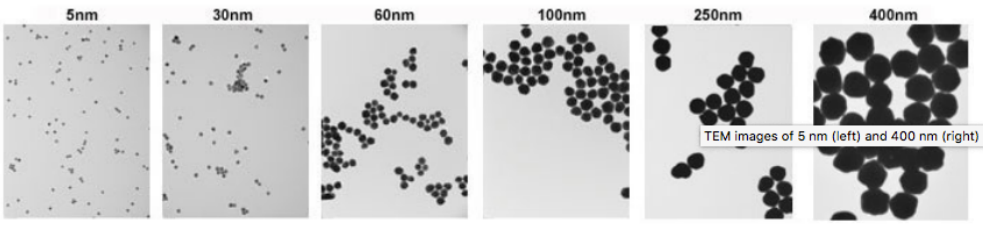

Figure 16: TEM imaged of gold nanoparticles from 5 nm (left) to 400 nm (right)

AuNPs are characterized by unique properties, such as size and shape that depend on optical and electronic features. Another feature is a high area to volume

ratio and the surface layer, which can be functionalized with different chemical groups such as thiols, phosphines, and amines, which exhibit affinity for gold shells. Thanks to the advantage of these functional groups, it is possible to confer greater functionality by anchoring ligands of various natures such as proteins, oligonucleotides, antibodies, etc.

The gold nano-conjugates formed have enabled a varied range of investigation, such as programmed assembly and crystallization of materials, arrangements of NPs into dimers and trimers onto DNA templates, bioelectronics, and new detection methods [137]. This spontaneous formation of proteins-AuNPs conjugate is well known [138,139].

Indeed, introducing NPs into the biological environments, immediately interface with the molecules immersed in it: nucleic acids, lipids, and proteins, which form a dynamic biomolecular corona around them [134].

Thus, as the first priority, it is necessary to understand the chemical nature of the conjugate's interaction, which in turn requires the knowledge of the structure of proteins on AuNPs surface [135].

1.3.2 **Protein-NPs interaction**

Among all of the potential applications of NPs, the most studied is the conjugation with proteins. These conjugations not only stabilize the system but also introduces biocompatible functionalities to the NPs, for further biological interactions or coupling [130,134]. The formation of this interaction is due to the varied composition, extensive properties, sizes, and shapes of NPs, and secondly to their low toxicity and unique optical, chemical, and physical properties. Moreover, NPs also offer the benefit of carrying functional groups (amino and carboxylic groups), which can be used for surface modification [128]. Furthermore, nanoparticles possess higher stability during storage, in vivo stability after administration, as well as being easily adjustable during preparation [128]. Because of all these features, it is challenging to generalize the behavior of the biomolecule-NP association to subtle changes to surface chemistry. Indeed, this can lead to large changes in binding behavior, altering both the soft and hard corona composition and dynamics.

Most of these conjugations are spontaneous without causing any protein aggregation. On the contrary, when aggregation does occur, NPs can be used as a good platform to modulate the orientation, structure, and function of the protein [134].

1.3.2.1 Nanoparticle role in protein aggregation

The interaction of NPs with proteins can affect both protein structure and functions [140]. In particular, in the presence of amyloid protein, NPs have the ability to modulate their aggregation [135,141,142]. Such an effect could be probably attributed to the enormous surface area of NPs that could influence protein structure and function. Recent evidence has shown that NPs can interfere with the aggregation process of amyloid proteins, going to up- or downregulate this mechanism [134,141]. Indeed, on one hand, the NPs may act as catalysts to facilitate the assembly of proteins into stable fibril aggregates by increasing the local concentration of those proteins [134,140]. On the other hand, NPs may act as an inhibitor of fibril propagation, determining a monomer depletion and/or trapping of sub- and near-critical nuclei [143]. Consequently, it is necessary to increase our knowledge of NP-protein interactions, and of established mechanisms of protein amyloid aggregation, in order to explore the possible scenarios in which NPs interfere with protein aggregation pathways [144].

1.3.2.2 Methods used to study Protein-Nanoparticle interactions

The interaction between protein and NPs has been widely studied with a range of different techniques such as mass spectrometry-based proteomics, surface plasmon resonance and gel filtration chromatography, especially in the spectroscopy field this interaction is deepen investigated [145–147].

Circular dichroism (CD) is used to obtain information of the interaction force and to monitor the changes in protein secondary structure after NPs addition [148]. Otherwise, Dynamic Light Scattering (DLS) is used to detect changes in hydrodynamic radii and electrokinetic surface potential of the NPs after the adsorption of biomolecules [149]. Moreover, with Isothermal Titration Calorimetry (ITC) it is possible determine the energy of the interactions [150]. Among all these spectroscopy techniques, solution NMR spectroscopy has proven to be an outstanding tool to

describe the coordination and exchange mechanisms of organic molecules at the NPs surface, as well as ligand shell composition [145,151]. Solution NMR spectroscopy is an established technique for the high-resolution characterization of biomolecules and recent studies are promoting new approaches to provide new information to understand these interactions.

1.4 Biomolecular NMR spectroscopy

Nuclear Magnetic Resonance (NMR) spectroscopy has proven to be a valuable tool in the studies of IDPs. Above all, in addition to its normal application for determination of 3D structure at atomic resolution of folded protein in solution, is unparalleled in its capability to provide detailed structural and dynamical information on unfolded proteins [152]. The proton chemical shift dispersion and line width give first information about the state of proteins: poor protein chemical shift chemical shift dispersion is indicative of disorder [152].
This powerful technique is one of the few comprehensive sources for information on unstructured/partly structured proteins and, moreover, on the protein folding process [153,154].

1.4.1 Protein NMR spectra

Nuclear Magnetic Resonance is a phenomenon that occurs when the nuclei of particular atoms are immersed in a static magnetic field and exposed to a second oscillating magnetic field. In a general NMR experiment the sample nuclei are oriented by a strong magnetic field (in the order units of Tesla), absorb radiation at characteristic radiofrequency (about 50-1000 MHz) and undergo an energetic transition between two states. Then, the magnetization decay (FID, free induction decay), necessary to reach the equilibrium state, is converted by Fourier-Transformation in the frequency-domain from the acquired time-domain data. Nuclei of the same element in different environments give rise to distinct spectral lines because they absorb radiation at characteristic frequencies. The different parameters that can be measured from the resulting spectra could give information about molecular structure, conformation and dynamics.

Different elements have nuclei suitable for NMR spectroscopy: hydrogen (^{1}H, the proton) is the most sensitive nucleus detected by NMR and it is by far the most important nucleus for the study of biological molecules. Other nuclei especially relevant are nitrogen (^{15}N isotope) and carbon (^{13}C isotope) which unfortunately represent only 0.4% and 1%, respectively, of the naturally occurring isotopes.

The main problem that occurs in NMR study of proteins is that these big molecules contain thousands of protons that determine the overlapping of signals in the ^{1}H spectrum. In order to overcome this problem, the common approach is labeling the molecule with isotope such as ^{15}N and ^{13}C which, together with multi-dimensional heteronuclear NMR, are crucial to extend NMR analysis to larger molecules. This can be done only thanks to the development of the molecular biology technique and to the ability to set overexpression systems, which allow obtaining a large quantity of isotopically labeled molecules in the order of milligrams (optimal quantity for NMR experiments).

The most basic parameters to consider during NMR experiments with IDPs includes buffer composition, pH, ionic strength and temperature [155]. Buffers are often used at low concentration (10-50 mM), and non-protonated buffers, such as phosphate buffers, are usually used to prevent overlap in NMR signals from the samples. In terms of pH, a physiological value, close to pH 7, is often chosen to obtain an optimal quality of the NMR data. The ionic strength, with IDPs, is an important parameter to be checked to acquire biologically relevant data. The ionic force, in fact, directly influences the formation of electrostatic interactions, going partially to shield the molecule's charges [156]; it may impact the association and dissociation rates of complexes [157]; and finally it may affect the data quality, because a high ionic strength (> 200 mM) needs setting longer pulses, thus increasing sample heating and reducing the signal to noise (especially using cryogenic probes).

NMR measurements of IDPs require several other components to be added to the sample: an internal chemical shift reference, such as 4,4-dimethyl-4-silapentane-1-sulfonic acid (DSS), for standardization of the resonance frequency to chemical shift values in ppm; 5%–10% (v/v) D_2O, to lock the instrument frequency, and NaN_3 can be added to prevent microbial growth. Lastly, several IDPs have free cysteines and need reducing agents for the measurements, such as β-mercaptoethanol or

dithiothreitol (DTT) or tris(2-carboxyethyl)phosphine hydrochloride (TCEP) [155,158]. NMR data acquisitions of IDPs are often conducted at low temperature (5-10°C) to slow down amide exchange.

1.4.2 **Protein Fingerprinting: ^{1}H-^{15}N-HSQC**

One of the applications of NMR is the investigation of the interaction sites in a protein-ligand complex, performed by monitoring the perturbations of chemical shifts (chemical shift perturbation, CSP), linewidths and/or intensity changes of HN and ^{15}N resonances upon binding or interaction with partners. Within the arsenal of NMR experiments, this analysis is often done with ^{1}H-^{15}N-HSQC, an invaluable tool for protein analysis.

The Heteronuclear Single Quantum Coherence (^{1}H-^{15}N-HSQC) experiments are the simplest and most useful two-dimensional (2D) pulse sequence, to study chemical shift and/or intensity variations of protein signals in a residue-specific manner. This kind of experiment is commonly used in the field of protein NMR, for correlating the ^{15}N nucleus with its attached proton in the backbone amide groups of proteins, by exploiting the coupling between the two nuclei (JHN= 92 Hz).

The resulting ^{1}H-^{15}N-HSQC spectrum represents the "fingerprint" of a protein, in which the number and the position of each signal are specific for each protein sample. Each signal is defined by parameters that provide different information on the changes in chemical environment: position (the resonance frequency or chemical shift), intensity (the concentration of each population), width and perturbation. Chemical shift (the resonance frequency position) and intensity changes are sensitive indicators of interactions among proteins in simple buffers and in presence of perturbing agents. Indeed, protein NMR signals are expected to be perturbed by the presence of ligands dispersed in the solutions or nanoparticles (NPs), and also by the nature of the interactions (protein-ligand/NP) and the physico-chemical properties of the perturbing agents. The chemical shift of a given nucleus, in presence of an interaction, will report on its local chemical environment, while, the signal intensity will depend on the number of nuclei resonating at a given frequency.

The chemical shift value, reported as parts per millions (or ppm), is a fundamental parameter in protein NMR. It defines the "NMR sensitivity", as it gives separately detectable signals for the hundreds of nuclei that can, therefore, be distinguished and assigned. The high NMR sensitivity of the chemical shift to structure and environment is very much evident in proteins. Chemical shift dispersion arises because different residues experience different microenvironments.

1.4.3 **Translational diffusion**

NMR spectroscopy is an optimal technique for studying protein-ligand interactions because a single analysis can give a big amount of structural information without destroying the sample. Many solution-state NMR techniques have been developed to study protein-ligand interactions, based, often, rely on monitoring changes in protein chemical shift and require labeled proteins [159].

An alternative approach for studying protein-ligand interaction are diffusion NMR experiment. This kind of experiment can be used to resolve different compounds spectroscopically in a mixture based on their differing diffusion coefficients, depending on the size and shape of the molecules. Moreover, it may be used to determine the size of molecules and aggregates, determining the degree of polymerization, size of a solvation shell or other microscopic structure. Typically, diffusion experiments refer to translational diffusion, which is the random translational (or Brownian) motion of molecules, driven by internal thermal energy. It is the basic mechanism by which molecules are distributed in space and it plays a central role in any chemical reaction since the reacting species have to collide before the reaction can occur. These NMR measurement represents an optimal approach to perform a qualitative and quantitative analysis of the samples [159]. It is an extremely useful method because it is very rapid, simple and selective, allowing to analyze simultaneously many different binding partners.

In the field of IDPs, diffusion measurement can be used to obtain information about the overall size of a complex in terms of hydrodynamic radii (R_h). Especially is useful in order to value the compactness among the free and bound states. Moreover, it can also be used to determine the K_D by measuring diffusion constants at different ligand concentrations [160].

In order to measure diffusion on free and bound states of the IDP, isotope labeling is combined with the use of filtered pulse schemes to avoid signals from the unlabeled binding partner [161]. The diffusion coefficient is inversely proportional to the hydrodynamic radii (R_h). Thus, binding partners (which assume the diffusion properties of the protein) can easily be distinguished from free-molecules by significant differences in diffusion coefficients [159], allowing to resolve otherwise intractable spectra of a mixture.

The diffusion NMR technique is achieved by combining radio-frequency pulses as used in routine NMR spectroscopy with magnetic field gradients that encode spatial information.

More simply, in this kind of experiment, the magnetization is parallel to the external field. Then the magnetization is excited with a 90° radiofrequency pulse then dispersed using a magnetic field gradient pulse. After a period of Δ/2, a 180° radiofrequency pulse inverts the dispersed magnetization such that after a period of Δ the magnetization is negative compared to the initial one (Figure 17).

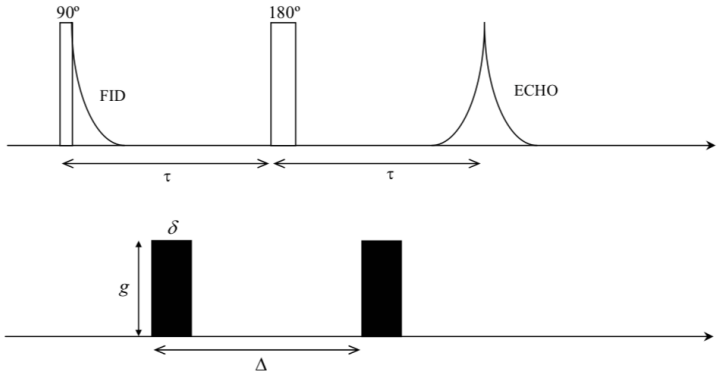

Figure 17: The main NMR sequences used to measure translational diffusion.

At this point, a second gradient pulse is applied to refocus the signal.

Diffusion causes some of the nuclei to move away from where their signals can be refocused, thereby reducing the intensity of the resulting signal. The pulse sequence is repeated, many times incrementing the gradient strength and keeping the delays constant.

The typical results of diffusion experiment are a plot of intensity against gradient strength (Figure 18).

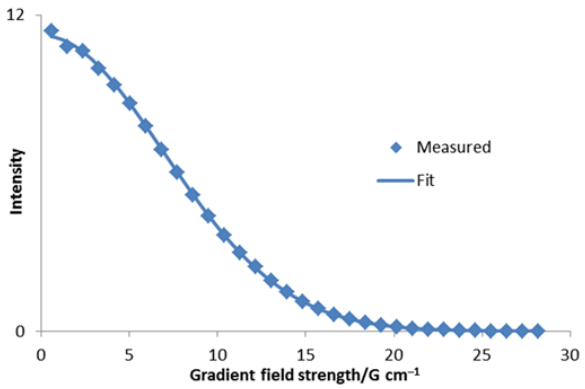

Figure 18: Gaussian fit to diffusion peak intensity using a non-linear fit.

Signal amplitudes are then extracted, and the translational diffusion coefficients (D) obtained by fitting the signal decay to the Stejskal–Tanner equation (Eq. 1):

$$I = I_0 \, e^{-g^2\gamma^2\delta^2\left(\Delta-\frac{\delta}{3}\right)D} \qquad (1)$$

Where g is the gradient strength, γ is the gyromagnetic ratio ($4257 s^{-1} G^{-1}$ for proton), δ and Δ are delays. Then, the D can be extracted using a non-linear curve fit to the resulting Gaussian decay (Figure 18).

Under conditions of fast exchange, the coefficient D measured on a protein sample in the presence of interacting partners, such as ligands, lipids, and NPs, is expected to decrease, due to the increased size of the complex/aggregate, according to the Stokes-Einstein law:

$$D = \frac{kT}{6\pi\eta R_h}$$

1.4.4 Dark-state exchange saturation transfer (DEST)

The ability to characterize the dynamics and the structure of increasingly large biological macromolecules in solution using recent NMR methods has expanded the understanding of biomolecular function at the atomic level [162]. Although several methods exist for high-resolution structural and dynamic characterization of proteins, none of traditional solution NMR techniques is able to observe, with atomic resolution, the dynamic equilibrium between an observable form and very-high-molecular-weight complexes. Some of these high-molecular complexes can be formed upon interaction with membranes, multiple copies of the same molecule,

or with nanoparticles. More specifically, the interaction of protein-NPs (P-NPs) can form particular large supramolecular adducts, whose understanding may provide useful information about what influences NP-clearance, their biodistribution, and their toxicity.

These adducts are characterized by slow molecular tumbling which causes very fast transverse spin relaxation (R_2). Traditional NMR experiments based on R_2 measurement are typically used to characterize the molecular dynamics. Especially ^{15}N-R_2 is used to measure the ^{15}N relaxation, directly probing the ^{15}N-^{1}H bond vectors of amide groups, because they are directly related to backbone internal motion and the over-all molecular tumbling. Relaxation is a phenomenon that happens, every time when the equilibrium of the system is regained and arises from the modulation of the effective local magnetic fields. Therefore, this phenomenon is susceptible to time-dependent modulation by protein motion, thus providing a direct relationship between internal dynamics and relaxation [163].

Unfortunately, when a small molecule binds to a high (≥1 MDa) molecular weight entity, this reduced the rate of molecular dynamics. Consequently, this leads to a marked increase in the R_2, thus precluding the observation by standard solution NMR techniques.

In recent years a novel solution NMR method has been developed, known as *Dark-State Exchange Saturation Transfer* (DEST) that allows obtaining interaction kinetics and residue-by-residue dynamic information in the "NMR-invisible" (dark) bound state [162,164]. However, with DEST is possible to observe the large difference in R_2 between the free and bound state.

DEST experiments are essentially based on the transfer of the ^{15}N-magnetization of the observable species by chemical exchange to the corresponding invisible state, partly perturbed, and therefore saturated. Subsequently, saturation is transferred back upon dissociation from the high-molecular-weight species [145,164]. In other words, it is based on a two-dimensional transfer-of-saturation NMR experiment in which is possible to exploit the exchange process between NMR invisible (“dark state”) and easily observed free unbounded state [162].

DEST allows an efficient partial saturation of ^{15}N longitudinal magnetization of the bound form by a weak radio-frequency field, even at large offsets where the free-molecules magnetization is completely unaffected [162].

DEST, unlike others NMR saturation methods, is a quantitative technique because it uses heteronuclear (i.e.^{15}N) saturation pulses [162,165]. Above all, this technique avoids possible problems with rapid dipolar-coupled magnetization transfers, that are observed for 1H saturation examples, even in the case of sparse protonation [162,166].

HSQC experiment in combination with DEST allows to obtain a single-residue resolution dynamic information on the NP-bound protein (the NMR-invisible state) in the form of ^{15}N- R_2 values [162].

2 Aim of the thesis project and brief summary of the research activities

The main focus of this Ph.D. thesis is the investigation of the molecular properties of protein Tau and their perturbations induced by post-translational modification and by the interaction with fatty acids and nanoparticles.

As part of this Ph.D. thesis, we investigate at a molecular level, the key role of ubiquitination of Tau and its effect on the propensity of Tau on its aggregation pathway to fibrils. We focused on the four-repeat domain of the MBD of Tau (Tau4RD), for which an accelerated aggregation into bona fide fibrillar structures was reported [167]. Taking the advantage ubiquitination process based *in vivo* we aim to ubiquitinate Tau by an *in vitro* reaction. The reaction was conducted exploiting the cascade of enzymes E1, E2N (human analogue of UbcH5B), and CHIP. The ubiquitinated products were characterized by mass spectroscopy and SDS-PAGE. Then the impact of this chemical modification on the propensity of Tau to aggregate into fibrils were monitored by aggregation assays based on changes in Thioflavin-T fluorescence during incubation with the aggregation inducer heparin. Finally, the morphology of the aggregates was inspected using AFM.

As a second goal of our research, we aimed to investigate the binding of Tau4RD to polyunsaturated fatty acids. Particularly, we are interested in identifying the polypeptide regions involved in the interactions and detecting conformational transitions experienced by Tau in the presence of lipid molecules. Interaction between these molecules was investigated by aggregation assays based on Thioflavin-T fluorescence. The acquisition of secondary structure elements was monitored by the use of circular dichroism measurements. The aggregated products were characterized by gradient SDS-PAGE to better identify the formation of high molecular weight species. NMR spectroscopy was used for the observation of lipid-induced perturbations at the single-residue level. Finally, AFM was used to characterize the morphology of the coaggregates.

As a third goal, in this Ph.D. project, we aimed to understand how amyloidogenic proteins, Tau (Tau4RD) and α-synuclein, interact with nanoparticles (NPs). Indeed, NP show promise as new-concept aggregation modulators, capable to redirect aberrant protein self-assembly. For our experiments we used ultrasmall gold-NPs functionalized with lipoic acid (Figure 19).

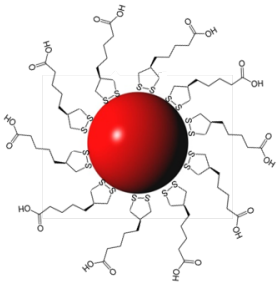

Lipoic Gold NPs

Figure 19: Schematic representation of Lipoic Gold Nanoparticles

Lipoic capped gold-NPs are uniform spherical gold-NPs with a high monodisperse size distribution. These nanoparticles bear a self-assembled monolayer of thioctic acid carrying a carboxylate end group, constituting a platform for many applications such as target-specific drug delivery, sensors, imaging probes for darkfield microscopy, cancer photothermal therapy and optoelectronic.

Solution NMR experiments have been increasingly used to describe protein-nanoparticle interactions at the individual residue level. Here, we wish to gather information about the conformations of the model proteins at NPs surfaces and to describe the relationship between particles features and conformational preference. Our studies challenge the current limits of the technique to obtain direct measurements on particle-protein or protein-protein assemblies.

3 Materials and Methods

3.1 Reagents

All reagent used in this PhD thesis were purchased from Sigma Aldrich except where indicated.

3.2 Material for protein expression

3.2.1 Plasmids and *Escherichia coli* strains for recombinant protein expression

Tau4RD

E. coli codon-optimized human Tau cDNA gene was purchased from Eurofins Genomics. Tau4RD (spanning residues Q244-E372 plus initial Met) (Figure 20) was cloned into a pET22b(+) vector via NdeI-BamHI sites with a stop codon to avoid insertion of a C-terminal histidine-tag.

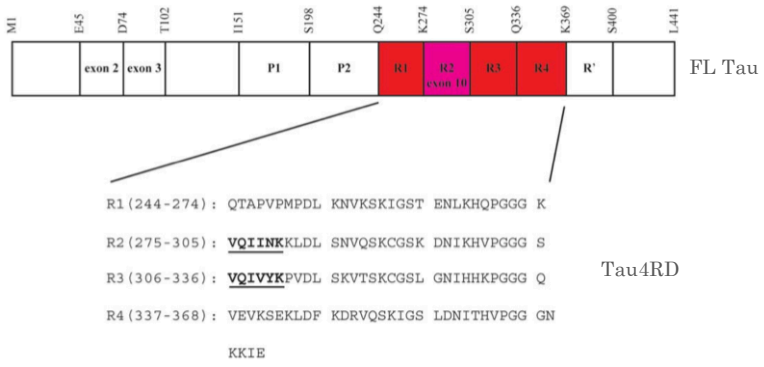

Figure 20: Schematic representation of the primary sequence of Tau protein full length, and the amino acid sequence of the Tau4RD construct used in all of these studies. (Adapted by Barrè et al, 2013) [168].

The plasmid pET22b(+) (purchased by Novagen) is a 5493bp expression vector with T7 promoter and terminator flanking MCS that accepts insert of interest. It is characterized by a pelB leader sequence for subcellular targeting and tag csd, amp resistance and many restrictions enzyme cloning. The Figure 21 shows the vector map of pET22 and the elements characterizing this vector.

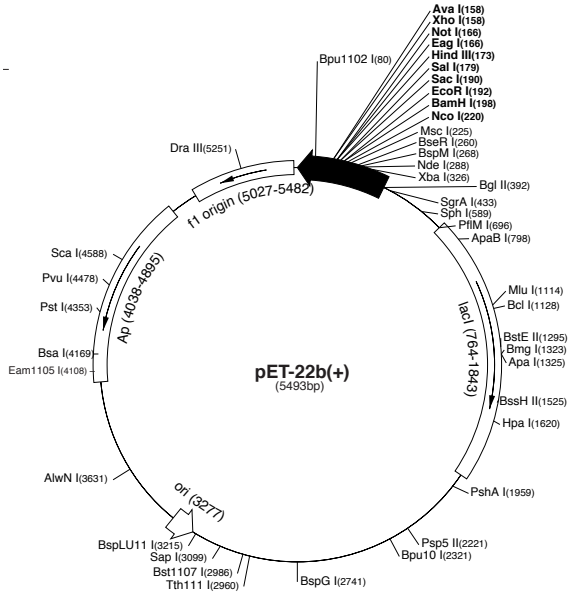

Figure 21: pET-22b(+) vector map.

BL21(DE3) host strain was transformed with the plasmid containing the Tau4RD sequence. This host strain is suitable for transformation and high-level protein expression using a T7 RNA polymerase-IPTG induction system.
In parallel, N-terminal histidine$_6$-tag Tau4RD gene was cloned into a pET15b vector via NdeI-BamHI sites and which was then inserted in BL21(DE).

Ubiquitin Machinery

The ubiquitin protein and all the enzymes necessary for the in vitro protein ubiquitination were expressed and purified using:

- N-terminal histidine$_6$-tagged **ubiquitin** gene cloned into a pET15 vector and expressed in *E. coli* Rosetta (DE3) cells;
- N-terminal histidine$_6$-tagged **Human E1** (UBE1) gene cloned into a pET21(+) and expressed in *E. coli* Rosetta (DE3) cells;
- N-terminal GST- tag **Ubc13** (human E2N, UniProtKBP61088) and E3 ubiquitin-protein ligase **CHIP** (UniProtKB Q9UNE7) gene cloned into a pGEX4T1 vector and expressed in *E. coli* Rosetta (DE3) cells;

3.2.2 Heat shock transformation

The following protocol has been used to transform BL21/Rosetta competent cells through heat shock:

- 50 µl of competent cells stored at -80 °C were placed in ice for thawing
- 30-50 ng of DNA were added, and the culture was incubated in ice for 30 minutes
- the heat shock was carried out by placing the culture in a water bath at 42 °C for 45 seconds without shaking
- the culture was immediately placed in ice for 2 minutes
- 500 µl of LB medium without antibiotic was added directly to the cells and then the culture was incubated at 37 °C for 1 hour with shaking (200-250 rpm)
- the cells were plated on selective LB agar and incubated overnight at 37 °C

3.3 Protein sample preparation

3.3.1 Glycerol stock

After transformation, bacterial colonies with plasmid coding for protein of interest were grown in 5 ml LB medium with antibiotic at 37 °C for 6 hours. A cell solution with a final concentration of 30% glycerol was prepared, vortexed and cooled in liquid nitrogen. Glycerol stocks were stored at -80 °C.

3.3.2 Culture growing media

The following media have been used for BL21/Rosetta growth. Sterilization was achieved in autoclave and media for bacterial growth were prepared as follows if not otherwise specified. Selective media were prepared adding chloramphenicol, ampicillin or kanamycin.

Luria-Bertani (LB) medium

For 1 L final volume:

Compound	Quantity
Tryptone	*10 g*
Yeast Extract	*5 g*
NaCl	*10 g*

pH was adjusted to 7.0 after sterilization, antibiotic was added

M9 medium

The **M9 medium** is used to achieve uniform ^{15}N isotope incorporation in proteins. This medium is prepared as follows:

For 1 L final volume:

Compound	Quantity
M9 salts	200 ml
$MgSO_4$	2 mM
$ZnSO_4$	0.1 mM
$CaCl_2$	0.01 mM
Glucose	4%
Tiamine	1 ng/ml
NH_4Cl*	**1g**
Sterile Water	**up to volume**

M9 salts (5X)

For 1L final volume:

Compound	Quantity
Na_2HPO_4	33,9 g
KH_2PO_4	15 g
NaCl	2.5 g

3.3.3 **Protein expression and cell lysis**

The expression of unlabeled proteins was achieved by adding 10 ml of the starter culture to 1 liter of LB medium, then incubated in a shaker at 37 °C till an OD600 value of 0.6/0.7 was reached. Protein expression was induced adding Isopropyl-β-D-1-thiogalactopyranoside (IPTG) at a final concentration of 0.5 mM and leaving the culture in the shaker at the best temperature and time (Table below) found in the preliminary protein expression evaluation.

	Time	**Temperature**
Tau4RD	5h	37 °C
His-UB	Over night	20 °C
His-E1	5h	37 °C
GST-E2N	Over night	20 °C
GST-CHIP	Over night	20 °C

After a centrifugation step at 10000g for 15 minutes, the pellet was resuspended in 2.5 ml/g of lysis buffer (Table A) and sonicated at the maximum sonication power for 7 cycles of 1 minute (except for the enzyme where we add more lysozyme), alternating the sample sonication time to an equal period on ice. The lysate was then centrifuged for 20 minutes at 10000 g at 4 °C and the supernatant solution was collected. The supernatant, containing the soluble protein fraction, was then processed for the purification._M9 medium was used for expression of ^{15}N labelled proteins and the same purification protocol was performed.

Lysis buffer Tau4RD	*Lysis buffer His-Ub, His E1*	*Lysis buffer GST-Chip, GST-E2N*
20 mM TrisHCl, pH 7.6	20 mM TrisHCl, pH 7.6	20 mM TrisHCl, pH 7.6
50 mM NaCl	1X Protease Inhibitor	150 mM NaCl
1X Protease Inhibitor	Triton X-100 0.05% (v/v)	1X Protease Inhibitor
PMSF 100mM	PMSF 100mM	Triton X-100 0.05% (v/v)
Lysozyme 0.4 mg/ml	Lysozyme 0.4 mg/ml	PMSF 100mM
Dnase 1 (20 µg/ml)	Dnase 1 (20 µg/ml)	Lysozyme 0.4 mg/ml
$MgCl_2$ 10 mM	$MgCl_2$ 10 mM	Dnase 1 (20 µg/ml)
EDTA 0.5 mM		$MgCl_2$ 10 mM

Table A: Recipes of Lysis Buffer

3.4 Protein and enzyme purification

- Tau4RD

The lysate was boiled at 100 °C for 10 min and then was centrifuged for 20 min at 10000 g at 4 °C. The soluble part was filtered and loaded onto a SP column, preequilibrated with Tris 20 mM, NaCl 25 mM buffer. The elution was made with a gradient of NaCl from 50 mM to 1 M in Tris 20mM buffer.

- His-Ubiquitin and His-E1

The lysate was centrifuged, and the soluble part extract was filtered and loaded onto Ni^{2+} charged-chelating Sepharose (GE Healthcare), preequilibrated with Tris 20 mM, NaCl 50 mM buffer. The elution was made with a gradient of imidazole from 50 to 500 mM in Tris 20 mM, NaCl 0.5 M buffer.

- GST-CHIP and GST-E2N

The lysate was centrifuged, and the soluble part extract was filtered and loaded onto Glutathione Sepharose beads (Molecular Probes, 10 ml bead suspension per liter culture) preequilibrated with PBS buffer, pH 7.4. Unbound proteins were washed out with 6-8 bed volumes of PBS buffer, and the fusion protein was eluted with 50 mM Tris pH 8, 10 mM glutathione.

Prior to storage, all protein samples were than concentrated using centrifugal filter units (Millipore) at the proper concentration (~ 0.5 mM). Then they were frozen with liquid nitrogen and stored at - 20 °C.
All samples for NMR measurements were buffer exchanged into a buffer suitable for NMR Experiments, in our case we use Potassium Phosphate 10 mM pH 6.8.

3.4.1 **Chromatography resins and columns**

Ion exchange chromatography resin: SP Sepharose FastFlow (GE Healthcare) with cationic exchanger has been used.
10 ml resin was then poured into a XK 16/20 (GE Healthcare) column and extensively washed 20 mM TrisHCl, 50 mM NaCl, pH 7.6 as running buffer. The cleared cellular lysate was loaded directly into the column and washed with 2 column volumes of running buffer and eluted with a NaCl gradient (0-1 M). Fractions of 2 ml were collected and analyzed by SDS-PAGE. After use the resin was regenerated according to the manufacturer's instructions.

Nickel affinity chromatography: Chelating Sepharose, when charged with Ni^{2+} ions, selectively binds to proteins if complex forming amino acid residues, in particular histidine, are exposed on the protein surface. The matrix Chelating Sepharose Fast Flow (Amersham Biosciences), which is able to bind metal cations around neutral pH values, was packed into a XK 16/20 column (GE Healthcare). First the resin was charged with Ni^{2+} using 1-2 volumes of a solution of 0.25 M $NiSO_4$, then the equilibration was achieved with 5 volumes of 20 mM Tris-HCl pH 7.6, 0.5 M NaCl, 10 mM imidazole (binding buffer). The protein elution was performed applying an imidazole gradient from 10 mM to 0.5 M, exploiting the ability of this compound to compete with the His6-tag for Ni^{2+} binding. Fractions of 2 ml were collected and analyzed by SDS-PAGE.

Glutathione Sepharose chromatography resin: 10 mL of Glutathione Sepharose resin (GE Healthcare) were packed in a XK 16/20 (GE Healthcare) column. The resin was first washed with 10-20 volumes of mQ water and successively with 20 mM Tris-HCl pH 7.6. The protein elution was performed adding 10 mM Glutathione in the buffer, at pH 8. Fractions of 2 ml were collected and analyzed by SDS-PAGE.

3.4.2 **SDS-PAGE**

Protein purity was evaluated using Sodium Dodecyl Sulphate Polyacrylamide Gel Electrophoresis (SDS-PAGE). Every protein sample (10 µl) was heated at 95 °C for 5 minutes after the addition of 5 µl of reducing loading buffer. Samples were loaded into a separate well of a discontinuous 10% or 17% polyacrylamide

gel together with 5 µL of molecular weight marker (GE Healthcare) loaded in a separate well internal referencing and to identify the proteins of interest after separation. Gels were run at 180 V for approximately one hour until the bromophenol blue exits the running gel. After running the gels were immersed in the staining solution for 20 minutes and de-stained with bidistilled hot water.

Reducing loading buffer

Compound	Quantity
Tris-HCl pH 6.8	*50 mM*
DTT	*100 mM*
SDS	*2%*
glycerol	*10%*
Bromophenol blue	*0.10%*

Polyacrylamide gel

Stacking gel solution

For a final 2 ml

Compound	Quantity
Acrylamide mix (30% stock solution)	*5%*
Tris-HCl pH 6.8 (1M stock solution)	*125 mM*
SDS (10% stock solution)	*0.10%*
Ammonium persulfate (10% stock solution)	*0.10%*
TEMED	*0.10%*
Water	*up to volume*

Running gel solution

For a final 5 ml at 10 or 17% of acrylamide

	Quantity	
Compound	**10%**	**17%**
Acrylamide mix (30% stock solution)	*10%*	*17%*
Tris-HCl pH 8.8 (1.5M stock solution)	0.39 mM	0.39 mM
SDS (10% stock solution)	0.10%	0.10%
Ammonium persulfate (10% stock solution)	0.10%	0.10%
TEMED	0.04%	0.04%
Water	*up to volume*	*up to volume*

Running solution

Compound	Quantity
Tris-HCl pH 8.3	*25 mM*
glycine	*192 mM*
SDS	*0.10%*

Staining solution

For a final 1L:

Compound	Quantity
Ethanol	*50%*
Acetic Acid	20%
Coomassie Brilliant Blue (R350)	3 g/L

Estimation of protein concentration

The absorbance at a wavelength of 280 nm was detected using Nanodrop spectrometer. Protein concentration (*c*) was calculated from the Beer-Lambert equation:

$$Abs = \varepsilon \times l \times c$$

A theoretical extinction coefficient at a wavelength of 280 nm measured in water (ε 280 nm) was estimated for each construct using the ProtParam Tool from the Expasy Tools server (http://www.expasy.ch/tools/protparam.html).

3.5 Tau and Ubiquitin Interaction

3.5.1 In vitro Ubiquitination Assay

In vitro ubiquitination reactions were carried out in 50 mM Tris-HCl buffer, pH 8, with 5 mM ATP, 5 mM $MgCl_2$ and 3 mM tris(2-carboxyethyl)phosphine hydrochloride (TCEP). All enzymes and substrate were used as follow:

His-E1	*1 µM*
GST-E2N	*10 µM*
GST-CHIP	*10 µM*
His-Ubiquitin	*70 µM*
Tau4RD	*35 µM*

3.5.2 Purification

To purify Tau4RD ubiquitinated by CHIP, a large volume of ubiquitination reaction was prepared (4 mL), using Tau4RD and His-Ubiquitin at a concentration of 110 and 140 µM, respectively. The reaction was incubated at 37 °C for 5 hours. Thus, the reaction was stopped and heated at 70 °C for ~ 15 min, in order to remove all enzymes from the solution. After centrifugation, the unreacted ubiquitin was removed, performing a SP-ion exchange chromatography. Finally, ubiquitinated Tau4RD was separated from unreacted Tau4RD by IMAC, taking advantage of the His_6-tag on Ubiquitin.

3.5.3 **Thioflavin-T Assay**

The kinetic of aggregation was monitored with Thioflavin-T assay. The 0.01 mM of samples were diluted in the aggregation buffer: in 20 mM NaPi, 50 mM NaCl, pH 7.4, with 5 mM DTT, 0.02% NaN_3 and protease inhibitors with EDTA, with the addition of 0.01 mM of heparin. Samples for ubiquitin, Tau4RD, Tau4RD in the presence of ubiquitin at 1:1 molar ratio, and Tau4RD ubiquitinated by CHIP were incubated in presence of 0.01 mM Thioflavin-T in a 96-well dark plates. The assay was carried out in a plate reader (FLUOstar Omega; BMG LABTECH) at 30 °C for 72 hours with cycles of 60 seconds of shaking (900 rpm, double-orbital) and 14 minutes of rest throughout the incubation. Thioflavin-T (ThT) fluorescence measurements (mean [slit width (SD)] excitation, 450 [10] nm; mean emission, 480 [10] nm [bottom read (reading the fluorescence signal from the bottom to the top of the well)]) were taken every 15 minutes. Proteins were filtered through a 100 kDa cut-off filter (Sartorius) before starting the aggregation to remove pre-existing large oligomers and fibrils. Error bars of ThT curves correspond to standard deviations of at least three independent experiments.

3.5.4 **Atomic Force Microscopy Measurements**

Solutions of 0.05 mM Tau4RD diluted in the aggregation buffer (as describe above) were incubated at 37 °C without agitation for 48 hours, using heparin at 1:1 molar ratio as aggregation initiator. 5 mM DTT was included only for Tau4RD and Tau4RD ubiquitinated by CHIP. After incubation, the buffer of protein samples was exchanged to mQ H_2O by filtration with a 100 kDa cut-off filter (Sartorius). Samples were then diluted in water to optimal concentration for AFM measurement (5 – 25 μM). About 20 μL of samples were deposited on freshly cleaved mica and allowed to dry in air. AFM images were acquired with a NT-MDT Solver Pro microscope, (Zelenograd, Moscow, RU), with single crystal silicon-antimony doped probe and a gold coated base (NSG-01 from NT-MDT) used in semi-contact mode. The hysteresis of the instrument was adjusted by a software correction of the data using calibration grid (TGQ1 from NT-MDT) before analysis. Images were processed and analyzed with the Gwyddion software [169].

3.6 Tau and Lipids Interaction

3.6.1 Lipids preparation

Sodium Oleate (*O7501*): a stock solution of ~ 48 mM in mQ H_2O was prepared, heated at 25 °C for ~ 10 minute and spinned. Then the solution was filtered with a 0.02 nm diameter filter (Anotop 10 plus Whatman).
For the experiments the sample was diluted at the final concentrations of 2 or 3 mM in H_2O and stored at RT.

Sodium Arachidonate (*SML1395*): in order to prevent the fatty acid oxidation, all the stock solutions were prepared under nitrogen flux in a glovebox. The powder was dissolved in H_2O to a final concentration of 15 mM in Wheaton glass serum bottle (Z113948) and then stored at -20 °C.

3.6.2 Dynamic Light Scattering measurements (DLS)

The presence of micelles was checked using dynamic light scattering (DLS). DLS measurements were performed with a Zetasizer Nano ZS instrument (Malvern Instruments, USA) operating at $\lambda = 633$ nm with backscatter detection at 173°. The samples were allowed to equilibrate for 5 min at the measurement temperature of 25 °C before starting acquisition. Measurement were repeated three time in order to check their repeatability. Acquisition were performed with serial dilution (1:2) in phosphate buffer from 2 mM to 0.01 mM. Autocorrelation function (ACF) was fitted in order to confirm the presence of large aggregates (micelles).

3.6.3 Tau aggregate assembly

Aggregation was performed in 10 mM Potassium Phosphate buffer at pH 6.8 in presence of DTT (2 mM or 0.5 mM for CD measurements) and protease inhibitor. Aggregation was induced by incubation soluble of Tau4RD at the concentration of 100 µM in volume of 0.5 ml at 37 °C with magnetic stirring in Wheaton glass serum bottle, respectively with heparin (molar ration of Tau to heparin 4:1[170]), with sodium oleate (molar ration of Tau to sodium oleate 1:3), with sodium arachidonate (1:3) [113,171]. All samples were incubated for ~ 24h – 48h. The formation of aggregates was monitored by SDS-PAGE.

3.6.4 **Thioflavin-T assay**

The kinetic of aggregation was monitored with Thioflavin-T assay. The samples were prepared in the same condition describe above and were incubated in the presence of 20 μM Thioflavin-T in a 96-well dark plate. The measurements were performed in a plate reader (TECAN Infinite M200 Pro) at 37 °C for 72 hours with cycles of 60 seconds of shaking (250 rpm, orbital) and 14 minutes of rest throughout the incubation. Thioflavin-T (ThT) fluorescence measurements (mean [SD] excitation, 450 nm; mean emission, 480 nm [bottom read]) were taken every 15 minutes. Proteins were filtered through a 100 kDa cut-off filter (Sartorius) before starting the aggregation to remove pre-existing large oligomers and fibrils. Error bars of ThT curves correspond to standard deviations of at least four independent experiments.

3.6.5 **Circular dichroism (CD) spectroscopy**

CD spectroscopy studies were performed with a Jasco 1500 spectropolarimeter equipped with a Peltier type thermostated cell holder. Far-UV spectra (190–260 nm) were recorded at 25 °C at a scan rate of 50 nm min^{-1}, a bandwidth of 1 nm and an integration time of 2 s. Five spectra accumulations were averaged for each sample, and the spectrum of the buffer was considered as a blank and subtracted. The protein concentration was 6 μM in 0.1 cm cuvettes.

3.6.6 **Gradient SDS-PAGE**

Gradient SDS-PAGE (10-17%) was employed on different samples under non-reducing conditions to analyze the aggregates states according to the protocol defined by Miller co-workers[172].

5 ml of the lower concentration gel buffer (10%) are drawn into a 10 ml serological pipet. Using the same pipet, the higher acrylamide concentration gel buffer (17%) is drawn up to 10 ml final volume (Figure 22A). Then one or two air bubbles are flowed up into the pipet to mix the interface, and to create a linear gradient (Figure 22B).

When this gel solution is injected into the casting plate sandwich, the higher acrylamide concentration is deposited on the bottom followed by the lower

concentration on top. This creates a “stacked” concentration gradient with very little mixing of the phases at the interface.

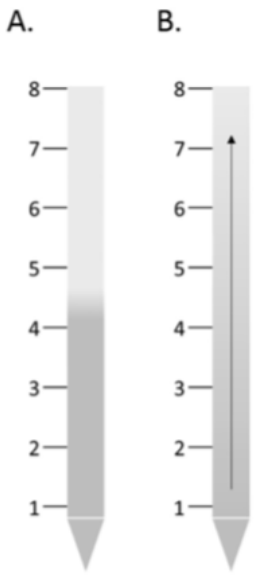

Figure 22: Example of sample acrylamide concentration differentials within the 10 ml pipet used to pour gel. A) The buffer with lower acrylamide concentration (10%) (light gray) is aspirated into pipet first followed by higher concentration (17%) (dark gray). B) The linear gradient is then created when a bubble is allowed to migrate up the pipet which will cause mixing at the phase inter-face. When the solution is ejected into the gel sandwich, the high concentration acrylamide is on the bottom.

3.6.7 Atomic Force Microscopy Measurements

After aggregation, the samples were diluted in mQ H_2O for AFM measurements. 20 µL of Tau4RD co-aggregates (5-10 µM) were deposited on freshly cleaved mica and allowed to dry in air.
AFM images were acquired and analyzed as describe in previous section.

3.7 Tau and Nanoparticles Interaction

3.7.1 Nanoparticles Preparation

Ultrasmall Lipoic Gold Nanoparticles (Lip@AuNPs) have been purchased by NanoImmunotech. The solution, stored in water at a concentration of 0.6 µM was concentrated by several centrifugation steps (5000 rpm, 20 min, 10 repetition) in order to have an enough concentration allowing their utilizations, especially for NMR measurement. Concentrations after centrifugation have been measured by

UV-vis spectroscopy using a method developed by Haiss et al. (Haiss et al., 2007). Depending of the stock solution, the concentration varies from 9 to 12 µM. In order to be in the Beer-Lambert law condition, each stock was diluted by a dilution factor from 20 to 40. A spectral width from 300 to 800 nm was used in each case. The absorbance at A_{450} nm measured using a Nanodrop spectrometer was divided by the extinction coefficient (ε_{450}nm) determined from the tables of the publication of *Haiss at al.*[14].

3.8 Protein NMR Analysis

3.8.1 NMR Samples Preparation

All protein samples for NMR measurements were centrifuged at 10000g for 10 minutes to remove any insoluble particles and the protein concentration was checked by measuring absorbance at 280 nm. The samples were prepared in 10 mM potassium phosphate aqueous buffer at pH 6.8, also containing protease inhibitors and 8% D_2O.

3.8.2 1D and HSQC

1D and 2D NMR experiments were acquired at 310 K and 298 K, respectively, on a Bruker Avance III spectrometer, operating at ^{1}H Larmor frequency of 600.13MHz, equipped with a triple resonance TCI cryogenic probe.

One-dimensional ^{1}H-NMR experiments were acquired with a standard pulse sequence incorporating the excitation sculpting water suppression scheme. A total of 128 transients were acquired over a spectral width of 12019 Hz, using a recycle delay of 2s. The spectra were processed applying an exponential window function prior to the Fourier transformation.

Typical sensitivity enhanced ^{1}H-^{15}N heteronuclear single quantum coherence (HSQC) were conducted by acquiring 256 complex points in the T_1 dimension, 1024 in the T_2 dimension. A total number of 4-8 transients were acquired for each spectrum with an interscan delay of 1.2s. Standard sequence schemes with pulsed field gradients were used to achieve suppression of the solvent signal and

cancellation of spectral artifacts. Data were processed using the Bruker software TOPSPIN 3.2 (Bruker, Karlsruhe) and analyzed with the program NMRFAM-SPARKY by Lee W, (https://nmrfam.wisc.edu/nmrfam-sparky-distribution/) [173].

3.8.3 **Diffusion**

NMR experiments were acquired at 310 K on a Bruker Avance III spectrometer, operating at ^{1}H Larmor frequency of 600.13MHz, equipped with a triple resonance TCI cryogenic probe.

Pulsed field gradient NMR diffusion experiments on Tau4RD were performed as using the standard Bruker *ledbpgp2s1dwsse* pulse sequence which implements the stimulated echo and longitudinal eddy current delay schemes, as well as bipolar gradient pulses for diffusion. Water signal suppression was achieved by pre-saturation and Watergate. The gradient was set to values in the range of 5–95% of the maximum gradient strength. The experiment was conducted with diffusion and gradient times of 200 ms and 4 ms. Data were analyzed by integrating resonances of the amide envelope region.

3.8.4 **R2 measurements**

NMR experiments were acquired at 283 K on a Bruker SB Avance III spectrometer, operating at ^{1}H Larmor frequency of 1000.13 MHz, equipped with a triple resonance TCI cryogenic probe.

Nitrogen-15 transverse relaxation (^{15}N-R_2) experiments were carried out in gradient-selected sensitivity enhanced mode and in interleaved fashion acquiring 2048 (^{1}H) × 200 (^{15}N) complex data points for each relaxation delay over spectral widths of 12 (^{1}H) and 23 (^{15}N) ppm. Optimal water signal suppression was obtained with optimized flip-back pulses. The recycle delay was set to 3 s and T2 relaxation delays were 0.016, 0.033, 0.050, 0.067, 0.084, 0.101, 0.135, 0.169, 0.203, 0.271, 0.033, 0.203 s (23.5 T). Relaxation times were determined by fitting peak volumes to a two-parameter single exponential function with the software NMRFAM-SPARKY by Lee W. (https://nmrfam.wisc.edu/nmrfam-sparky-distribution) [173].

3.8.5 **DEST measurement**

NMR experiments were acquired at 283 K on a Bruker SB Avance III spectrometer, operating at ^{1}H Larmor frequency of 1000.13 MHz, equipped with a triple resonance TCI cryogenic probe.

2D ^{15}N-DEST experiments were performed using the pulse sequence available online from Dr. M. Clore (http://spin.niddk.nih.gov/clore/). The sequence was slightly modified to obtain an interleaved pseudo-3D version directly processable with spectrometer acquisition software (Bruker Topspin 3.2). ^{15}N continuous wave saturation was applied for 0.9 s with field strengths of 0 Hz (reference) and 350 Hz. Saturation was applied at 17 offsets distributed symmetrically around 0 Hz (35, 20, 10, 5, 4, 2, 1, 0.5, 0, -0.5, -1, -2, -4, -5, -10, -20, -35 kHz at 23.5 T). Acquisition times were 127 ms (^{1}H) and 23 ms (^{15}N) at 23.5 T. 16 transients were collected per free induction decay in the indirect dimension and an interscan delay of 1.3 s was used. A 2.1 ms (23.5 T) *IBURP2* pulse was applied to achieve amide proton decoupling. Water flip-back pulses were used for optimal water suppression. All of the spectra were processed with Topspin 3.2 (Bruker, Karlsruhe), while peak intensities were analyzed and quantified with the program NMRFAM-SPARKY by Lee W. (https://nmrfam.wisc.edu/nmrfam-sparky-distribution) [173].

DEST experiments were analyzed with DESTfit by Fawzi N.L. (http://spin.niddk.nih.gov/clore/Software/software.html) [162].

4 Results and Discussion

4.1 Semisynthetic and enzyme-mediated conjugate preparations illuminate the ubiquitination-dependent aggregation of protein Tau

Angew Chem Int. Ed. Engl. 2020 Feb 5. doi:10.1002/anie.201916756

Francesca Munari, [a] Carlo G. Barracchia, [a] Cinzia Franchin, [b].[c] Stefano Capaldi, [a] Alessandro Romeo,[d] Michael Assfalg, [a] Giorgio Arrigoni, [b].[c] and Mariapina D'onofrio*[a]

[a]. Department of Biotechnology, University of Verona , Strada Le Grazie 15, 37134 Verona (Italy) E-mail: mariapina.donofrio@univr.it
[b]. Department of Biomedical Sciences, University of Padova, Padova (Italy)
[c]. Proteomics Center, University of Padova and Azienda Ospedaliera di Padova, Padova (Italy)
[d]. Department of Computer Science, University of Verona, Strada Le Grazie 15, 37134 Verona (Italy)

In the brain of individuals with Alzheimer's disease, the regulatory protein ubiquitin is found conjugated to different lysine residues of protein Tau assembled into pathological paired helical filaments. To shed light on the hitherto unexplored ubiquitination-linked conformational transitions of Tau, the availability of in vitro ubiquitin conjugation methods is of primary importance. In our work, we focused on the four-repeat domain of Tau and assembled an enzymatic machinery formed by UBE1, Ubc13, and CHIP enzymes. The enzymatic reaction resulted in monoubiquitination at multiple sites, reminiscent of the ubiquitination pattern observed in vivo. We further exploited chemo-selective disulfide coupling reactions to construct three Tau regio-isomers with site-specific monoubiquitination. Protein aggregation experiments revealed that the multiple enzyme-derived products were unable to convert into amyloid fibrils, while the semisynthetic conjugates exhibited diverse capability to form filaments. This study contributes novel insight into the effects of a key post-translational modification on aberrant protein self-assembly.

Intracellular aggregates of the protein Tau, with the properties of amyloid fibrils, are the defining feature of a group of neurological disorders known as Tauopathies, which include Alzheimer's disease (AD) [1,2]. Tau pathology has been recognized as a target for the development of disease-modifying therapies, the success of which requires to acquire a deep knowledge on the multiple molecular factors that contribute to the formation of neurotoxic aggregates [3] . Tau is an intrinsically disordered protein, occurring in six distinct isoforms in adult brain and playing

a fundamental role in microtubule assembly and stabilization in neurons [4,5] . Under normal conditions, Tau function is regulated by extensive post- translational modifications (PTMs), primarily phosphorylation [6,7] . Both missense mutations and aberrant PTMs render Tau aggregation-prone, ultimately leading to accumulation of insoluble filaments [7–9] . Two hexapeptide motifs in the microtubule-binding domain (MBD) were proposed to be implicated in the nucleation of pathological Tau aggregates [10] and recent cryo-EM investigations of Tau paired helical filaments (PHFs), isolated from AD brain, identified the polypeptide region (residues 306-378 within the MBD) forming the core of the amyloid [11].

It is plausible that several distinct PTMs concur towards Tau dysfunction [9,12]. Besides being hyperphosphorylated, Tau of PHFs isolated from AD brains (AD-PHFs) was found conjugated to ubiquitin at multiple lysine residues within the MBD [13,14]. In particular, the protein was reported to be monoubiquitinated at Lys254, Lys257, Lys311 and Lys317 [13] and modified at Lys254, Lys311 and Lys353 with polyubiquitin chains [14]. It is noteworthy that monoubiquitination has been recently recognized as an esteemed proteasomal targeting signal in addition to the canonical Lys48-polyubiquitin signal [15], suggesting an additional strategy of the ubiquitin proteasome system (UPS) to clear Tau aggregates.

A thorough understanding of the determinants of PTM- associated conformational transitions of Tau necessitates approaches for protein modification in vitro to enable subsequent molecular-level characterization [16,17]. Indeed, the recent successful development of chemical methods for the site- specific modification of Tau allowed to obtain unprecedented insight into the role of phosphorylation, GlcNAcylation, acetylation, and carboxymethylation on the self-aggregation and binding behavior of Tau [18–21]. However, the study of ubiquitination has lagged behind in the ensemble of PTMs of Tau.

In our work, we focused on the four-repeat region (TauK18 or Tau4RD) of the MBD of Tau (Figure 1A) which contains all acceptor lysine residues found ubiquitinated in AD-PHFs [13,14]. For the preparation of ubiquitinated Tau4RD, we adopted two distinct approaches: i) enzyme-mediated conjugation employing CHIP, an E3 ligase able to ubiquitinate Tau in cells and found to ameliorate the toxic effects of various neurodegenerative disease-related proteins [22,23], ii)

disulphide-coupling chemistry [24-26] to produce to produce Tau regio-isomers with site-specific monoubiquitination in positions 254, 311, or 353, as three representatives of the ubiquitinated Tau species found in vivo. By use of mass spectrometry we identified the sites targeted by the enzymatic machinery, we further performed Thioflavin-T (ThT) fluorescence aggregation assays and inspected the morphology of Tau aggregates using atomic force microscopy (AFM).

In the first approach, we reconstituted enzymatic ubiquitination in vitro after selecting appropriate enzymes. We identified CHIP, an E3 ligase that was found to interact with and ubiquitinate Tau [22,27], and that plays a key role in UPS-mediated Tau degradation [27,28]. CHIP can act in combination with distinct E2-conjugating enzymes [29] and, according to previous structural studies, it interacts with Ubc13 but not with its assistant Uev1a [30]. Therefore, we assembled an enzymatic machinery formed by CHIP, the E1 enzyme UBE1, and human Ubc13, to promote the reaction between Tau4RD and ubiquitin (Scheme 1A). SDS-PAGE analysis of the reaction products revealed a new band corresponding to a molecular weight of ~25 kDa (Figure 1B and S1), compatible with monoubiquitinated-Tau4RD (hereafter ub-Tau4RD). Immunoblot analysis further confirmed the formation of this conjugate (Figure S2). These results demonstrate that CHIP can act in tandem with hUbc13, in the absence of Uev1a, to monoubiquitinate Tau in vitro.

To identify the ubiquitinated sites, we carried out mass spectrometry (MS) analysis of trypsin-digested monoubiquitinated Tau4RD, obtained after a five-hours conjugation reaction. The analysis (Table 1 and SupportingDataSheet1) revealed that ubiquitination occurred on nine out of the twenty lysine residues present in Tau4RD. The nine sites are distributed across the four repeats (Figure 1C), however with greater prevalence in R2. Interestingly, after an overnight reaction the number of distinct sites of modification increased to twelve (Figure S3, TableS1, SupportingDataSheet2), matching almost completely the ubiquitinated sites found in Tau samples isolated from mouse [6]. Notably, CHIP-mediated ubiquitination occurred, among others, at Lys311 and Lys353, which are two sites found ubiquitinated in human brain filaments [13,14].

To investigate the effect of enzymatic ubiquitination on Tau filaments assembly, the ubiquitinated protein was first purified from unconjugated components by

affinity chromatography exploiting a His6-tag placed at the ubiquitin N-terminus (Figure S1). Aggregation kinetics experiments were then performed, based on a ThT assay. Unmodified Tau4RD exhibited a rapid increase in filaments formation (Figure 1D): the fluorescence signal displayed a typical sigmoidal growth profile characterized by a lag phase of ~8 hours and a plateau phase starting at ~16 hours. In contrast, the fluorescence signal measured on the ub-Tau4RD sample displayed a non-sigmoidal growth profile with modest increase in intensity over the duration of the experiment. This marked difference appears to reflect a reduction in the rates of elongation and secondary nucleation which are two key molecular processes governing fibrillation [31]. Thus, the data suggest that CHIP-mediated ubiquitination of Tau4RD, which results in a set of monoubiquitinated products, strongly interferes with Tau fibril formation. To confirm that the observed inhibitory effect was indeed caused by the covalent modification of Tau4RD, we performed a control experiment with unconjugated Tau4RD and His6-ubiquitin. Interestingly, this protein mixture exhibited similar aggregation kinetics as unmodified Tau, excluding that the sole presence of ubiquitin could interfere with fibril formation.

The morphology of the aggregated samples was analyzed by AFM. Unmodified Tau4RD was found to form mature filaments, however only small aggregates of 10-40 nm in height and 150-350 nm in length were observed for ub-Tau4RD (Figure 1E). The latter species were not reactive with the A11 antibody (Figure 1F) which recognizes prefibrillar oligomers of a number of different proteins [32], including Tau4RD.

Together, these findings indicate that the unresolved mixture of monoubiquitinated Tau isomers had a strong inhibitory effect on the formation of prefibrillar and filamentous structures. Notably, several modified sites fall within the 272-330 region which constitutes the core of heparin-induced Tau filaments [33]. Thus, the attachment of a bulky macromolecule to those sites appears to cause steric hindrance, preventing the formation of an ordered cross-β/β-helix structure.

The lack of site-specificity of the CHIP-based ubiquitination reaction prevents us from understanding the role of each ubiquitinated site in the mechanism of Tau aggregation. To overcome this limitation, we sought to produce Tau proteins homogenously ubiquitinated at unique sites. In this second approach, we adopted an

effective semisynthetic method already successfully applied to obtain ubiquitin-modified substrates [24,26]. The conjugation between ubiquitin and Tau was based on a disulfide-forming reaction between a cysteine residue placed at a desired position on Tau and a ubiquitin molecule modified with a C-terminal thiol (Scheme 1B). Since Tau4RD contains two native cysteines, we first produced the C291A/C322ATau4RD double mutant (hereafter Tau4RDΔC) and then introduced a single cysteine in place of either Lys254, Lys311, or Lys353. We finally produced three monoubiquitinated Tau4RD isomers with linkages in those positions (hereafter ub-Tau4RD(254), ub-Tau4RD(311), and ub-Tau4RD(353)) (Figures 2A and S4-S8) as representatives of the ubiquitinated Tau species found in AD-PHFs.

The impact of ubiquitination at three different sites (occurring in three distinct repeats) on the aggregation kinetics of Tau was then evaluated in comparison with the unconjugated cysteine- free protein. The ThT assay (Figure 2B) and AFM analysis (Figure 2C) showed that Tau4RDΔC retained the ability to form filaments, in agreement with previous data on cysteine-free Tau variants [34,35]. The formation of fibrils by Tau4RDΔC increased rapidly over time with a sigmoidal trend and a lag time shorter than 4 hours. Interestingly, the three ubiquitinated derivatives exhibited different behavior. The aggregation kinetics of ub-Tau4RD(254) and ub-Tau4RD(353) followed a sigmoidal trend that suggested the formation of cross-β structures. However, with a lag time of ~8 hours, the aggregation process was markedly slowed down compared to that of Tau4RDΔC. AFM images further indicated the presence of short filaments (Figure 2C). Instead, the ThT signal of the ub-Tau4RD(311) sample increased with an almost linear time-dependence, suggesting that ubiquitination at this site strongly interferes with the conformational transitions that progress towards amyloid formation. Short sticks of 6-12 nm in height and 0.1-1 μm in length were formed (Figure 2C) and were not immunoreactive with the A11 antibody (Figure 2D). On the contrary, A11 recognized the ub-Tau4RD(254) and, to a lesser extent, the ub-Tau4RD(353) aggregates (Figure 2D).

Differences in the aggregation kinetics profiles of the three ubiquitin-Tau conjugates reflect changes at the level of the microscopic aggregation process: our data indicate that modification at Lys254 and Lys353 slows down the aggregation but permits the formation of filaments. Accordingly, the two conjugates were found to

produce A11-positive oligomers and short filaments detected by AFM. Notably, the two sites fall outside the 272-330 region forming the core of filaments [33], implying that attached ubiquitin molecules were too distant to determine steric hindrance against filament assembly. Both the aggregation kinetics experiments, and AFM analysis showed instead that ubiquitination in position 311 inhibited the formation of filaments more strongly: the small aggregates observed by AFM were indeed unable to elongate and lacked an A11- reactive epitope. The fact that Lys311 is located within the PHF motif of the R3 domain, which becomes part of the ordered core of heparin-induced [33] and AD-brain Tau filaments [11], explains why the presence of a bulky modifier at this site makes Tau unable to convert to cross-β/β-helix structures. Based on this consideration, we speculate that the ubiquitinated Lys311 found in AD-PHFs may originate from a modification event that follows the formation of the fibrils core. In conclusion, we have successfully applied enzyme-based and semisynthetic methods to ubiquitinate protein Tau. We demonstrated for the first time the possibility to use the CHIP ligase for the ubiquitination of Tau in vitro. The enzyme-based reaction produced a mixture of monoubiquitinated Tau isomers, reminiscent of the modifications observed in vivo, which were resistant to fibril formation. We used semisynthesis to obtain single monoubiquitinated Tau regio-isomers with which we could clarify the impact of the specific ubiquitination sites in Tau fibrillogenesis. Ubiquitination is an important PTM playing critical roles in Tau degradation and in neurodegeneration. By use of a combination of preparation procedures we have expanded our capability to interrogate the effects of ubiquitin modification at the molecular level and made a step forward in understanding the complex PTM-linked conformational transitions of amyloidogenic proteins.

4.1.1 **Acknowledgements**

This work was supported by a grant from the Alzheimer's Association (AARG-17-529221, MD). University of Verona is acknowledged for funding (Progetto Ricerca di Base 2015, MD). FM thanks "Fondazione Umberto Veronesi" for granting a postdoctoral fellowship. We thank Dr. Rossella Gottardo for ESI- MS analysis and Prof. Gianluigi Zanusso for kindly providing access to the FLUOstar Omega plate

reader. Centro Piattaforme Tecnologiche of the University of Verona is acknowledged for providing access to the Mass Spectrometry Platform. We thank Cassa di Risparmio di Padova e Rovigo (Cariparo) holding for funding the acquisition of the LTQ-Orbitrap XL mass spectrometer.

4.1.2 **Author Contribution**

Dr. Barracchia performed experiments and analyzed data on ubiquitinated samples obtained by enzymatic reactions.
In particular he prepared protein samples (Tau4RD, Ubiquitin, enzymes) and performed Tau4RD enzymatic ubiquitination. Performed aggregation and Thioflavin-T assay. Prepared AFM samples and performed their measurements.

4.1.3 **Figures**

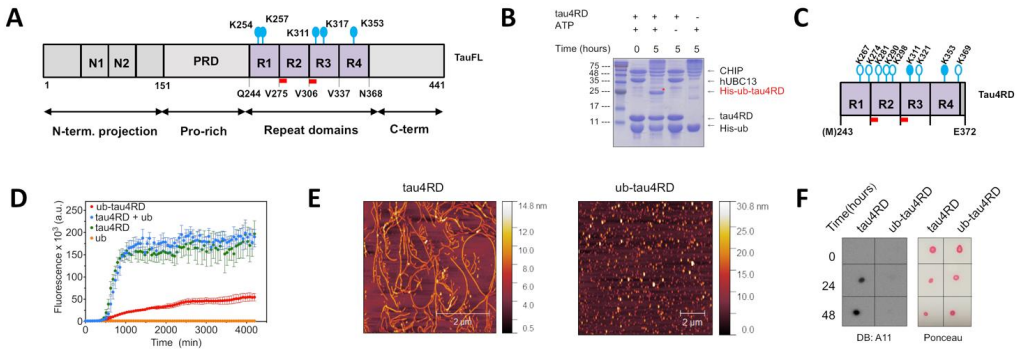

Figure 1: A) Schematic representation of full-length Tau (TauFL) sequence showing domains organization; the red boxes label the hexapeptide PHF motifs; ubiquitinated sites found in AD brains are visualized on the top. B) SDS-PAGE showing enzymatic ubiquitination of Tau4RD after incubation at 37 °C for 5 hours. C) Scheme of ubiquitinated sites in Tau4RD upon enzymatic reaction identified by MS; filled symbols represent ubiquitinated sites in AD-PHFs. D) Kinetics of protein aggregation followed by ThT-fluorescence; the aggregation assay was done at 30 °C for ubiquitin, Tau4RD, Tau4RD in the presence of ubiquitin at 1:1 molar ratio and ub-Tau4RD. E) AFM images of Tau4RD and ub-Tau4RD after 48 hours of incubation at 37 °C under static condition (scale bar: 2 µm). F) Dot Blot of samples in panel E, probed with the A11 antibody; proteins were also stained with Ponceau.

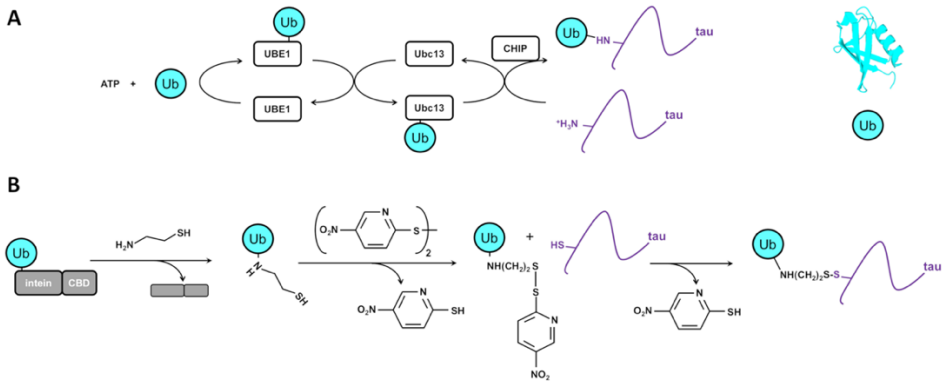

Scheme 1: A) Enzymatic cascade leading to ubiquitin (Ub) conjugation of Tau4RD: UBE1 activating, Ubc13 conjugating, CHIP ligase enzymes. B) Semisynthetic disulfide-based site-specific ubiquitination of Tau4RD.

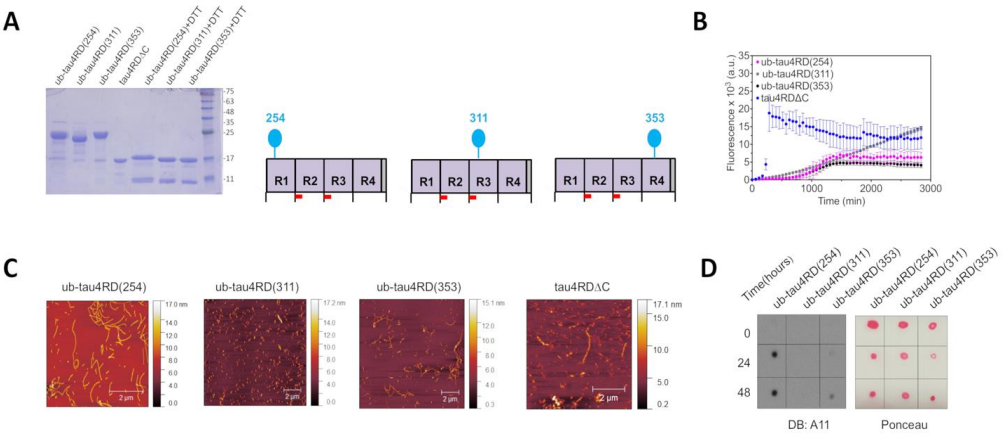

Figure 2: A) SDS-PAGE showing the purified site-specific monoubiquitinated Tau regio-isomers; incubation with dithiothreitol cleaved the ub-Tau disulfide linkage as expected; the schemes of Tau4RD modified at specific positions are shown. B) Kinetics of protein aggregation followed by ThT-fluorescence; aggregation experiments were carried out on Tau4RDΔC, ub-Tau4RD(254), ub-Tau4RD(311), and ub-Tau4RD(353) at 30 °C. C) AFM images of the same proteins after 48 hours of incubation at 37 °C under static condition (scale bar: 2 µm). D) Dot Blot of samples in C, probed with the A11 antibody; proteins were also stained with Ponceau.

Table 1: Modified peptides identified by MS analysis on ub-Tau4RD conjugate obtained by enzymatic reaction at 37 °C for 5 hours.[a]

Peptide sequence	K(GG) position	PEP
IGSTENLK(GG)HQPGGGK	267	3.29E-08
HQPGGGK(GG)VQIINK	274	1.75E-10
K(GG)LDLSNVQSK	281	1.11E-10
LDLSNVQSK(GG)CGSK	290	6.28E-07
DNIK(GG)HVPGGGSVQIVYKPVDLSK	298	1.91E-14
HVPGGGSVQIVYK(GG)PVDLSK	311	1.40E-10
HVPGGGSVQIVYKPVDLSKVTSK(GG)	321	1.37E-05
VQSK(GG)IGSLDNITHVPGGGNK	353	6.70E-15
IGSLDNITHVPGGGNK(GG)K	369	1.85E-12

[a] For each identified K-ε-GG peptide obtained with trypsin digestion of the sample the table reports: the sequence of peptides containing ubiquitinated lysines (indicated as K(GG)); K(GG) peptide position numbered according to the human Tau 441 isoform; Posterior Error Probability (PEP).

4.1.4 References

[1] V. M.-Y. Lee, M. Goedert, J. Q. Trojanowski, Annu. Rev. Neurosci. 2001, 24,1121–1159.

[2] E. Mandelkow, Trends Cell Biol. 1998, 8, 425–427.

[3] E. E. Congdon, E. M. Sigurdsson, Nat. Rev. Neurol. 2018, 14, 399–415.

[4] M. D. Weingarten, A. H. Lockwood, S. Y. Hwo, M. W. Kirschner, Proc. Natl. Acad. Sci. U. S. A. 1975, 72, 1858–1862.

[5] J. Avila, J. J. Lucas, M. Pérez, F. Hernández, Physiol. Rev. 2004, 84, 361–384.

[6] M. Morris, G. M. Knudsen, S. Maeda, J. C. Trinidad, A. Ioanoviciu, A. L. Burlingame, L. Mucke, Nat. Neurosci. 2015, 18, 1183–1189.

[7] L. Martin, X. Latypova, F. Terro, Neurochem. Int. 2011, 58, 458–471.

[8] Y. Wang, E. Mandelkow, Nat. Rev. Neurosci. 2016, 17, 22–35.

[9] C. Kontaxi, P. Piccardo, A. C. Gill, Front. Mol. Biosci. 2017, 4, DOI 10.3389/fmolb.2017.00056.

[10] M. von Bergen, P. Friedhoff, J. Biernat, J. Heberle, E.-M. Mandelkow, E. Mandelkow, Proc. Natl. Acad. Sci. 2000, 97, 5129–5134.

[11] A. W. P. Fitzpatrick, B. Falcon, S. He, A. G. Murzin, G. Murshudov, H. J. Garringer, R. A. Crowther, B. Ghetti, M. Goedert, S. H. W. Scheres, Nature 2017, 547, 185–190.

[12] M. Goedert, D. S. Eisenberg, R. A. Crowther, Annu. Rev. Neurosci. 2017, 40, 189–210.

[13] M. Morishima-Kawashima, M. Hasegawa, K. Takio, M. Suzuki, K. Titani,Y. Ihara, Neuron 1993, 10, 1151–1160.

[14] D. Cripps, S. N. Thomas, Y. Jeng, F. Yang, P. Davies, A. J. Yang, J. Biol. Chem. 2006, 281, 10825–10838.

[15] I. Livneh, Y. Kravtsova-Ivantsiv, O. Braten, Y. T. Kwon, A. Ciechanover, BioEssays News Rev. Mol. Cell. Dev. Biol. 2017, 39, DOI 10.1002/bies.201700027.

[16] C. D. Spicer, B. G. Davis, Nat. Commun. 2014, 5, 4740.

[17] M. Broncel, E. Krause, D. Schwarzer, C. P. R. Hackenberger, Chem. - Eur. J. 2012, 18, 2488–2492.

[18] O. Reimann, C. Smet-Nocca, C. P. R. Hackenberger, Angew. Chem. Int. Ed. 2015, 54, 306–310.

[19] S. Schwagerus, O. Reimann, C. Despres, C. Smet-Nocca, C. P. R. Hackenberger, J. Pept. Sci. 2016, 22, 327–333.

[20] M. Haj-Yahya, H. A. Lashuel, J. Am. Chem. Soc. 2018, 140, 6611– 6621.

[21] D. Ellmer, M. Brehs, M. Haj-Yahya, H. A. Lashuel, C. F. W. Becker, Angew. Chem. Int. Ed. 2019, 58, 1616–1620.

[22] L. Petrucelli, Hum. Mol. Genet. 2004, 13, 703–714.

[23] H. Shimura, D. Schwartz, S. P. Gygi, K. S. Kosik, J. Biol. Chem. 2004, 279, 4869–4876.

[24] C. Chatterjee, R. K. McGinty, B. Fierz, T. W. Muir, Nat. Chem. Biol. 2010, 6, 267–269.

[25] J. Chen, Y. Ai, J. Wang, L. Haracska, Z. Zhuang, Nat. Chem. Biol. 2010, 6, 270–272.

[26] F. Meier, T. Abeywardana, A. Dhall, N. P. Marotta, J. Varkey, R. Langen, C. Chatterjee, M. R. Pratt, J. Am. Chem. Soc. 2012, 134, 5468–5471.

[27] S. Hatakeyama, M. Matsumoto, T. Kamura, M. Murayama, D.-H. Chui, E. Planel, R. Takahashi, K. I. Nakayama, A. Takashima, J. Neurochem. 2004, 91, 299–307.

[28] M. J. Lee, J. H. Lee, D. C. Rubinsztein, Prog. Neurobiol. 2013, 105, 49– 59.

[29] S. E. Soss, Y. Yue, S. Dhe-Paganon, W. J. Chazin, J. Biol. Chem. 2011, 286, 21277–21286.

[30] M. Zhang, M. Windheim, S. M. Roe, M. Peggie, P. Cohen, C. Prodromou, L. H. Pearl, Mol. Cell 2005, 20, 525–538.

[31] P. Arosio, T. P. J. Knowles, S. Linse, Phys. Chem. Chem. Phys. PCCP 2015, 17, 7606–7618.

[32] R. Kayed, E. Head, J. L. Thompson, T. M. McIntire, S. C. Milton, C. W. Cotman, C. G. Glabe, Science 2003, 300, 486–489.

[33] W. Zhang, B. Falcon, A. G. Murzin, J. Fan, R. A. Crowther, M. Goedert, S. H. Scheres, eLife 2019, 8, e43584.

[34] E. Akoury, M. Pickhardt, M. Gajda, J. Biernat, E. Mandelkow, M. Zweckstetter, Angew. Chem. Int. Ed Engl. 2013, 52, 3511–3515.

[35] Y. K. Al-Hilaly, S. J. Pollack, D. M. Vadukul, F. Citossi, J. E. Rickard, M. Simpson, J. M. D. Storey, C. R. Harrington, C. M. Wischik, L. C. Serpell, J. Mol. Biol. 2017, 429, 3650–3665.

4.1.5 **Supplementary information**

Experimental Procedures:

Reagents

Cysteamine, Tris(2-carboxyethyl)phosphine, 2,2′-Dithiobis(5-nitropyridine), Thioflavin-T, IPTG, Heparin (H3393), dithiothreitol, NH_4HCO_3, acetonitrile, formic acid, methyl methanethiosulfonate, were purchased from Sigma.

Protein expression and purification

E. coli codon-optimized human Tau cDNA sequence was purchased from Eurofins Genomics. Tau4RD (spanning residues Q244-E372 plus initial Met) was cloned into a pET22 vector via NdeI-BamHI sites with a stop codon to avoid insertion of a C-terminal histidine-tag. N-terminal histidine$_6$-tag Tau4RD was cloned into a pET15 vector via NdeI-BamHI sites. Tau4RD mutants C291A, C322A; C291A, C322A, K254C; C291A, C322A, K311C and C291A, C322A, K353C were obtained by site-directed mutagenesis. While the last two mutants could be easily produced in pET22 vector, the triple mutant C291A, C322A, K254C Tau4RD was obtained in pET15 only.

All Tau4RD variants were expressed in BL21 (DE3) cells grown in LB medium, at 37 °C for 5 hours with 0.5 mM IPTG. Protein purification was achieved either by thermal treatment of the soluble bacterial extract (80 -100 °C) and SP-ion exchange chromatography or by immobilized nickel affinity chromatography (IMAC) for histidine-tag proteins. Where necessary, the histidine tag was removed by thrombin and a second step of IMAC.

Wilde-type human ubiquitin was produced as previously described[(1)].

N-terminal histidine$_6$-tagged ubiquitin was cloned into a pET15 vector via NdeI-BamHI sites and expressed in *E. coli* Rosetta (DE3) cells grown in LB medium, at 20 °C overnight with 0.5 mM IPTG. His$_6$-tagged ubiquitin was purified by IMAC according to standard protocols.

Ubiquitin used in the semisynthetic reaction was produced with the GyrA intein and the chitin binding domain fused at its C-terminus. Plasmid ptXB1 encoding for this construct was kindly provided by Prof. David Fushman, University of Maryland (USA). The fusion protein was produced in BL21 (DE3) cells at 37 °C

overnight in auto-inducing medium and purified by affinity chromatography using the chitin resin (NEB) in Tris-HCl 20 mM at pH 7.5, NaCl 200 mM, EDTA 1 mM, Triton 0.05%. Elution of ubiquitin bearing an aminoethanethiol C-terminal group (Ub-SH) was obtained by incubating the clean fusion protein attached to the chitin resin with Tris-HCl 20 mM, NaCl 200 mM, EDTA 1 mM, cysteamine, and Tris(2-carboxyethyl)phosphine (TCEP) 50 mM at pH 7.5 for 24 h. Ub-SH was further purified by a superdex-75 gel filtration column. The protein was verified by ESI-MS (Figure S4), which yielded an observed mass value of 8624.6 Da (expected: 8625 Da). Human E1 (UBE1) with an N-terminal histidine tag was produced as previously described [2]. The pET21 plasmid encoding UBE1 gene was a gift from Cynthia Wolberger (Addgene plasmid #34965; http://n2t.net/addgene:34965; RRID:Addgene_34965[3]).

HUbc13 (human E2N, UniProtKB P61088) and human E3 ubiquitin-protein ligase CHIP (UniProtKB Q9UNE7) were both amplified from a HEK293 cells cDNA library and cloned into a pGEX4T1 vector via EcoRI/BamHI sites. Both enzymes were produced with an N-terminal GST-tag in *E. coli* Rosetta (DE3) cells in LB medium at 20 °C overnight with 0.4 mM IPTG and purified with GSH-chromatography by standard procedures.

Activation of Ub-SH by 2,2′-Dithiobis(5-nitropyridine)

Ub-SH was activated with 2,2′-dithiobis(5-nitropyridine) (DTNP) to generate an asymmetric disulfide. 8 mg of DTNP were dissolved in 3 mL of acetic acid and then added to 1 mL of Ub-SH in mQ H_2O at a concentration of 1 mg/mL. The mixture was incubated for 24 h at 25 °C, and then dialysed against mQ H_2O. The resulting product, Ub-S-nitro-2-pyridinesulfenyl disulfide adduct (Ub-S-pNpys) was verified by ESI-MS (figure S5), which measured a mass value of 8778.5 Da (expected: 8779.0 Da).

Reaction of Ub-S-nitro-2-pyridinesulfenyl disulfide adduct with Tau4RD cysteine mutants

Tau4RD cysteine mutants were incubated with a large excess of DTT. The latter was then removed by buffer-exchange with dialysis or desalting column prior the coupling reaction.

Typically, 2 mg of Tau4RD cysteine mutant was incubated with 2 mg of Ub-S-pNpys (twofold molar excess of activated ubiquitin) in 1 ml of 100 mM Hepes buffer, pH 7, for 40' at 25 °C with continuous shaking. The reaction product was then purified by SP-ion exchange chromatography and verified by MALDI. We obtained mass values of 22637, 22353 and 22363 Da for the ubiquitin-Tau4RD adducts conjugated in position 254 (expected mass 22629: this value corresponds to a Tau mutant with an additional N-terminal GSH peptide resulting from thrombin-processing of an N-terminal histidine tag), 311 (expected mass 22348), and 353 (expected mass 22348), respectively.

Dot blotting

About 3 µg of each protein sample were spotted on a PVDF membrane (Millipore). After blocking in TBS-T (0.1% Tween-20, 150 mM NaCl, 10 mM Tris at pH 8.0) with 5% (w/v) fat-free dry milk at room temperature, the membrane was washed three times with TBST and incubated with the anti-oligomer antibody A11 (1:2000, ThermoFisher) at 4 °C overnight. Membranes were washed three times with TBS-T and incubated with the goat HRP-conjugated secondary antibody (1:10000, ThermoFisher) in blocking buffer for 2 hours at room temperature. After washing three times with TBS-T, the blot was developed with ECL reagents (Pierce) on a Chem-iDoc imager (BioRad).

Enzymatic ubiquitination

Ubiquitination reactions were carried out in 50 mM Tris-HCl buffer, pH 8, also containing 5 mM ATP, 5 mM $MgCl_2$ and 3 mM TCEP, using 1 µM His-tagged E1, 10 µM GST-tagged Ubc13, and 10 µM GST-tagged CHIP. Ubiquitin and Tau4RD substrates were used at 70 and 35 µM concentration, unless otherwise specified.

Trypsin digestion for LC-MS/MS analysis

SDS-PAGE bands corresponding to Tau4RD before and after the reaction with E1-hUbc13-CHIP were excised and divided in small pieces. A digestion with trypsin was performed in gel according to published protocols[4] with some modifications. Briefly, after washing several times the gel pieces alternatively with 50 mM NH_4HCO_3 and acetonitrile (ACN), samples were dried under vacuum.

Reduction of cysteine residues was carried out by incubating the gel pieces with 50 µL of TCEP (2 mM in 50 mM NH_4HCO_3) for 1 h at 56 °C. Successively, the reducing solution was discarded and gel pieces were treated with 50 µL of the alkylating agent methyl methanethiosulfonate (MMTS) (4 mM in 50 mM NH_4HCO_3) for 15 min at room temperature. The solution was discarded and the samples were washed with 50 mM NH_4HCO_3 and ACN, and dried under vacuum. 10 µL of sequencing grade modified trypsin (12.5 ng/µL) were added and the digestion was allowed to proceed overnight at 37 °C before stopping it with the addition of 1 µL of pure formic acid (FA).

Peptides were extracted from the gel by several passages in 10 mM NH_4HCO_3, in 50% ACN/0.1% FA and in 75% ACN/0.1% FA. Samples were finally dried under vacuum and stored at -20 °C until the LC-MS/MS analysis was performed.

LC-MS/MS and data analysis

The analysis was performed using an LTQ-Orbitrap XL mass spectrometer (Thermo Fisher Scientific) interfaced to a nano-HPLC Ultimate 3000 (Dionex – Thermo Fisher Scientific). Samples were dissolved in 15 µL of 3% ACN/0.1% FA and 3 µL were loaded into a trap column (NanoEase Symmetry300, C_{18}, 5 µm, Waters) using a flow rate of 8 µL/min. Peptides were then transferred to a 10 cm pico-frit column (75 µm I.D., New Objective) packed in house with C_{18} material (Aeris Peptide 3.6 µm XB-C18, Phenomenex) and separated using a linear gradient of ACN/0.1% FA (from 3% to 40% in 20 min) with a flow rate of 250 nL/min. MS spectra were acquired in the Orbitrap (60000 nominal resolution) in the range 300-1700 m/z, while MS/MS spectra were acquired in the linear ion trap. The instrument operated in a data-depended mode, with a cycle consisting of a full MS scan

followed by the MS/MS scans of the 10 most intense ions. Mono-charged ions were excluded from fragmentation.

Raw data were analyzed with the software Proteome Discoverer 1.4 (Thermo Fisher Scientific) interfaced to a Mascot server (version 2.2.4, Matrix Science). Search was done against the human section of the Uniprot database. Trypsin was selected as digesting enzyme with up to 2 missed cleavages allowed. Peptide and fragment tolerance were set to 10 ppm and 0.6 Da respectively. Methyltio-cysteine was set as fixed modification, while methionine oxidation and Gly-Gly modification of lysine residues were set as variable modifications. The algorithm percolator was used in combination with a search against a randomized database to assess the False Discovery Rate (FDR). Results were filtered to keep into account only proteins identified with at least 2 unique peptides with high confidence (FDR $\leq$ 0.01).

MS analysis of intermediates of semisynthesis

ESI-MS analyses were carried out on a MicrOTOF mass spectrometer (Bruker Daltonics, Bremen, Germany). Capillary voltage was – 4.5 kV, source temperature 200 °C. Nitrogen was used both as drying and nebulizing gas (drying gas flow rate: 5 l/min, nebulizer pressure: 6 psi). The mass spectrometer was operated in the positive ion scan mode from 50 to 3000 *m/z*, with acquisition scan rate of 20 spectra per second.

Samples were dissolved in a mixture of ACN/water (50/50) added with 0.1 % FA and then directly infused into the ESI source of the TOF mass spectrometer with a flow of 5 µl/min delivered by a syringe pump (Cole-Parmer, Vernon Hill, IL, USA). External calibration was obtained by infusing for one minute at the beginning of each analysis a solution composed of 10 mM sodium hydroxide in isopropanol and 0.2% FA (1:1, v/v), using seven calibration ions corresponding to the formulas Na(NaCOOH)x, with x ranging from 2 to 9. Data processing was fully carried out using Data Analysis software (Version 3.2, Bruker Daltonics).

Maldi TOF MS analysis was performed on a Bruker Ultraflextreme MALDI-TOF/TOF instrument (Bruker Daltonics).

Samples were resuspended and acidified with ACN/H_2O solution (30:70 (v/v) acetonitrile:0.1% TFA in water) and incubated for 30 min at room temperature. The

resulting solution was mixed 1:1 (v/v) with the matrix Sinapinic acid (trans-3,5-dimethoxy-4-hydroxycinnamic acid) (10 mg/ml in ACN:H_2O 1:1 with 0.1% TFA), and then 1 µl of the sample/matrix solution was spotted in triplicate onto a Ground steel MALDI target plate (Bruker Daltonics), allowed to dry at room temperature. Mass spectra were collected from m/z 5000 to 20000 in positive linear mode and mass calibration was performed using a protein standard mixture composed by myoglobin, cytochrome C, ubiquitin I and insulin. Instrument settings were: ion source 1: 19.93 kV; ion source 2: 18.77 kV; lens: 8.57 kV; delay time:104 ns with a scale factor of 800; acceleration voltage: 20 kV; number of shots: 2000 in six different positions for one spectrum. All the data were analysed with FlexAnalysis Software (Bruker Daltonics)

Purification of Tau4RD ubiquitinated by CHIP

To purify Tau4RD ubiquitinated by CHIP, a large volume of ubiquitination reaction was prepared (4 mL), using Tau4RD and His_6-tagged ubiquitin at a concentration of 110 and 140 µM, respectively. After incubation at 37 °C for 5 hours, the reaction was stopped and heated at 70 °C for 15 minutes: this thermal treatment removes all the enzymes from the solution. Removal of unreacted ubiquitin was then achieved by SP-ion exchange chromatography. Finally, ubiquitinated Tau4RD was separated from unreacted Tau4RD by IMAC, taking advantage of the His_6-tag on ubiquitin.

Thioflavin-T aggregation assay

Solutions of 0.01 mM Tau4RD variants in 20 mM sodium phosphate buffer at pH 7.4 and 50 mM NaCl (with 0.02% NaN_3 and protease inhibitors with EDTA) were incubated in the presence of 0.01 mM Thioflavin-T and 0.01 mM heparin in 96-well dark plates in a plate reader (FLUOstar Omega; BMG LABTECH) at 30 °C for 72 hours with cycles of 60 seconds of shaking (900 rpm, double-orbital) and 14 minutes of rest throughout the incubation. The aggregation assay for ubiquitin, Tau4RD, Tau4RD in the presence of ubiquitin at 1:1 molar ratio, and Tau4RD ubiquitinated by CHIP was performed in the presence of 5 mM DTT. In the latter samples, ubiquitin carries a His_6-tag at its N-terminus. Thioflavin-T (ThT) fluorescence measurements (mean [SD] excitation, 450 [10] nm; mean emission, 480 [10] nm

[bottom read]) were taken every 15 minutes. Proteins were filtered through a 100 kDa cut-off filter (Sartorius) before starting the aggregation to remove pre-existing large oligomers and fibrils. Error bars of ThT curves correspond to standard deviations of at least three independent experiments.

Aggregation of Tau4RD variants for AFM analysis

Solutions of 0.05 mM Tau4RD variants in 20 mM sodium phosphate buffer at pH 7.4 and 50 mM NaCl (with 0.02% NaN_3 and protease inhibitors with EDTA) were incubated at 37 °C without agitation for 48 hours, using heparin at 1:1 molar ratio as aggregation initiator. 5 mM DTT was included only for Tau4RD and Tau4RD ubiquitinated by CHIP. After incubation, the buffer of protein samples was exchanged to mQ H_2O by filtration with a 100 kDa cut-off filter (Sartorius).

AFM analysis

For AFM measurements, 20 µL of Tau4RD variant aggregates (5-25 µM) in mQ H_2O were deposited on freshly cleaved mica, and allowed to dry in air. AFM images were acquired with a NT-MDT Solver Pro microscope, (Zelenograd, Moscow, RU), with single crystal silicon-antimony doped probe and a gold coated base (NSG-01 from NT-MDT) used in semi-contact mode. The hysteresis of the instrument was adjusted by a software correction of the data using calibration grid (TGQ1 from NT-MDT) before analysis. Images were processed and analyzed with the Gwyddion software.

4.1.6 **Supplementary figures and tables**

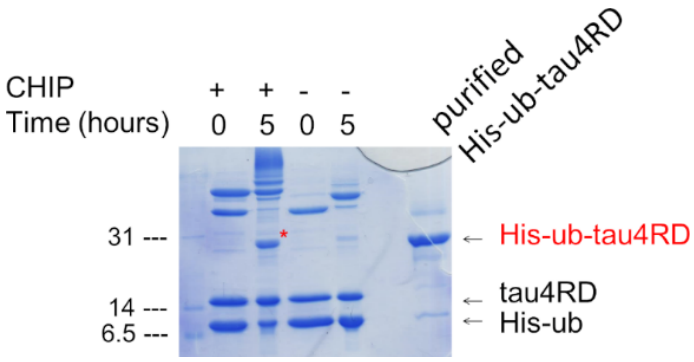

Figure S1. Coomassie Blue-stained SDS-PAGE showing His_6-ub-Tau4RD obtained from the enzymatic reaction performed at 37 °C for 5 hours with UBE1, hUbc13 and CHIP. A control in the absence of CHIP is also reported. In the last lane, the purified His_6-ub-Tau4RD, obtained after thermal treatment and SP-ion exchange is shown.

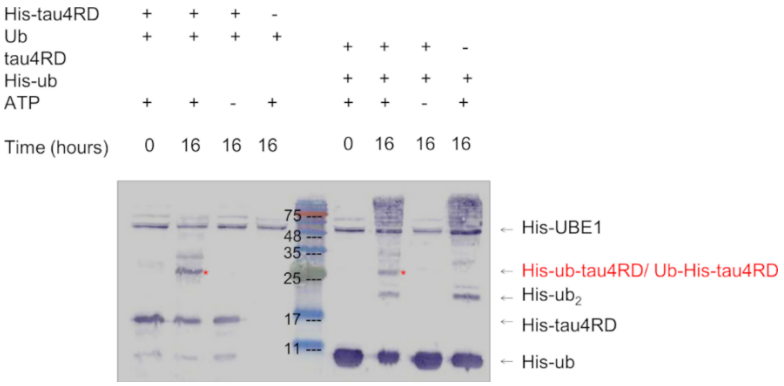

Figure S2. Immunoblot analysis of the *in vitro* enzymatic ubiquitination reaction of Tau4RD incubated overnight at 30 °C with UBE1, hUbc13 and CHIP. The analysis was performed with anti-his-tag mAb in assays done with the His_6-tag fused at the N-terminus of either ubiquitn or Tau4RD. Enzymatic reactions carried out without ATP or Tau4RD were used as controls. The blot revealed the presence of a new band running close to the 25 kDa marker, corresponding to His_6-ub-Tau4RD or ub-His_6-Tau4RD, that was absent in the negative controls. Bands corresponding to monoubiquitinated Tau4RD are highlighted with a red asterisk. A positive band corresponding to slightly larger molecular weight (close to the 35 kDa marker) could instead represent a diubiquitinated species of Tau4RD. Unexpectedly, we also found an immunoreactive band running between 17 and 25 kDa, which was only present when the His_6-tag was on ubiquitin, and could be attributed to free diubiquitin chains (Ub_2). The high molecular weight band close to the 48 kDa marker that is positive to anti-his tag mAb in all lanes, could correspond to degradation products of His_6-tagged E1. Higher molecular weight bands in the reaction with His_6-ubiquitin could instead be assigned to ubiquitinated enzymes: indeed, those bands are not present at time 0 and in the absence of ATP, while they show up after 15 hours and in the absence of Tau.

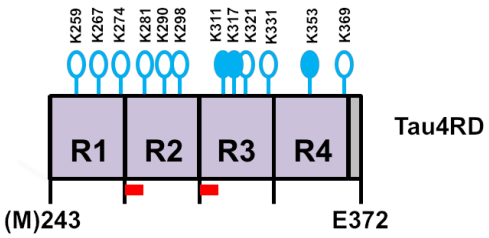

Figure S3. Scheme of ubiquitinated sites found by MS in Tau4RD upon enzymatic reaction performed at 30 °C for 16 hours. Filled symbols represent ubiquitinated sites in AD-PHFs.

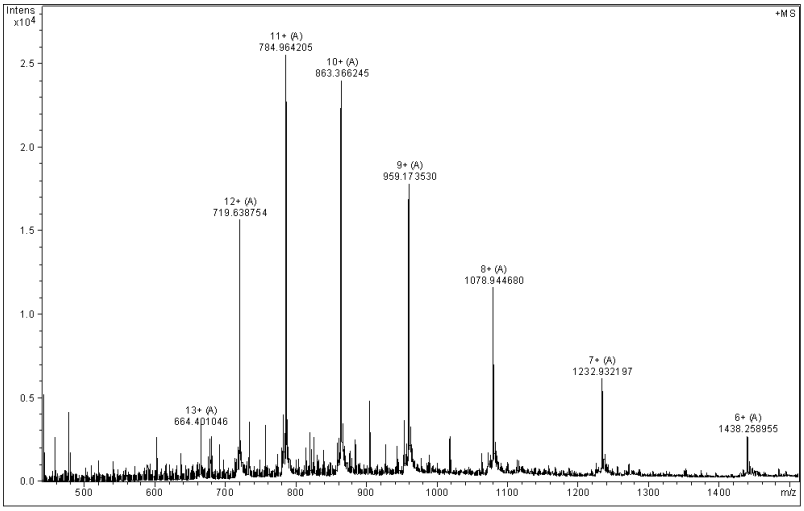

Figure S4. ESI-MS analysis of the Ub-SH sample. The experimental mass value was 8624.6 Da (expected: 8625 Da).

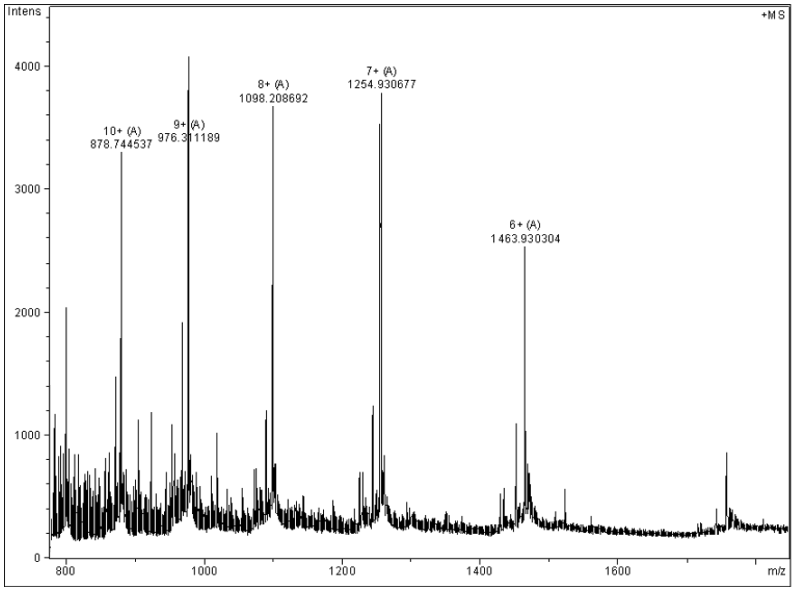

Figure S5. ESI-MS analysis of Ub-S-pNpys. The experimental mass value was 8778.5 Da (expected: 8779.0 Da).

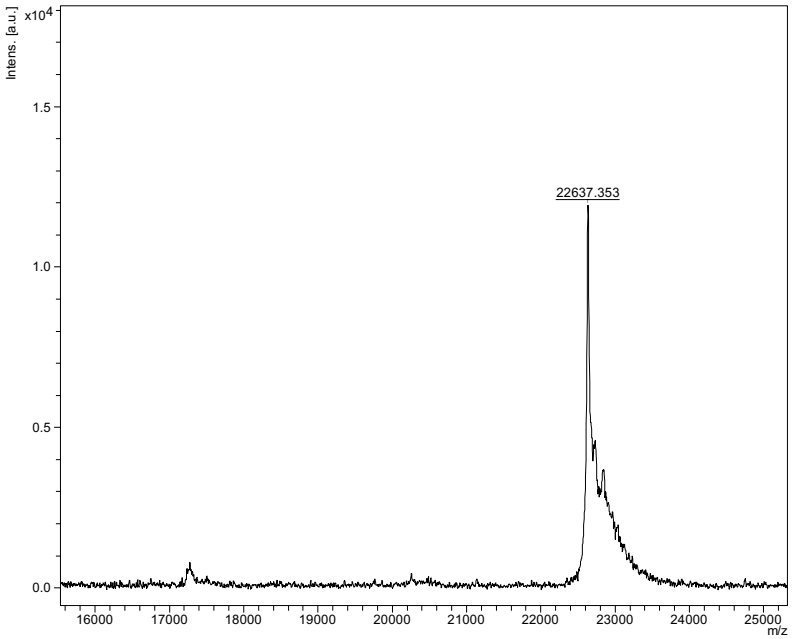

Figure S6. Maldi TOF MS analysis of ub-Tau4RD(254). The experimental mass value was 22637 Da (expected mass 22629 Da).

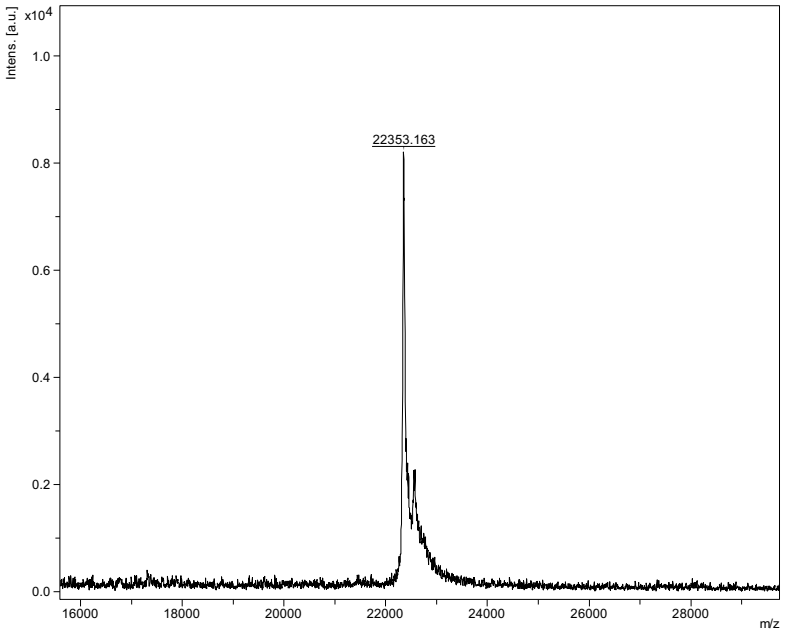

Figure S7. Maldi TOF MS analysis of ub-Tau4RD(311). The experimental mass value was 22353 Da (expected mass 22348 Da).

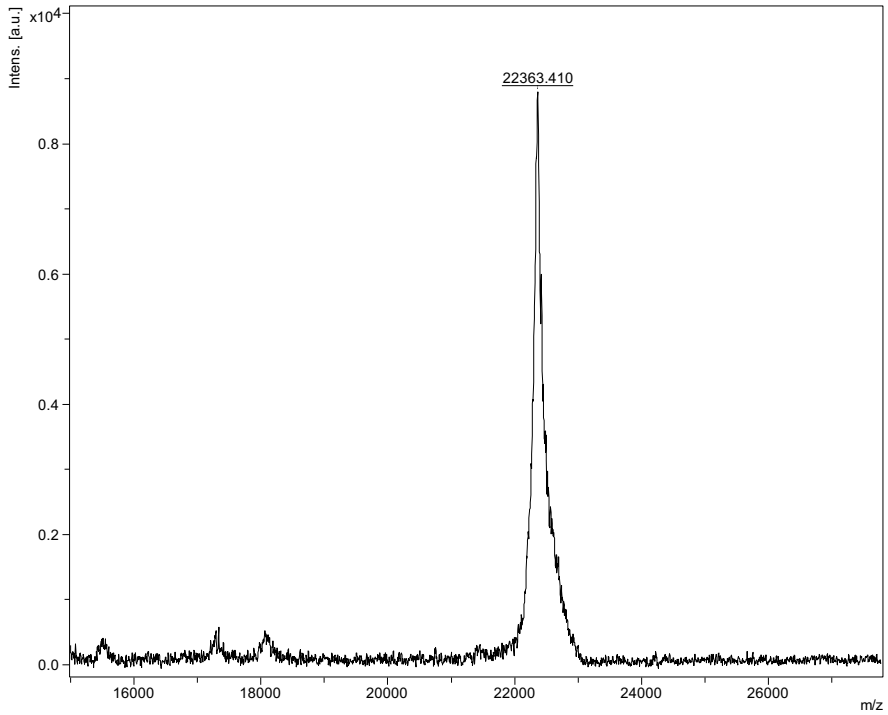

Figure S8. Maldi TOF MS analysis of ub-Tau4RD(353). The measured mass value was 22363 Da (expected mass 22348 Da).

Table S1. Modified peptides identified by MS analysis on ub-Tau4RD conjugate obtained by enzymatic reaction at 30 °C for 16 hours.[a]

Peptide sequence	K(GG) position	PEP
SK(GG)IGSTENLK	259	3.69E-02
IGSTENLK(GG)HQPGGGK	267	7.37E-5
HQPGGGK(GG)VQIINK	274	2.51E-05
K(GG)LDLSNVQSK	281	1.35E-8
LDLSNVQSK(GG)CGSK	290	9.24E-4
DNIK(GG)HVPGGGSVQIVYKPVDLSK	298	1.78E-6
HVPGGGSVQIVYK(GG)PVDLSK	311	5.11E-11
HVPGGGSVQIVYKPVDLSK(GG)VTSK	317	5.47E-5
VTSK(GG)CGSLGNIHHKPGGGQVEVK	321	4.01E-9
CGSLGNIHHK(GG)PGGGQVEVK	331	8.87E-7
VQSK(GG)IGSLDNITHVPGGGNK	353	5.00E-8
IGSLDNITHVPGGGNK(GG)K	369	8.16E-11

[a] For each identified K-ε-GG peptide obtained with trypsin digestion of the sample the table reports: the sequence of peptides containing ubiquitinated lysines (indicated as K(GG)); K(GG) peptide position numbered according to the human Tau 441 isoform; Posterior Error Probability (PEP).

References

[1] Munari, F.; Bortot, A.; Zanzoni, S.; D'Onofrio, M.; Fushman, D.; Assfalg, M. Identification of Primary and Secondary UBA Footprints on the Surface of Ubiquitin in Cell-Mimicking Crowded Solution. *FEBS Lett.* **2017**, *591* (7), 979–990.

[2] Munari, F.; Bortot, A.; Assfalg, M.; D'Onofrio, M. Alzheimer's Disease-Associated Ubiquitin Mutant Ubb+1: Properties of the Carboxy-Terminal Domain and Its Influence on Biomolecular Interactions. *Int. J. Biol. Macromol.* **2018**, *108*, 24–31.

[3] Berndsen, C. E.; Wolberger, C. A Spectrophotometric Assay for Conjugation of Ubiquitin and Ubiquitin-like Proteins. *Anal. Biochem.* **2011**, *418* (1), 102–110.

[4] Arrigoni, G.; Pagano, M. A.; Sarno, S.; Cesaro, L.; James, P.; Pinna, L. A. Mass Spectrometry Analysis of a Protein Kinase CK2beta Subunit Interactome Isolated from Mouse Brain by Affinity Chromatography. *J. Proteome Res.* **2008**, *7* (3), 990–1000.

4.2 Unsaturated fatty acid-induced conformational transitions and aggregation of the repeat domain of Tau

The concentration and composition of Unsaturated Fatty Acids (UFAs) in the brain are altered with age and are associated with neurological disorders, including Alzheimer's Disease.

Several reports propose that, in these conditions, Tau protein could interact with free fatty acids in a micellar state [1-3]. Therefore, investigations of lipid-protein co-assembly are necessary to deepen our understanding of both the healthy and aberrant action of amyloidogenic proteins, also providing the basis for the development of therapeutic strategies against devastating neurodegenerative diseases.

In our work, we aimed to study the binding of Tau4RD protein to unsaturated fatty acids/salts, proposed as aggregation inducers. Mostly we were interested in identifying the polypeptide regions involved in the interactions and detecting conformational transitions experienced by Tau4RD in the presence of these molecules. Two of the most abundant FA (Figure 1) in the grey matter of the human brain were used to investigate the nature of this interaction: Arachidonic Acid (ARA) (20:4), a polyunsaturated fatty acid (PUFA), and Oleic Acid (OLA) (18:1), a monounsaturated fatty acid (MUFA), which constitutes the 45% of unsaturated fatty acid in the cerebral spinal fluid (CSF).

In our work, these FAs were used in the form of micelles (Supplementary information (SI1)) in order to mimic the elevated levels of FAs in pathological conditions and to produce lipid vesicles exhibiting a negatively charged surface, predicted to interact with the positively charged Tau4RD.

The interaction was characterized using NMR spectroscopy for the observation of lipid-induced perturbations at the single-residue level and Circular Dichroism (CD) measurements to monitor the perturbations at the level of secondary structure elements. Aggregation assays were further conducted by monitoring time-dependent changes in Thioflavin-T fluorescence while the protein was incubated in the presence of UFAs. The co-aggregates were subsequently characterized in terms of size and morphology by SDS-PAGE and Atomic Force Microscopy (AFM).

4.2.1 Aggregation of Tau4RD in the presence of Unsaturated Fatty Acids

The formation of Tau4RD aggregates in the presence of ARA and OLA (molar ratio 1:3 P/FA) (samples prepared as described in Material and Method paragraph 3.6) was followed by the Thioflavin-T (ThT) fluorescence assay. The interaction of Tau4RD with FAs micelles exhibits an increase in fluorescence intensity after 2 days of incubation a 37 °C (Figure 2A and B), which continues over time (blue curves). In contrast, the fluorescence signals measured on the two controls, Tau4RD (green curves) and fatty acid (red curves) display no time-dependent increase in intensity. This observation indicates that the interaction of protein and FA promotes the formation of ThT-positive Tau aggregates. However, at this concentration and molar ratio, the fibrils formation remains less pronounced compared to the sample incubated with heparin, another anionic cofactor. The data collected show that after a few hours of incubation, the curve plateau is reached (Figure 2C).

To analyze the co-aggregates, gradient polyacrylamide gel electrophoresis was performed on these samples, under non-reducing condition. Gradient polyacrylamide concentration was used because it can offer some advantages compared to fixed concentration gels [4]:

1. Separating a wide range of protein sizes into a single gel
2. High resolving power of distinct proteins with close molecular weights

Tau4RD shows a clear and concentrated band of monomer at about 14 KDa (the molecular weight has been estimated based on previously run SDS-PAGE with molecular weight standards), whose intensity does not appear to decrease significantly over time. However, after 72 h of incubation, the presence of large oligomers was observed in the gel. Furthermore, the presence of insoluble protein material in the loading wells indicates also the formation of SDS-resistant high molecular weight co-aggregates. A similar pattern of bands was observed in a control sample incubated with Heparin. In contrast, Tau4RD migrates as a compact band, without precipitated material in the well, showing only an increase in the formation of the dimers. These evidences appear in agreement with what observed in the ThT assay. Thus, these data suggest the ability of lipids to induce co-aggregates formation of Tau4RD protein.

4.2.2 ^{1}H-NMR measurement of Tau4RD monomer depletion and translational diffusion

In our work, we also used NMR spectroscopy to explore the protein-lipid interaction. The addition of a threefold molar excess of FA to Tau4RD perturbed the protein ^{1}H-NMR profile to very little extent: virtually no chemical shift changes were observed, and intensities were only slightly reduced (Figure 4). On the contrary, the signals of the FAs became undetectable and they did not add to the protein signals. Based on translational diffusion measurements, the observable protein ^{1}H-NMR signals could be attributed to Tau4RD molecules which were freely diffusing in solution and were not part of larger aggregates (Figure S1). Thus, a small portion of protein molecules appeared to interact with the bulk of FAs, determining a major change in lipid aggregation state and/or dynamics. We note that in our aggregation studies, both FAs were predominantly in the micellar state (Figure S5), however, signals of free monomers of ARA were also observed (not shown).

To monitor protein aggregation, ^{1}H-NMR spectra were recorded on P/FA samples immediately after mixing and after 24 h or 48 h of incubation. In the presence of OLA, the spectrum intensity decreased by 67% after 24 h (Figure 5A), indicating that the population of free protein was reduced, likely due to the formation of protein-containing aggregates. Unexpectedly, the translational diffusion of the species observed in the spectrum did not decrease but instead was slightly faster (~10%) compared to that measured on the freshly prepared mixture (Figure 5B). This result can be likely attributed to the structural compaction induced by the formation of intramolecular disulfide bridges upon progressive decrease of DTT reducing activity.

In the case of ARA, the protein spectrum displayed reduced intensity after 24 h (30% reduction) and after 48 h (60%) (Figure 5C). Again, it was remarkable to observe that the protein diffusion coefficient became larger (~20% at 48h) after prolonged incubation with the FA (Figure 5D).

4.2.3 ^{1}H-^{15}N-NMR measurements

To better understand the conformational properties of the free Tau4RD and co-aggregates, HSQC spectra were recorded on protein alone and immediately after the addition of FAs, and after 24 h and 48 h of incubation. The spectrum of Tau4RD (Figure 6A) exhibits a dense cluster of cross-peaks over a narrow ppm range in agreement with its unfolded nature. The spectra obtained after the immediate addition of FAs are quite similar to those previously recorded in their absence (Figure 6B and C), indicating that the conformational properties of the observable protein species are unchanged with respect to those of the free protein.

As expected, the spectra obtained after 24h (data not shown) and 48h of incubation of the protein alone (Figure S6) are identical to those previously recorded, indicating that the protein largely maintains its unfolded nature also after 48 h of incubation.

The spectra obtained after 24 h and 48 h of incubation in the presence of FAs are interesting (Figure 7A and C) (data 24 h are not shown). The interaction with each FA did not change significantly peaks position but caused evident perturbation in peak intensity, that continued during the incubation. The plot of normalized intensities as a function of residue number (Figure 7B and D) shows only a uniform perturbation of the values, which is characteristic of an interaction which is not residue-specific.

4.2.4 FA-induced protein secondary structure perturbations monitored by circular dichroism

Circular dichroism (CD) spectroscopy was used to gain insight into changes in secondary structure of Tau4RD induced by the presence of FA. The far-UV CD spectrum of Tau4RD is characteristic of a largely disordered protein, featuring a deep minimum centred at 198 nm and the absence of strong negative signals above 205 nm (Figure 8A).

Firstly, to evaluate the effects of micelles on the conformation of Tau4RD, the spectra of the protein were collected after the immediate addition of different molar excess of FA (P/FA = 1:3, 1:10, 1:25). The CD data (Figures 8B and C) show that as the fatty acid concentration increases, the protein spectrum gradually vanishes.

This trend is completely different in the presence of another amphipathic micelle, formed by SDS. Indeed, the addition of SDS produces a quantitative conversion to α-helical structure (Figure 8D), which increases with increasing molar ratio, as reported [5]. These data indicate that in the presence of distinct types of micelles, the interaction can perturb the unfolded nature of Tau4RD.

According to these results, the evolution of the perturbation of the secondary structure of Tau4RD was monitored in the presence of FA at different time points, choosing as the optimal molar ratio, P/FA 1:3.

On addition of OLA, the protein spectrum remained unperturbed (Figure 9A), however, after incubation for 24 h, significant changes were observed. The lineshape showed two minima, at 202 and 218 nm, and positive ellipticity was observed below 195 nm. This lineshape can be attributed to a mixture of protein molecules in disordered state and in partially ordered conformations, however with no uniquely defined secondary structure elements.

In analogy with OLA, the addition of ARA did not immediately perturb the CD spectrum of Tau4RD, but changes were observed after longer incubation (Figure 9B). The lineshapes observed appeared quite similar to the previous sample and exhibited two minima centred at about 200 and 220 nm.

To better understand the structural perturbations induced by FA, experiments were also performed with heparin, as a further control. The transition of Tau4RD from the disordered state to a β-sheet structure after incubation for 24 h with heparin was clear from the CD spectrum (Figure 9C), in agreement with previous studies [6].

For comparison purposes, we investigated the interaction of FA with another amyloidogenic protein, α-synuclein (αS). αS can easily form amyloid fibrils *in vitro* without the addition of inducers, and the corresponding CD spectrum was consistent with the presence of β-sheet structure (Figure 10A). In the presence of ARA, however, the protein turned immediately to α-helical structure and the CD spectrum displayed little changes after longer incubation, in agreement with the results of Klenerman and co-workers [7] (Figure 10B). Analogous results were observed in αS incubated with OLA (Figure 10C).

4.2.5 **Lipid co-aggregates characterization**

Atomic force microscopy (AFM) studies were performed to examine the morphology of the co-aggregates formed by interaction with fatty acids. Samples were prepared in the same conditions employed for the above-described NMR and CD measurements. Samples were diluted to the optimal concentration and were adsorbed on the surface of the mica for AFM imaging.

After the immediate addition of the Fatty Acid (OLA or ARA) (Figures 11A and B), no significant particles were found adsorbed to the surface of the mica. The presence of small particles could be due to homotypic (lipid-only or protein-only) assemblies or impurities. After incubation (24 h at 37 °C) samples were diluted and adsorbed to the mica again. As evident in the micrography in Figure 11C and D, Tau4RD appeared to interact with the bulk of FAs, showing the presence of large amorphous aggregates.

Thus, although very preliminary, the collected results show clearly that the interaction of Tau4RD with FAs determine the formation of larger assemblies which do not exhibit the typical fibrillar form of amyloids.

4.2.6 **Conclusions**

In vitro studies have shown to be particularly useful to investigate the interaction effects of fatty acids on Tau4RD aggregates formation. In our work, we demonstrate that fatty acids can affect the kinetics and the type of aggregations, as well as the structural properties of Tau. Samples characterization shows how Arachidonic Acid and Oleic Acid can induce the formation of Tau adducts, suggesting that these phenomena could be correlated firstly to the specific property of FAs to form micelles and secondly to their elevated concentration levels in AD.

4.2.7 **Figures**

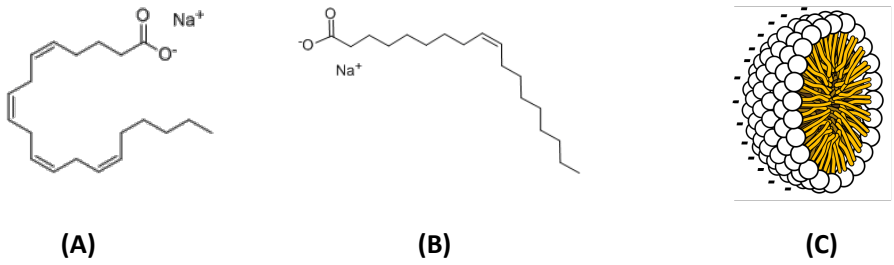

Figure 1: Chemical Structures of FAs used in this work and illustration of a Micelle structure. (A) Arachidonic Acid (20:4); (B) Oleic Acid (18:1), (C) Fatty acid micelles.

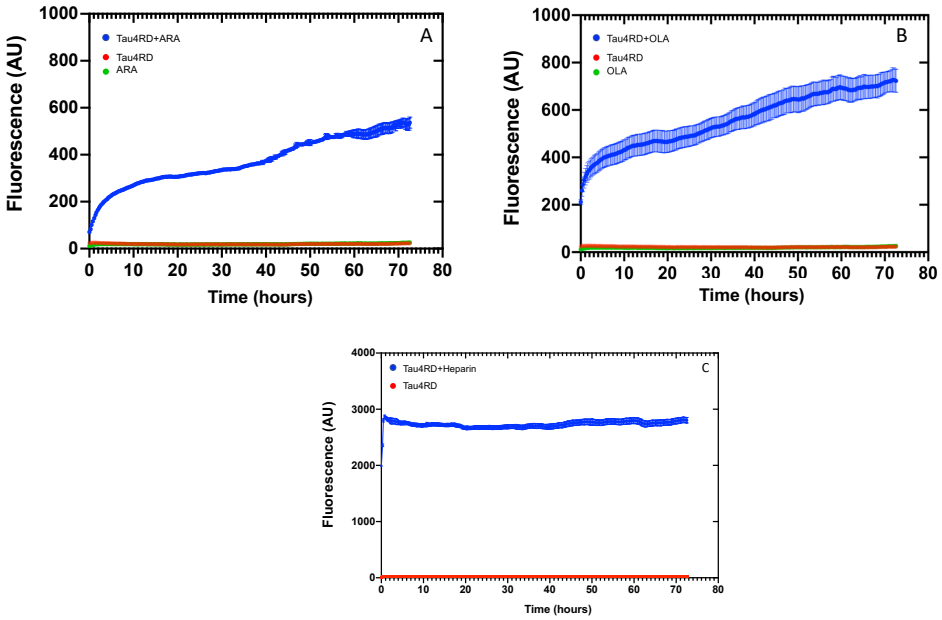

Figure 2: Kinetics of protein aggregation followed by ThT-fluorescence. Aggregation assay was done at 37 °C for 72 h. Samples contained Tau4RD and FAs at 1:3 molar ratio (A) Tau4RD+Arachidonic Acid; (B) Tau4RD+Oleic Acid. (C) Tau4RD in the presence of Heparin at 4:1 molar ratio.

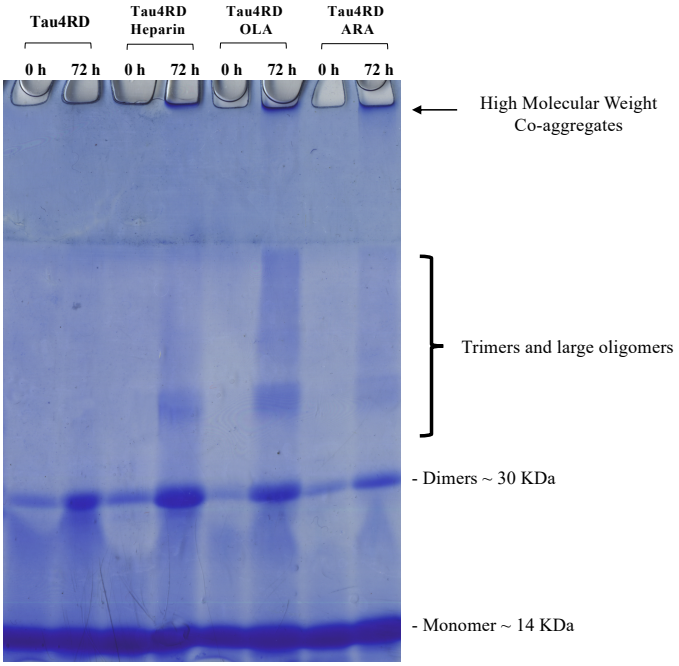

Figure 3: Non-reducing gradient SDS-PAGE (10-17%) shows the formation of high molecular weight co-aggregates, trimers and large oligomers, of Tau4RD in presence of heparin or fatty acids after 72 h of incubation.

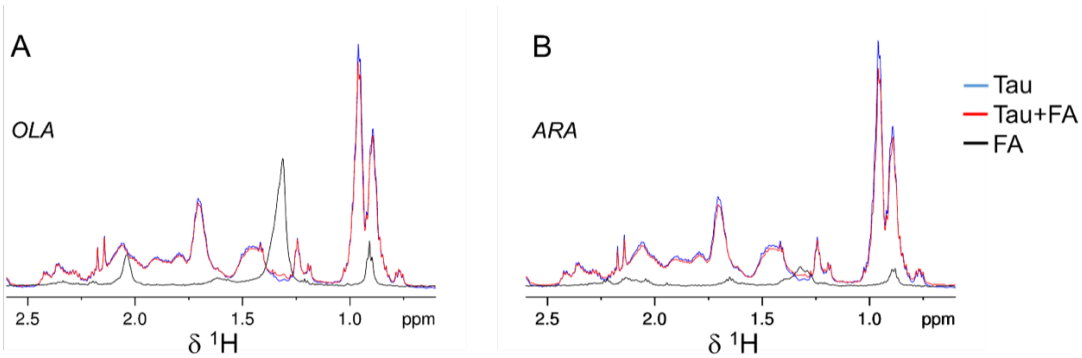

Figure 4: 1H-NMR profiles of Tau4RD and fatty acids. High-field portion of 1H-NMR spectra of 25 µM Tau4RD (blue), 75 µM fatty acid (FA, black), and 25 µM Tau4RD mixed with 75 µM fatty acid (red). Measurements were performed at 37 °C.

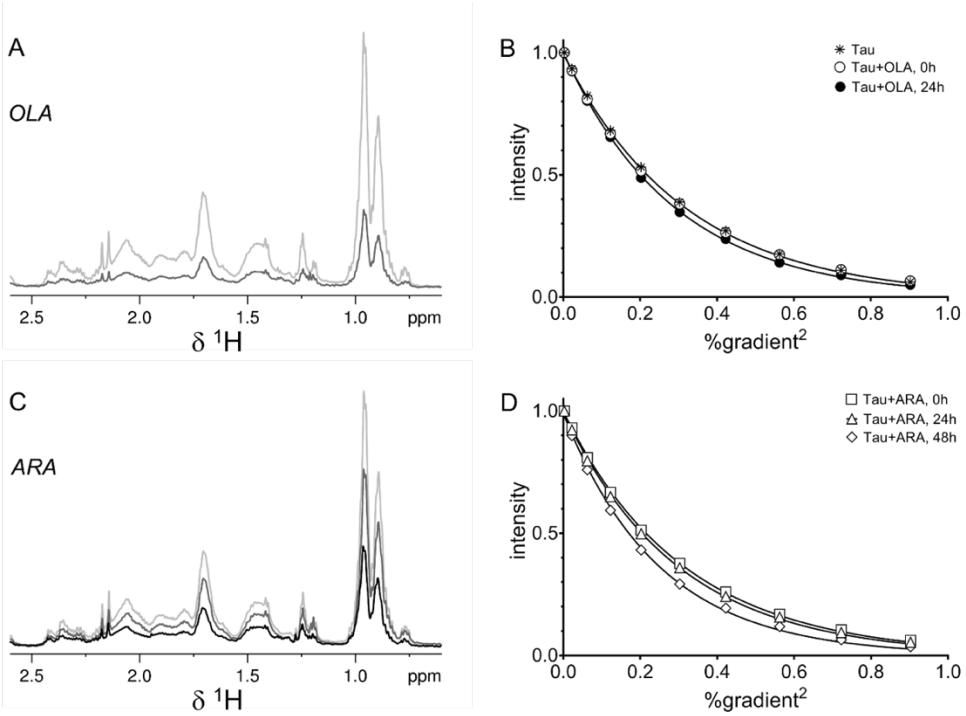

Figure 5: *[1]H-NMR measurements of Tau4RD monomer depletion and translational diffusion*. High-field region of [1]H-NMR spectra (A) and translational diffusion experiments (B) recorded on Tau4RD in the presence of OLA. High-field region of [1]H-NMR spectra (C) and translational diffusion experiments (D) recorded on Tau4RD in the presence of ARA. In B and D, the intensity of a selected signal is shown as a function of the square of the fraction of gradient used. Samples contained 25 µM Tau4RD and 75 µM fatty acid. A, C) Spectra were collected on samples that were incubated 0 h (gray), 24 h (dark gray), and 48 h (black). B) Samples were incubated 0 h (empty circles) and 24 h (filled circles), and asterisks denote data collected on Tau4RD in the absence of fatty acid. D) Samples were incubated 0 h (empty squares), 24 h (empty triangles), 48 h (empty diamonds). B, D) Lines are fitted exponential curves. Aggregation of 100 µM protein was induced with 300 µM fatty acid and magnetic stirring. Samples were kept at 37 °C during both incubation and measurement.

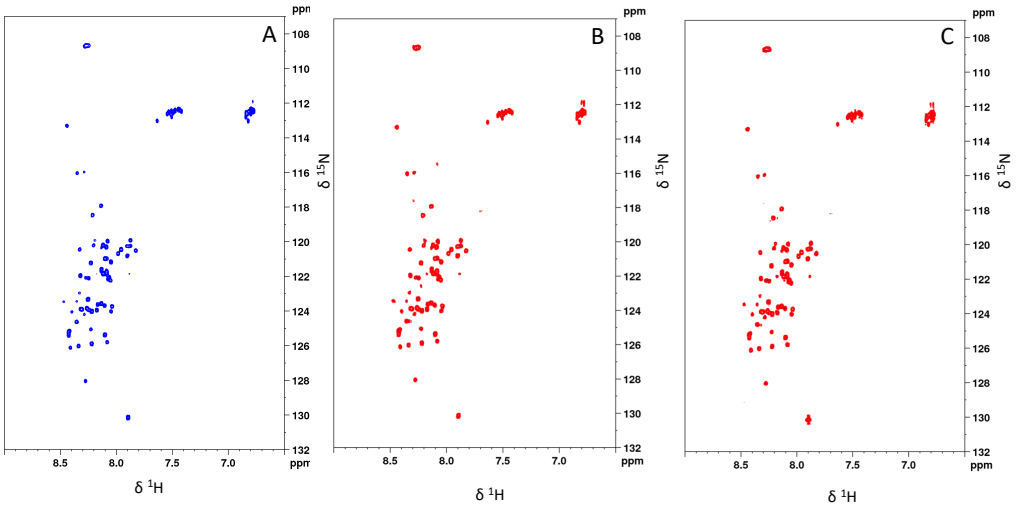

Figure 6: [1]H-[15]N-NMR spectra of Tau4RD in absence of fatty acid (panel A) and after the immediate addition of Arachidonic Acid (panel B) an Oleic Acid (panel C).

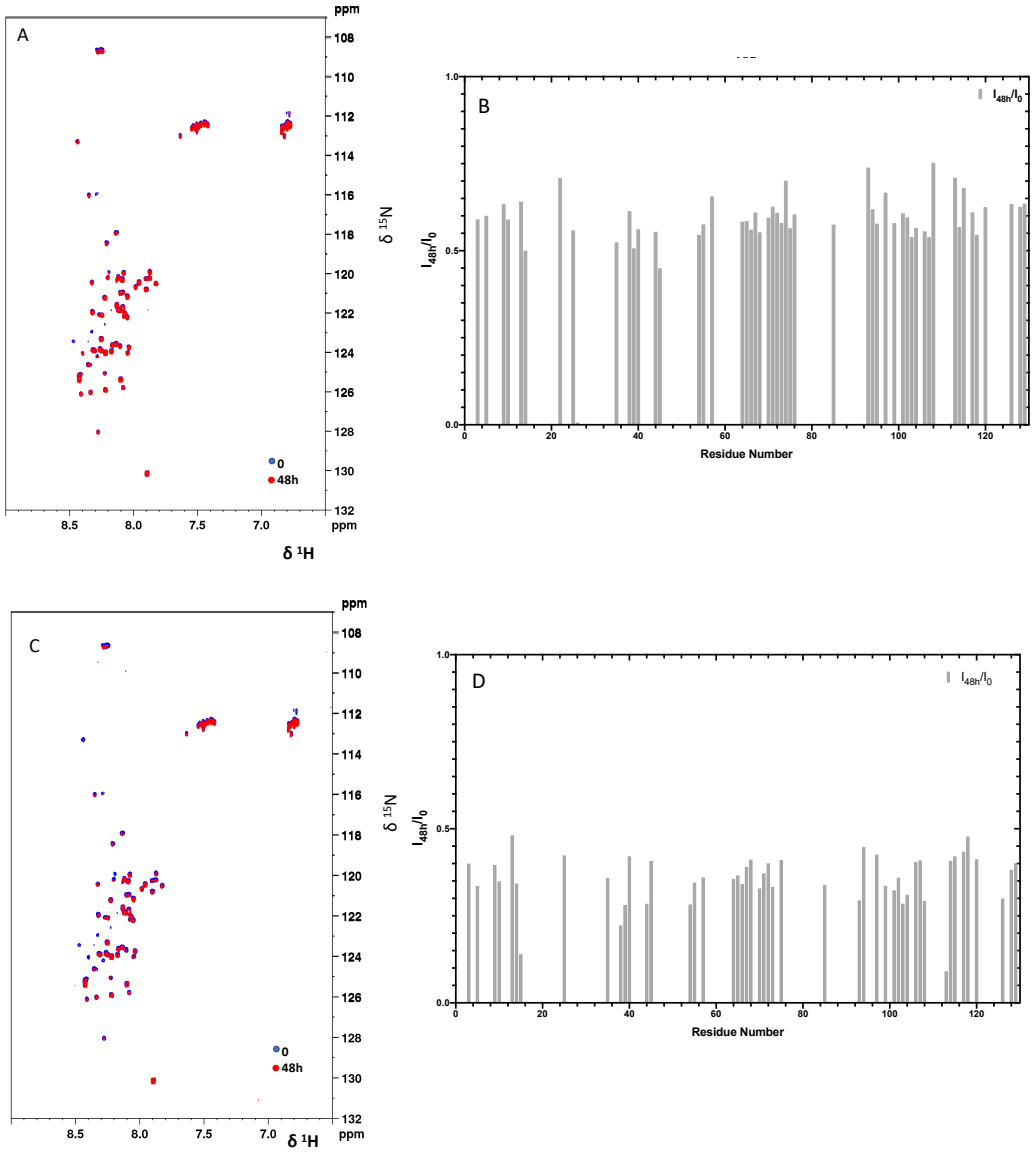

Figure 7: Superimposition of two 1H-15N-HSQC NMR spectra of ^{15}N-Tau4RD: (A) after the immediate addition of ARA (blue spectrum) and after 48 h of incubation at 37 °C (red spectrum); (C) after the immediate addition of OLA (blue spectrum) and after 48 h of incubation at 37 °C (red spectrum). Relative signal intensity obtained from HSQC spectra measured on (C) ^{15}N-Tau4RD: ARA and (D) ^{15}N-TauRD:OLA, after the immediate addition of FA (I_0) and after 48h (I_{48h}).

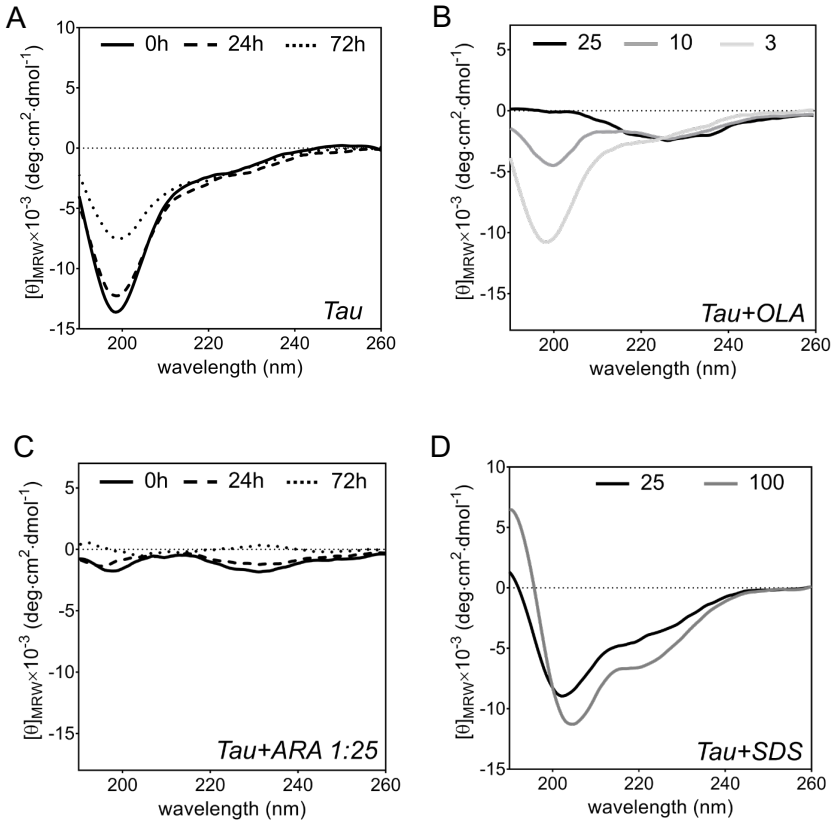

Figure 8: Effect of micelles on the secondary structure of Tau4RD. Far-UV CD spectra of Tau4RD (A) recorded after 0h-24h-72h of incubation at 37°C; (B) in the presence of OLA micelles at different molar ratios (P:FA = 1:3, 1:10, 1:25); (C) in the presence of of ARA micelles at a P:FA molar ratio of 1:25 after 0 h, 24 h, 72 h of incubation at 37°C. (D) Effect of SDS micelles on Tau4RD at P:SDS molar ratios of 1:125 and 1:100.

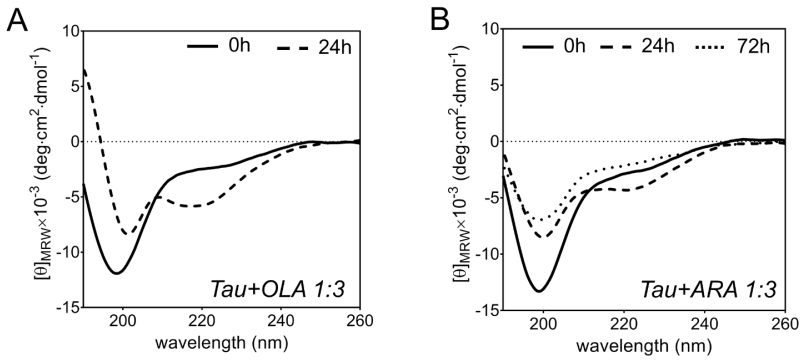

Figure 9: CD spectra of Tau4RD in presence of ARA (A) and OLA (B) after incubation at 37 °C. Incubation times are indicated in the figures.

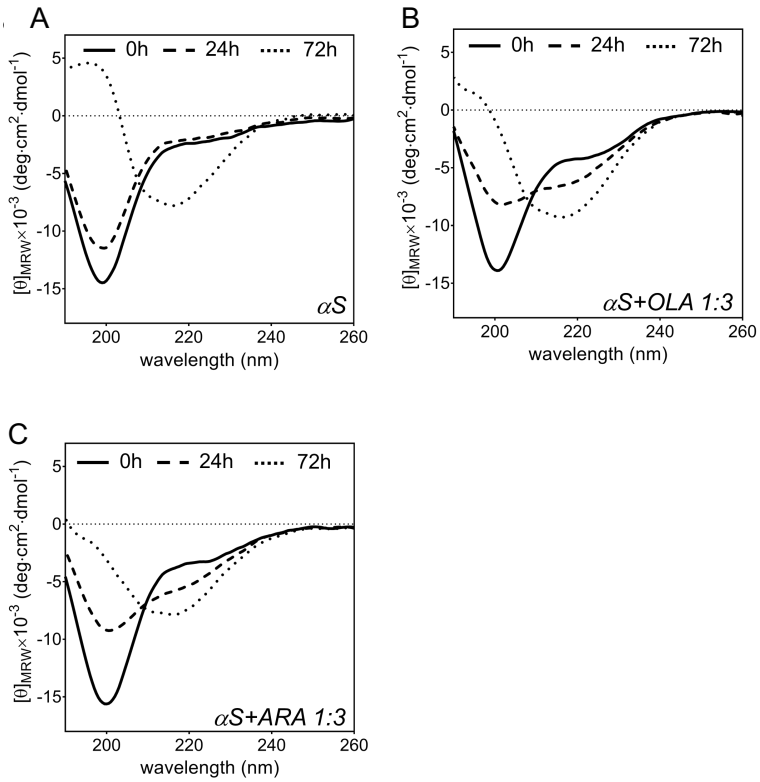

Figure 10: CD spectra of α-synuclein (A), in presence of Arachidonic Acid (B) and Oleic Acid(C) (P/FA 1:3). Incubation times are indicated in the figures.

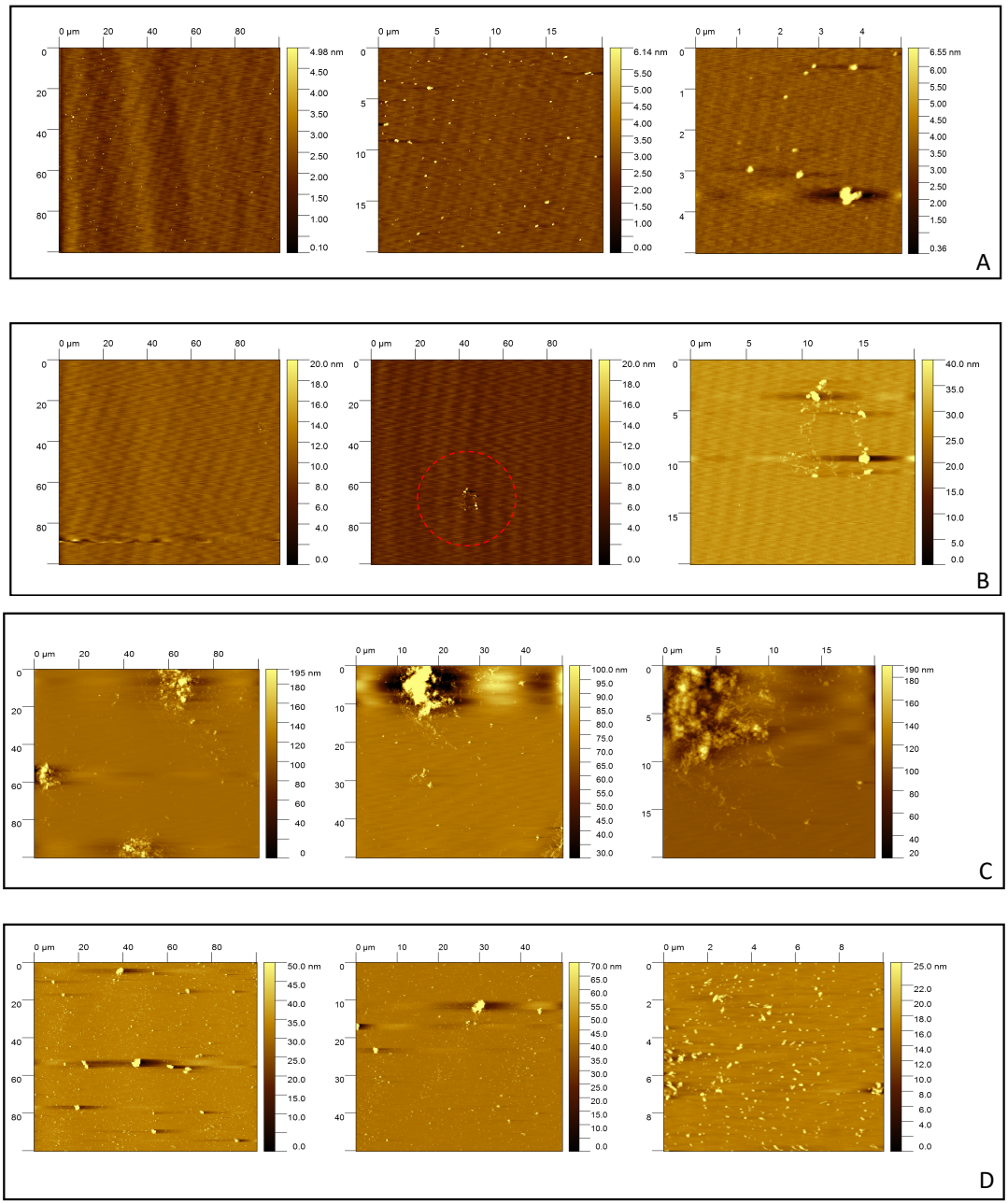

Figure 11: AFM micrographs of Tau4RD co-aggregates obtained from the aggregation of Tau4RD in presence of micelles of fatty acid, immediately after mixing and after 24h of incubation. Oleic Acid micelles at t0 (A) and 24h (C), arachidonic acid at t0 (B) and 24h (D).

4.2.8 References

[1] Brandt, R.; Léger, J.; Lee, G. Interaction of Tau with the Neural Plasma Membrane Mediated by Tau's Amino-Terminal Projection Domain. *Journal of Cell Biology* **1995**, *131* (5), 1327–1340. https://doi.org/10.1083/jcb.131.5.1327.

[2] Wilson, D. M.; Binder, L. I. Free Fatty Acids Stimulate the Polymerization of Tau and Amyloid Beta Peptides. In Vitro Evidence for a Common Effector of Pathogenesis in Alzheimer's Disease. *Am J Pathol* **1997**, *150* (6), 2181–2195.

[3] Martin, L.; Latypova, X.; Terro, F. Post-Translational Modifications of Tau Protein: Implications for Alzheimer's Disease. *Neurochem. Int.* **2011**, *58* (4), 458–471. https://doi.org/10.1016/j.neuint.2010.12.023.

[4] Miller, A. J.; Roman, B.; Norstrom, E. A Method for Easily Customizable Gradiet Gel Electrophoresis. *Analytical Biochemistry* **2016**, *509*, 12–14. https://doi.org/10.1016/j.ab.2016.07.003.

[5] Karikari, T. K.; Turner, A.; Stass, R.; Lee, L. C. Y.; Wilson, B.; Nagel, D. A.; Hill, E. J.; Moffat, K. G. Expression and Purification of Tau Protein and Its Frontotemporal Dementia Variants Using a Cleavable Histidine Tag. *Protein Expr. Purif.* **2017**, *130*, 44–54. https://doi.org/10.1016/j.pep.2016.09.009.

[6] Barré, P.; Eliezer, D. Structural Transitions in Tau K18 on Micelle Binding Suggest a Hierarchy in the Efficacy of Individual Microtubule-Binding Repeats in Filament Nucleation. *Protein Sci.* **2013**, *22* (8), 1037–1048. https://doi.org/10.1002/pro.2290.

[7] Iljina, M.; Tosatto, L.; Choi, M. L.; Sang, J. C.; Ye, Y.; Hughes, C. D.; Bryant, C. E.; Gandhi, S.; Klenerman, D. Arachidonic Acid Mediates the Formation of Abundant Alpha-Helical Multimers of Alpha-Synuclein. *Sci Rep* **2016**, *6*, 33928. https://doi.org/10.1038/srep33928.

[8] Wiśniewska-Becker, A.; Gruszecki, W. I. 2 - Biomembrane Models. In *Drug-Biomembrane Interaction Studies*; Pignatello, R., Ed.; Woodhead Publishing Series in Biomedicine; Woodhead Publishing, 2013; pp 47–95. https://doi.org/10.1533/9781908818348.47.

[9] Gundloori, R. V.; Singam, A.; Killi, N. Chapter 19 - Nanobased Intravenous and Transdermal Drug Delivery Systems. In *Applications of Targeted Nano Drugs and Delivery Systems*; Mohapatra, S. S., Ranjan, S., Dasgupta, N., Mishra, R. K., Thomas, S., Eds.; Micro and Nano Technologies; Elsevier, 2019; pp 551–594. https://doi.org/10.1016/B978-0-12-814029-1.00019-3.

4.2.9 Supporting Information

Lipid Micelles

The chemical structure of lipid molecules is characterized by a hydrophobic and hydrophilic region, that determines their behavior in an aqueous environment. Hydrophobic regions tend to self-associate, whereas hydrophilic moieties preferably interact with water and with each other. This leads to the spontaneous formation of particular structures such as micelles [8].

Micelle represents the simplest association structure, in which the lipid hydrophilic head group is in direct contact with the surrounding aqueous phase, whereas the hydrophobic region is forming the micelle core (Figure S3). Micelles are approximately spherical in shape, although other shapes, are possible, depending on concentration, temperature, pH and ionic strength. Usually, association in micelles occurs when the lipid molecules reach a threshold concentration in solution known as the Critical Micelle Concentration (CMC) [9]. Below this value, the molecules exist as a single chain in a molecular dispersion. However, when molecule concentration is increased, aggregation takes place within a rather narrow concentration range. The CMC is therefore defined as the concentration of surfactant at a given temperature where the first micelle begins to form [9].

Dynamic light scattering (DLS) was used in this work to perform a qualitative analysis of the CMC value of micelles formed in solution. When the CMC is reached in solution, there is a sudden increase in intensity of scattered light due to the formation of micelles (Figure S4). Evidence for micelle formation comes from the correlation function curves. Experimental correlation function data for all the concentration of DLS measurement are given in Figure S4. The correlation functions show very poor signal at very low interception, at very low concentration (below the CMC) $\leq$ 0.01 mM.

However, when the CMC is reached, the intensity of scattered light increases due to the presence of micelles, and the intercepts of correlation function become much higher, 0.6-0.9, as seen in the DLS measurement (Figure S4).

4.2.10 **Supplementary figures**

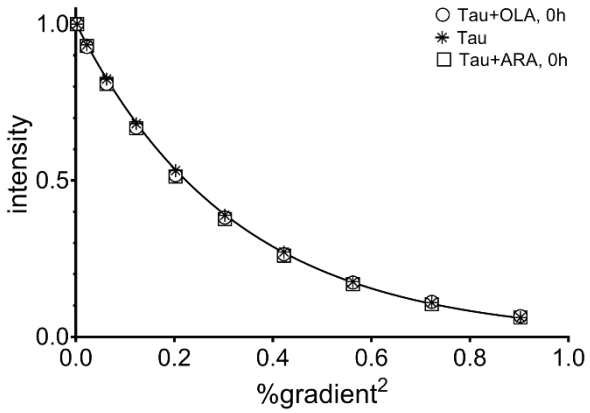

Figure S1. *Translational diffusion of Tau^{4RD} in the presence of fatty acids*. The intensity of a selected signal is shown as a function of the square of the fraction of gradient used. Samples contained 25 µM Tau^{4RD} and no fatty acid (asterisks and fitted curve), 75 µM OLA (empty circles), or 75 µM ARA (empty squares). Measurements were performed immediately after sample preparation, at 37 °C.

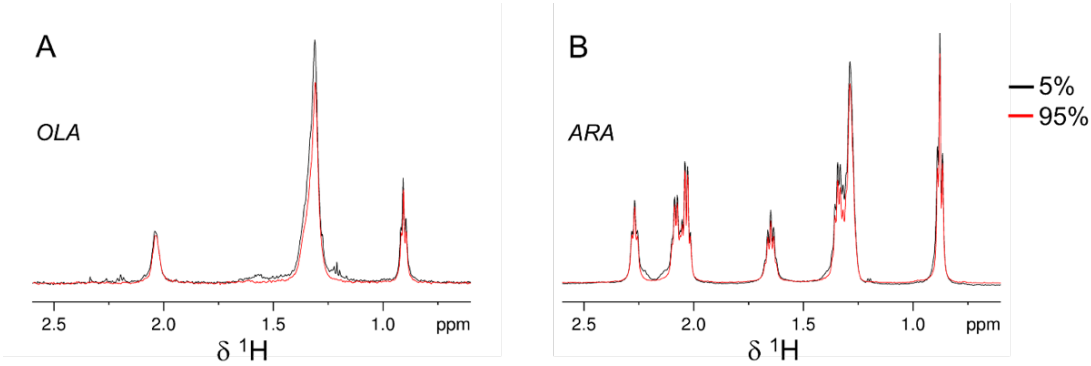

Figure S2. *Translational diffusion of fatty acid*. The displayed NMR diffusion spectra were recorded with 5% (black) and 95% (red) of the maximum gradient strength (53.5 G/cm) and a diffusion delay of 200 ms. The samples contained 75 µM OLA (A) or 500 µM ARA (B). The measurement temperature was 37 °C.

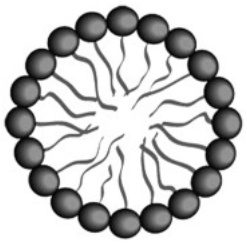

Figure S3: Representation of fatty acid micelle

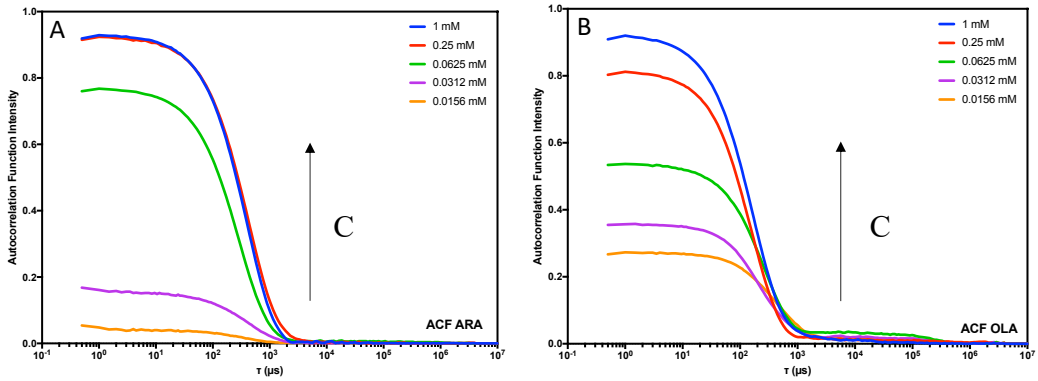

Figure S4: Investigation of micelles formation of fatty acids. Autocorrelation Function (ACF) of Arachidonic Acid (A) and Oleic Acid (B) at various concentrations

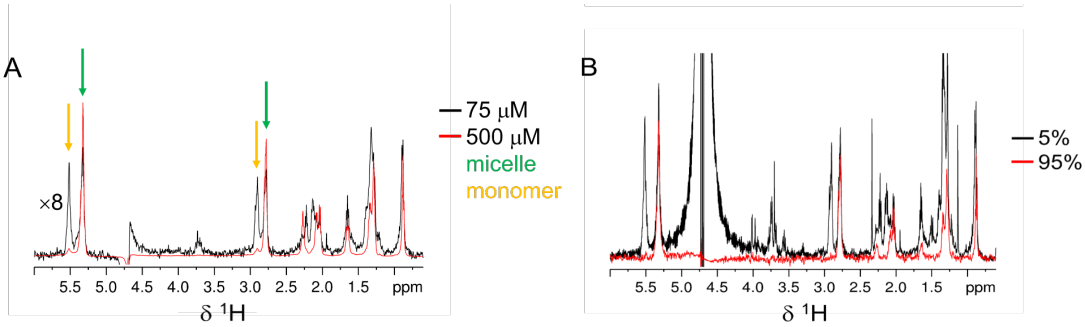

Figure S5: *NMR analysis of ARA micelle formation*. A) Portion of ^{1}H NMR spectrum of ARA dissolved at a concentration of 75 μM (black) or 500 μM (red). The intensity of the spectrum at lower concentration was multiplied by 8 for better comparison. B) Diffusion NMR spectra recorded on 75 μM ARA with 5% (black) and 95% (red) of the maximum gradient strength. Peaks indicated by green (orange) arrows are attributed to ARA micelles (monomers).

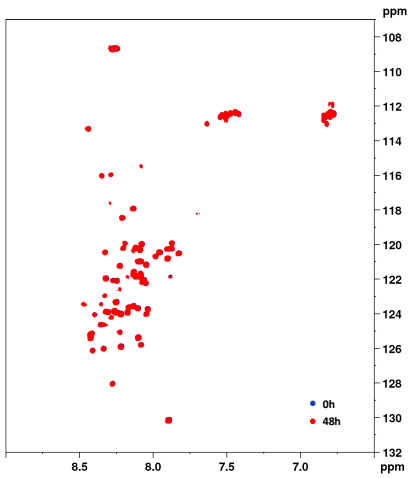

Figure S6: Superimposition of two1H-15N-HSQC NMR spectra of ^{15}N-Tau4RD (blue spectrum) and after 48h of incubation at 37 °C (red spectrum), as expected no perturbation are observed.

4.3 Study of nanoparticle-induced conformational transitions of amyloidogenic protein Tau at single residue resolution

Aberrant aggregation of specific proteins and peptides and their progressive accumulation as insoluble deposits of amyloid fibrils are hallmarks of a growing number of neurodegenerative diseases [1,2]. Among these proteins, Tau, a prototypical amyloidogenic protein, in solution populates an ensemble of rapidly interconverting structures that eventually transition to higher-order aggregates such as oligomers and fibrils [3]. Perturbing the dynamic interconversion among conformational states with small molecules, macromolecules, and nanoparticles (NPs) offers the possibility to redirect the formation of neurotoxic aggregates [4-7].

In recent years, NPs have attracted increasing interest as aggregation modulators, and have been proposed as systems to either accelerate or inhibit fibrillogenesis. The specific effects depend on their properties (size, charge, hydrophobicity, material), the environment (pH, ionic strength, temperature), NP/P molar ratios, and the protein intrinsic aggregation propensities [10]. However, despite intense investigations, our understanding of how amyloidogenic proteins interact with NPs remains limited, and general paradigms are still lacking [12].

Solution NMR experiments have been increasingly used to describe the interaction of proteins with NPs at the individual residue level [13]. Indeed, recent efforts demonstrated that several NMR observables, such as chemical shifts, signal intensities, amide exchange rates and relaxation parameters, together with newly designed saturation transfer experiments, could be successfully employed to characterize the orientation, structure and dynamics of proteins adsorbing onto NP surfaces [14-22]. In addition, methodologies have been proposed to investigate protein molecules in higher order supramolecular structures [8].

In our work, we aimed to explore the general effects of NPs-proteins hybrid assemblies, with the goal of contributing to sustained nanotechnology and safe nanomedicine against amyloid diseases. We selected Ultrasmall Gold Nanoparticles (Figure 23), with a core size of about 3 nm, and conjugated with lipoic acid to enhance their stabilization, convenient for the investigation of NP-protein supramolecular complexes by NMR spectroscopy.

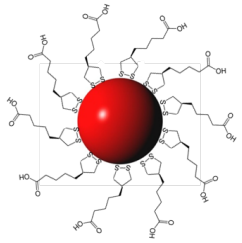

Lipoic Gold NPs

Figure 23: Schematic representation of Lipoic Gold Nanoparticles

The size is one of the key parameters that can influence NP-biomolecular interaction. Thus, these ultrasmall NPs were selected because may not form a protein corona and possibly lead to a 1:1 protein:NP assembly [9]. Moreover, gold was selected as the NPs core material because AuNPs are readily synthesized, easily functionalized, and highly stable against oxidative dissolution [10-11].

4.3.1 ^{1}H-^{15}N-NMR measurements

In order to investigate changes in chemical environment of the individual amino acid of Tau4RD in presence of NPs, we performed experiments on a high-resolution NMR spectrometer operating at 1 GHz proton frequency.

Two-dimensional ^{1}H-^{15}N-HSQC spectra were recorded on Tau4RD in the absence (Figure 1A) and in the presence of Lip@AuNPs at different molar ratios (6:1 and 3:1) (Figure 1B and C). In these experiments, the protein in the hybrid assemblies was in excess with respect to the NPs, therefore both free and bound protein molecules were present in solution.

The addition of NPs (Figure 1B and C) did not change significantly peaks position but caused evident perturbation in peak intensities. Indeed, a progressive decrease of protein peaks intensity was observed, due to the formation of larger hybrid assemblies where the protein experiences slower rotation tumbling.

The plots of normalized intensities as a function of residue number (Figure 2) show that the interaction is not residue specific but show only a uniform perturbation across the residues.

4.3.2 **Transverse Relaxation Measurements**

Further investigation about the possibility to obtain information about the NP-bound state of Tau4RD, through the analysis of transverse relaxation rate values, ^{15}N-R_2, was explored. The ^{15}N-R_2 values for Tau4RD (Figure 3A) plotted versus residue number, displayed a fairly homogeneous relaxation profile for the unbound state (red dots), as expected for a disordered protein. After addition of NPs, the relaxation rates plot (blue dots) displayed only small values, reflecting the fast-rotational tumbling of all amino acids along the protein sequence, in analogy with the sample containing only protein.

Normally, when NPs are added to the solution containing proteins, the protein signals are expected to be perturbed depending on the nature of the NP-protein interaction. On the contrary, in our sample, after the addition of Lip@AuNPs, ^{15}N-R_2 values for all residues did not show increased values indicative of slow rotational dynamics (red dots) and all residues exhibited similar behavior as the free state. This could be due to a slow exchange regime, in which the bound species dissociates at a slow rate from the surface of the NPs. In other words, the observed signals report on the unbound state and do not appear to be exchange-averaged over the bound and unbound forms.

For comparison purposes, we investigated the transverse relaxation changes with another amyloidogenic protein, α-synuclein. As Tau4RD, the ^{15}N-R_2 values for α-synuclein (Figure 3B) are consistent with the fast mobility of the entire protein (blue dots). However, after the addition of NPs, it's possible to observe a modification of the relaxation profile (red dots). The values of the first sixty amino acids became much larger compared to the values of α-synuclein alone. Followed, then, by a gradual decrease towards the C-terminus region, with values that were essentially identical to those of the free protein. This effect could be due to a lifetime line-broadening effect originating from an exchange between free and bound states during experiment acquisition.

4.3.3 **Saturation Transfer Measurements**

In order to obtain information on the interaction kinetics and a residue-by-residue dynamics, dark-state exchange saturation transfer (DEST) measurements

were performed. This innovative solution-NMR method, developed by Fawzi and co-workers, relies on saturation transfer to provide information on the invisible state ("dark") (nanoparticles-protein) in chemical exchange with visible states (protein). In other words, in this kind of experiment, when the invisible state is saturated [8,12], the saturation will be transferred by the chemical exchange to the visible state, leading to a decrease in the intensity of the latter [13]. Combining DEST and two-dimensional ^{1}H-^{15}H-HSQC experiments allows for a single residue resolution of dynamic information of the relaxation. Furthermore, combining the measurement of the relaxation rate in the presence and absence of nanoparticles (ΔR_2), it is possible characterize the interaction kinetic and molecular motion of bound states.

The experimental ^{15}N-DEST profiles and ΔR_2 data, collected from the sample Tau4RD:Lip@AuNP, molar ratio 6:1, as described in Materials and Method (3.8.5) were plotted using *DESTfit* software [12] (Figure 5A) .

The obtained saturation profiles clearly display the absence of an optimal match between the experimental best-fit parameters obtained with *DESTfit* (Figure 5). This result could be explained by the direct observation of the ΔR_2. The values of ΔR_2 (Figure 4A) were equal to zero at all residue positions, thus a ΔR_2 not greater than 0.2 s^{-1} is directly connected with an insufficient population of dark state, or a timescale not appropriate for observing the effect. Consequently, as next step, it will necessary to modify sample conditions on order to promote an increased conversion rate from the NMR-visible to the dark species. This can often be accomplished by increasing the concentration of the dark state. However, the absence of saturation could also due to saturation power too weak. Thus, it will be necessary also to increase the saturation power, in the next experiment.

On the contrary, for the sample α-syn:Lip@AuNPs, the large difference of ΔR_2 values between the bound and the free state, enable the observation of DEST (Figure 4B and 5B). The observed residue-specific saturation transfer profile can be attributed to a lifetime line-broadening effect originating from an exchange between free and bound states during experiment acquisition.

4.3.4 **Conclusion**

The interaction between Ultrasmall Gold Nanoparticles and Tau4RD has been highlighted notably by NMR spectroscopy. The presence of nanoparticles produced a variation of the protein fingerprint observed with ^{1}H-^{15}N-HSQC spectra. Indeed, the 2D NMR data indicated a general decrease in signals intensity, due to the formation of the hybrid assemblies (Figure 1 and 2). At present, we were not able to gather information on the bound state based on relaxation measurements and DEST spectroscopy, possibly due unfavorable kinetics of exchange (Figure 5).

Thus, further investigations are needed to fully characterize the inter-structure between these two species. In order to later characterized the implication of this interaction in the protein aggregation processes.

4.3.5 **Figures**

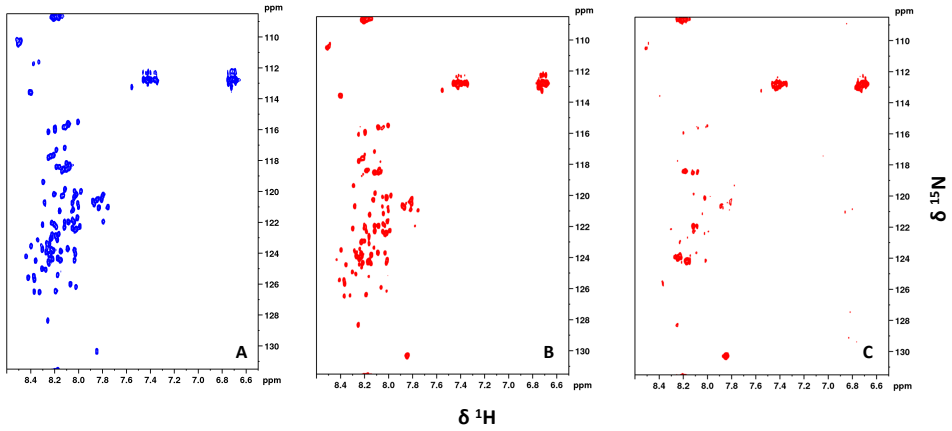

Figure 1: HSQC of Tau4RD in absence/presence of Lip@AuNPs. (A) Tau4RD; (B) Tau4RD:Lip@AuNPs (6:1); (C) Tau4RD:Lip@AuNPs (3:1). Spectra were collected on 1 GHz NMR spectrometer equipped with solution-state cryogen probe. Experiment temperature: 283 K. (Upon addition of NPs, almost negligible chemical shift variations are observed).

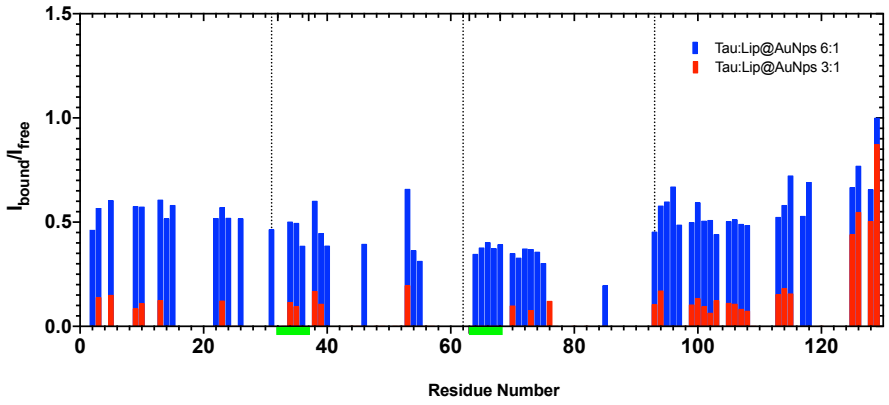

Figure 2: Relative signal intensities obtained from ^{15}N-HSQC spectra measured on 15N-Tau4RD in 10mM KPi pH 6.8 at 283 K, in presence of Lip@AuNPs at different molar ration 6:1 in blue and 3:1 in red.

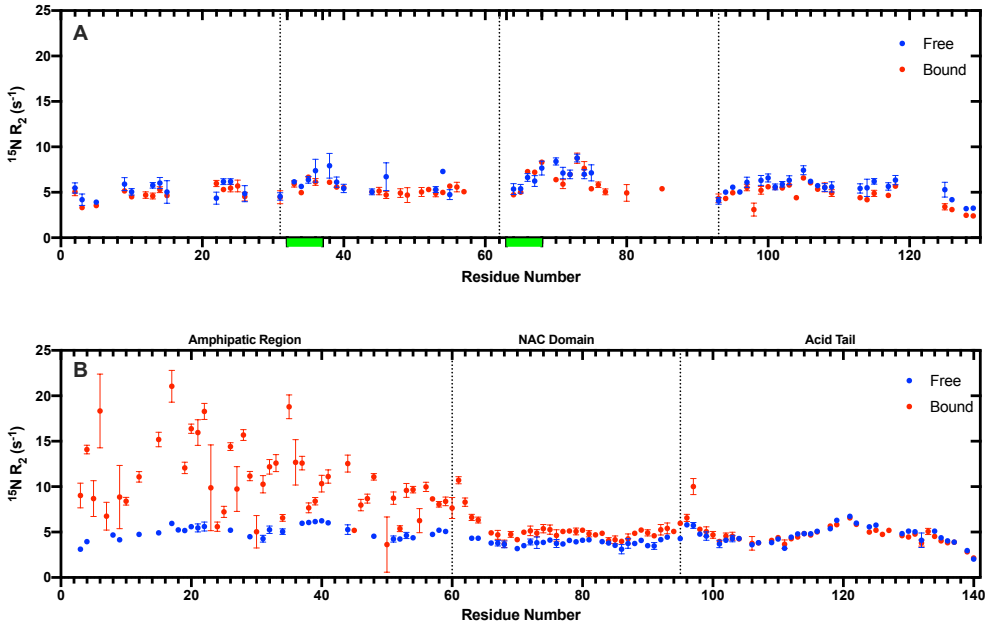

Figure 3: ^{15}N transverse relaxation rate value. (A) Plot of 15N-R2 values of Tau4RD measured in the absence (blue dots) and presence of Lip@AuNPs, for a molar ratio of 6:1 (red dots) (green regions represent the two hexapeptide motifs). (B) Plot of R2 value of α-Synuclein measure in the absence (blue dots) and presence of Lip@AuNPs, for a molar ratio of ~ 20:1 (red dots).

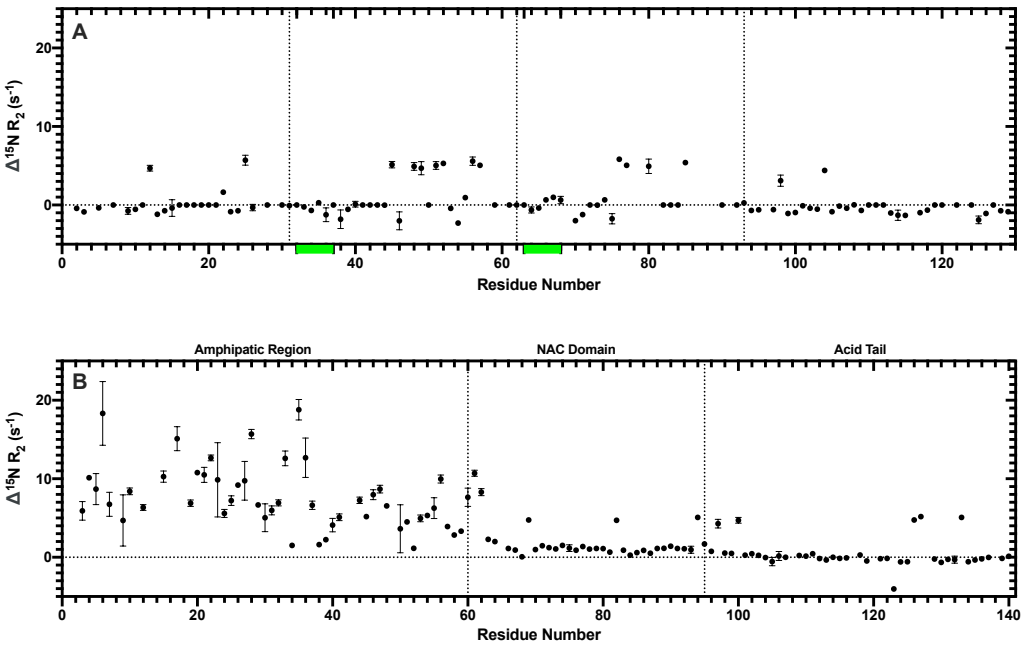

Figure 4: ΔR_2 value. Difference of R_2 values (showed in figure 3A and B) measured on samples of (A) Tau4RD and (B) α-synuclein, in the absence and presence of NPs. (green regions represent the two hexapeptide motifs).

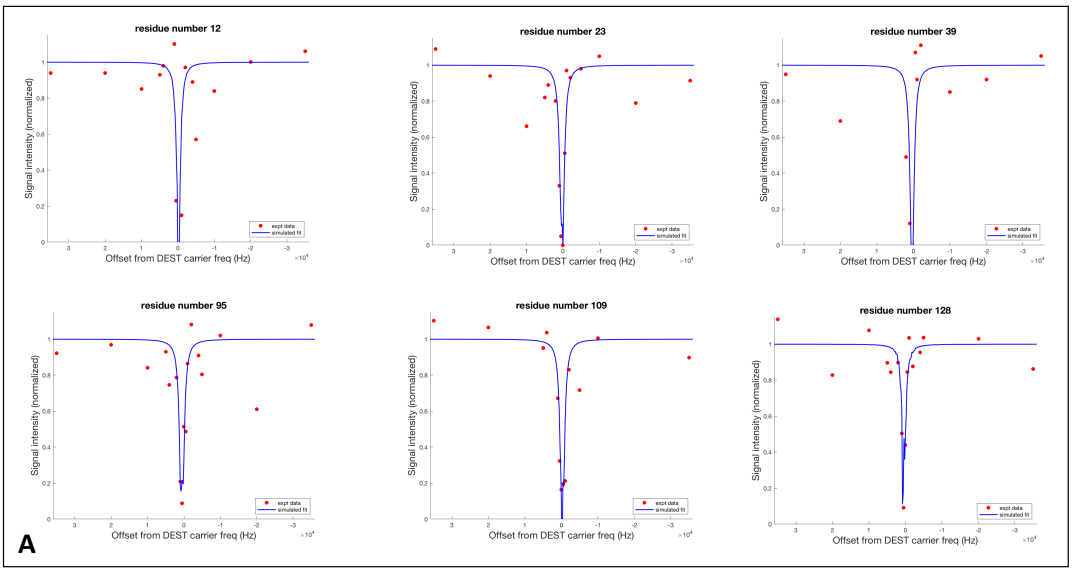

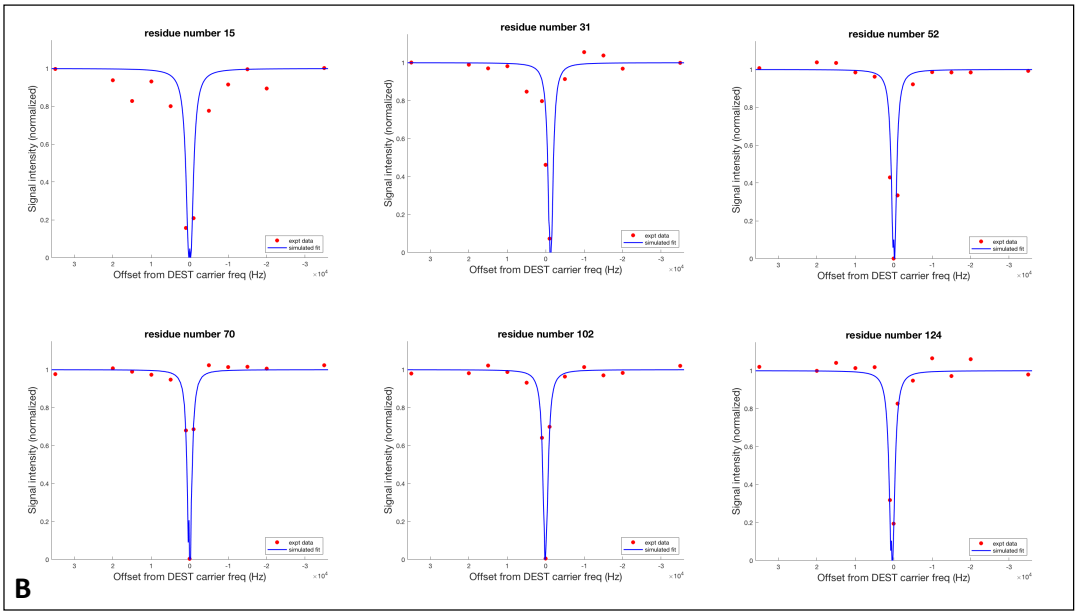

Figure 5: 15N-DEST profiles observed for some representative residue for Tau4RD (A) and α-synuclein (B) in presence of Lip@AuNPs. Screenshots of figure output from the *DESTfit* software: comparison of experimental (red dots) and calculated (blue lines) data.

4.3.6 References

[1] Ross, C. A.; Poirier, M. A. Protein Aggregation and Neurodegenerative Disease. *Nat. Med.* **2004**, *10 Suppl*, S10-17. https://doi.org/10.1038/nm1066.

[2] Soto, C.; Pritzkow, S. Protein Misfolding, Aggregation, and Conformational Strains in Neurodegenerative Diseases. *Nat Neurosci* **2018**, *21* (10), 1332–1340. https://doi.org/10.1038/s41593-018-0235-9.

[3] Nath, A.; Sammalkorpi, M.; DeWitt, D. C.; Trexler, A. J.; Elbaum-Garfinkle, S.; O'Hern, C. S.; Rhoades, E. The Conformational Ensembles of α-Synuclein and Tau: Combining Single-Molecule FRET and Simulations. *Biophysical Journal* **2012**, *103* (9), 1940–1949. https://doi.org/10.1016/j.bpj.2012.09.032.

[4] Álvarez, Y. D.; Fauerbach, J. A.; Pellegrotti, J. V.; Jovin, T. M.; Jares-Erijman, E. A.; Stefani, F. D. Influence of Gold Nanoparticles on the Kinetics of α-Synuclein Aggregation. *Nano Lett.* **2013**, *13* (12), 6156–6163. https://doi.org/10.1021/nl403490e.

[5] Eisele, Y. S.; Monteiro, C.; Fearns, C.; Encalada, S. E.; Wiseman, R. L.; Powers, E. T.; Kelly, J. W. Targeting Protein Aggregation for the Treatment of Degenerative Diseases. *Nat Rev Drug Discov* **2015**, *14* (11), 759–780. https://doi.org/10.1038/nrd4593.

[6] Kurnik, M.; Sahin, C.; Andersen, C. B.; Lorenzen, N.; Giehm, L.; Mohammad-Beigi, H.; Jessen, C. M.; Pedersen, J. S.; Christiansen, G.; Petersen, S. V.; et al. Potent α-Synuclein Aggregation Inhibitors, Identified by High-Throughput Screening, Mainly Target the Monomeric State. *Cell Chemical Biology* **2018**, *25* (11), 1389-1402.e9. https://doi.org/10.1016/j.chembiol.2018.08.005.

[7] Pujols, J.; Peña-Díaz, S.; Lázaro, D. F.; Peccati, F.; Pinheiro, F.; González, D.; Carija, A.; Navarro, S.; Conde-Giménez, M.; García, J.; et al. Small Molecule Inhibits α-Synuclein Aggregation, Disrupts Amyloid Fibrils, and Prevents Degeneration of Dopaminergic Neurons. *PNAS* **2018**, *115* (41), 10481–10486. https://doi.org/10.1073/pnas.1804198115.

[8] Fawzi, N. L.; Ying, J.; Ghirlando, R.; Torchia, D. A.; Clore, G. M. Atomic-Resolution Dynamics on the Surface of Amyloid-β Protofibrils Probed by Solution NMR. *Nature* **2011**, *480* (7376), 268–272. https://doi.org/10.1038/nature10577.

[9] Lira, A. L.; Ferreira, R. S.; Torquato, R. J. S.; Zhao, H.; Oliva, M. L. V.; Hassan, S. A.; Schuck, P.; Sousa, A. A. Binding Kinetics of Ultrasmall Gold Nanoparticles with Proteins. *Nanoscale* **2018**, *10* (7), 3235–3244. https://doi.org/10.1039/C7NR06810G.

[10] Daniel, M.-C.; Astruc, D. Gold Nanoparticles: Assembly, Supramolecular Chemistry, Quantum-Size-Related Properties, and Applications toward Biology, Catalysis, and Nanotechnology. *Chem. Rev.* **2004**, *104* (1), 293–346. https://doi.org/10.1021/cr030698+.

[11] De Roe, C.; Courtoy, P. J.; Baudhuin, P. A Model of Protein-Colloidal Gold Interactions. *J. Histochem. Cytochem.* **1987**, *35* (11), 1191–1198. https://doi.org/10.1177/35.11.3655323.

[12] Fawzi, N. L.; Ying, J.; Torchia, D. A.; Clore, G. M. Probing Exchange Kinetics and Atomic Resolution Dynamics in High-Molecular-Weight Complexes Using Dark-State Exchange Saturation Transfer NMR Spectroscopy. *Nat Protoc* **2012**, *7* (8), 1523–1533. https://doi.org/10.1038/nprot.2012.077.

[13] Giuntini, S.; Cerofolini, L.; Ravera, E.; Fragai, M.; Luchinat, C. Atomic Structural Details of a Protein Grafted onto Gold Nanoparticles. *Sci Rep* **2017**, *7* (1), 1–6. https://doi.org/10.1038/s41598-017-18109-z.

[14] Haiss, W.; Thanh, N. T. K.; Aveyard, J.; Fernig, D. G. Determination of Size and Concentration of Gold Nanoparticles from UV−Vis Spectra. *Anal. Chem.* **2007**, *79* (11), 4215–4221. https://doi.org/10.1021/ac0702084

4.3.7 **Supporting Information**

Gold Nanoparticle Preparation

Ultrasmall Lipoic Gold Nanoparticles were concentrated by several centrifugation from 0.6 μM (stock) to enough concentration that allowing their utilization for NMR measurement, and finally washed in the final buffer (10mM KPi pH 6.8). The concentration was calculated according the method developed by Haiss et al. [14].

Depending on the stock solution, the concentration obtained varies from 10 to 12 μM. UV-vis measurements were performed on a Nanodrop 2000C spectrophotometer (Thermo Scientific) at room temperature. In order satisfy the Beer-Lambert law condition, each stock was diluted by a dilution factor from 20 to 40. A spectral width from 300 to 800 nm was used in each case (Figure S1).

The measured absorbance at A_{450} nm was then divided by the extinction coefficient (ε_{450}nm) determined from the tables of the publication of *Haiss at al.* [14].

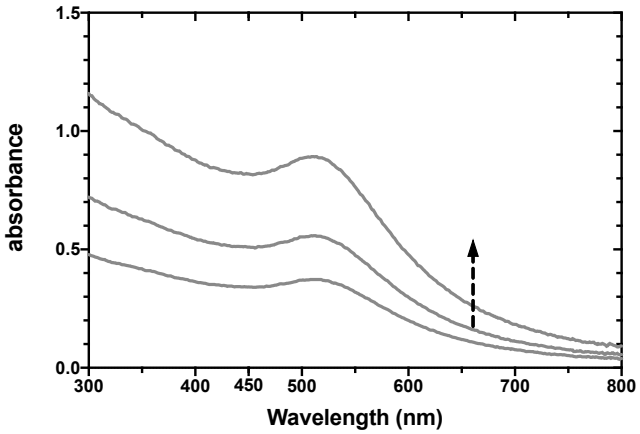

Figure 1: **UV-vis absorption spectrum of Lip@AuNPs**. The spectrum shows the absorbance of 1:20 diluted NPs solution.

5 References

(1) Moya-Alvarado, G.; Gershoni-Emek, N.; Perlson, E.; Bronfman, F. C. Neurodegeneration and Alzheimer's Disease (AD). What Can Proteomics Tell Us About the Alzheimer's Brain? *Mol Cell Proteomics* **2016**, *15* (2), 409–425. https://doi.org/10.1074/mcp.R115.053330.

(2) Heemels, M.-T. Neurodegenerative Diseases. *Nature* **2016**, *539* (7628), 179. https://doi.org/10.1038/539179a.

(3) Gitler, A. D.; Dhillon, P.; Shorter, J. Neurodegenerative Disease: Models, Mechanisms, and a New Hope. *Disease Models & Mechanisms* **2017**, *10* (5), 499–502. https://doi.org/10.1242/dmm.030205.

(4) World Alzheimer Report 2018 - The State of the Art of Dementia Research: New Frontiers. *Alzheimer's Disease International* **2018**, 48.

(5) Guo, T.; Noble, W.; Hanger, D. P. Roles of Tau Protein in Health and Disease. *Acta Neuropathol.* **2017**, *133* (5), 665–704. https://doi.org/10.1007/s00401-017-1707-9.

(6) Mark S Forman, V. M.-Y. L. Neurodegenerative Diseases: A Decade of Discoveries Paves the Way for Therapeutic Breakthroughs. *Nature Medicine* **2004**, *10*, 1055–1063. https://doi.org/10.1038/nm1113.

(7) Ernst, R. L. Cognitive Function and the Costs of Alzheimer Disease: An Exploratory Study. *Arch Neurol* **1997**, *54* (6), 687. https://doi.org/10.1001/archneur.1997.00550180013006.

(8) Skovronsky, D. M.; Lee, V. M.-Y.; Trojanowski, J. Q. Neurodegenerative Diseases: New Concepts of Pathogenesis and Their Therapeutic Implications. *Annual Review of Pathology: Mechanisms of Disease* **2006**, *1* (1), 151–170. https://doi.org/10.1146/annurev.pathol.1.110304.100113.

(9) Goedert, M.; Spillantini, M. G. A Century of Alzheimer's Disease. *Science* **2006**, *314* (5800), 777–781. https://doi.org/10.1126/science.1132814.

(10) Gustafson, L. Psychiatric Symptoms in Dementia with Onset in the Presenile Period. *Acta Psychiatrica Scandinavica* **1975**, *Suppl 257*, 9–35.

(11) Burns, A. Dementia—a Clinical Approach, 2nd Edn. Jeffrey Cummings and Frank Benson. Butterworth Heinemann, Boston, 1992. No. of Pages: 548. Price: $95. *International Journal of Geriatric Psychiatry* **1992**, *7* (12), 920–920. https://doi.org/10.1002/gps.930071213.

(12) Fratiglioni, L.; De Ronchi, D.; Agüero-Torres, H. Worldwide Prevalence and Incidence of Dementia. *Drugs Aging* **1999**, *15* (5), 365–375. https://doi.org/10.2165/00002512-199915050-00004.

(13) Johannes Wancata; M. Musalek,; R. Alexandrowicz; M. Krautgartner. Number of Dementia Sufferers in Europebetween the Years 2000 and 2050. *European Psychiatry* **2003**, *18*, 306–313. https://doi.org/10.1016/j.eurpsy.2003.03.003.

(14) Rönnemaa, E.; Zethelius, B.; Lannfelt, L.; Kilander, L. Vascular Risk Factors and Dementia: 40-Year Follow-Up of a Population-Based Cohort. *DEM* **2011**, *31* (6), 460–466. https://doi.org/10.1159/000330020.

(15) Rogers, J.; Webster, S.; Lue, L.-F.; Brachova, L.; Harold Civin, W.; Emmerling, M.; Shivers, B.; Walker, D.; McGeer, P. Inflammation and Alzheimer's Disease Pathogenesis. *Neurobiology of Aging* **1996**, *17* (5), 681–686. https://doi.org/10.1016/0197-4580(96)00115-7.

(16) Drouin, E.; Drouin, G. The First Report of Alzheimer's Disease. *The Lancet Neurology* **2017**, *16* (9), 687. https://doi.org/10.1016/S1474-4422(17)30258-2.

(17) Goedert, M.; Sisodia, S. S.; Price, D. L. Neurofibrillary Tangles and β-Amyloid Deposits in Alzheimer's Disease. *Current Opinion in Neurobiology* **1991**, *1* (3), 441–447. https://doi.org/10.1016/0959-4388(91)90067-H.

(18) Iqbal, K.; del C. Alonso, A.; Chen, S.; Chohan, M. O.; El-Akkad, E.; Gong, C.-X.; Khatoon, S.; Li, B.; Liu, F.; Rahman, A.; Tanimukai, H.; Grundke-Iqbal, I. Tau Pathology in Alzheimer Disease and Other Tauopathies. *Biochimica et Biophysica Acta (BBA) - Molecular Basis of Disease* **2005**, *1739* (2), 198–210. https://doi.org/10.1016/j.bbadis.2004.09.008.

(19) Petersen, R. C. Aging, Mild Cognitive Impairment, and Alzheimer's Disease. *Neurologic Clinics* **2000**, *18* (4), 789–805. https://doi.org/10.1016/S0733-8619(05)70226-7.

(20) Ezio Giacobini, G. G. Alzheimer Disease Therapy—Moving from Amyloid-β to Tau. *Nature Reviews Neurology* **2013**, *9*, 677–686. https://doi.org/10.1038/nrneurol.2013.223.

(21) Villemagne, V. L.; Burnham, S.; Bourgeat, P.; Brown, B.; Ellis, K. A.; Salvado, O.; Szoeke, C.; Macaulay, S. L.; Martins, R.; Maruff, P.; Ames, D.; Rowe, C. C.; Masters, C. L. Amyloid β Deposition, Neurodegeneration, and Cognitive Decline in Sporadic Alzheimer's Disease: A Prospective Cohort Study. *The Lancet Neurology* **2013**, *12* (4), 357–367. https://doi.org/10.1016/S1474-4422(13)70044-9.

(22) Allsop, D.; Mayes, J. Amyloid β-Peptide and Alzheimer's Disease. *Essays In Biochemistry* **2014**, *56*, 99–110. https://doi.org/10.1042/bse0560099.

(23) Hardy, J.; Selkoe, D. J. The Amyloid Hypothesis of Alzheimer's Disease: Progress and Problems on the Road to Therapeutics. *Science* **2002**, *297* (5580), 353–356. https://doi.org/10.1126/science.1072994.

(24) Ittner, L. M.; Ke, Y. D.; Delerue, F.; Bi, M.; Gladbach, A.; van Eersel, J.; Wölfing, H.; Chieng, B. C.; Christie, M. J.; Napier, I. A.; Eckert, A.; Staufenbiel, M.; Hardeman, E.; Götz, J. Dendritic Function of Tau Mediates Amyloid-β Toxicity in Alzheimer's Disease Mouse Models. *Cell* **2010**, *142* (3), 387–397. https://doi.org/10.1016/j.cell.2010.06.036.

(25) Chabrier, M. A.; Cheng, D.; Castello, N. A.; Green, K. N.; LaFerla, F. M. Synergistic Effects of Amyloid-Beta and Wild-Type Human Tau on Dendritic Spine Loss in a Floxed Double Transgenic Model of Alzheimer's Disease. *Neurobiology of Disease* **2014**, *64*, 107–117. https://doi.org/10.1016/j.nbd.2014.01.007.

(26) de Vrij, F. M. S.; Fischer, D. F.; van Leeuwen, F. W.; Hol, E. M. Protein Quality Control in Alzheimer's Disease by the Ubiquitin Proteasome System. *Progress in Neurobiology* **2004**, *74* (5), 249–270. https://doi.org/10.1016/j.pneurobio.2004.10.001.

(27) Lee, M. J.; Lee, J. H.; Rubinsztein, D. C. Tau Degradation: The Ubiquitin-Proteasome System versus the Autophagy-Lysosome System. *Prog. Neurobiol.* **2013**, *105*, 49–59. https://doi.org/10.1016/j.pneurobio.2013.03.001.

(28) Hershko, A.; Ciechanover, A. The Ubiquitin System. *Annu. Rev. Biochem.* **1998**, *67*, 425–479. https://doi.org/10.1146/annurev.biochem.67.1.425.

(29) Jackson, M. P.; Hewitt, E. W. Cellular Proteostasis: Degradation of Misfolded Proteins by Lysosomes. *Essays In Biochemistry* **2016**, *60* (2), 173–180. https://doi.org/10.1042/EBC20160005.

(30) Glickman, M. H.; Ciechanover, A. The Ubiquitin-Proteasome Proteolytic Pathway: Destruction for the Sake of Construction. *Physiological Reviews* **2002**, *82* (2), 373–428. https://doi.org/10.1152/physrev.00027.2001.

(31) Kisselev, A. F.; Akopian, T. N.; Castillo, V.; Goldberg, A. L. Proteasome Active Sites Allosterically Regulate Each Other, Suggesting a Cyclical Bite-Chew Mechanism for Protein Breakdown. *Molecular Cell* **1999**, *4* (3), 395–402. https://doi.org/10.1016/S1097-2765(00)80341-X.

(32) Goldstein, G.; Scheid, M.; Hammerling, U.; Schlesinger, D. H.; Niall, H. D.; Boyse, E. A. Isolation of a Polypeptide That Has Lymphocyte-Differentiating Properties and Is Probably Represented Universally in Living Cells. *PNAS* **1975**, *72* (1), 11–15. https://doi.org/10.1073/pnas.72.1.11.

(33) Komander, D.; Rape, M. The Ubiquitin Code. *Annual Review of Biochemistry* **2012**, *81* (1), 203–229. https://doi.org/10.1146/annurev-biochem-060310-170328.
(34) Pickart, C. M.; Fushman, D. Polyubiquitin Chains: Polymeric Protein Signals. *Current Opinion in Chemical Biology* **2004**, *8* (6), 610–616. https://doi.org/10.1016/j.cbpa.2004.09.009.
(35) Komander, D. The Emerging Complexity of Protein Ubiquitination. *Biochemical Society transactions* **2009**, *37* (Pt), 937–953. https://doi.org/10.1042/BST0370937.
(36) Thrower, J. S.; Hoffman, L.; Rechsteiner, M.; Pickart, C. M. Recognition of the Polyubiquitin Proteolytic Signal. *The EMBO Journal* **2000**, *19* (1), 94–102. https://doi.org/10.1093/emboj/19.1.94.
(37) Varadan, R.; Assfalg, M.; Haririnia, A.; Raasi, S.; Pickart, C.; Fushman, D. Solution Conformation of Lys63-Linked Di-Ubiquitin Chain Provides Clues to Functional Diversity of Polyubiquitin Signaling. *J. Biol. Chem.* **2004**, *279* (8), 7055–7063. https://doi.org/10.1074/jbc.M309184200.
(38) Pickart, C. M. Back to the Future with Ubiquitin. *Cell* **2004**, *116* (2), 181–190. https://doi.org/10.1016/S0092-8674(03)01074-2.
(39) Breuzard, G.; Hubert, P.; Nouar, R.; Bessa, T. D.; Devred, F.; Barbier, P.; Sturgis, J. N.; Peyrot, V. Molecular Mechanisms of Tau Binding to Microtubules and Its Role in Microtubule Dynamics in Live Cells. *J Cell Sci* **2013**, *126* (13), 2810–2819. https://doi.org/10.1242/jcs.120832.
(40) Weingarten, M. D.; Lockwood, A. H.; Hwo, S. Y.; Kirschner, M. W. A Protein Factor Essential for Microtubule Assembly. *Proc Natl Acad Sci U S A* **1975**, *72* (5), 1858–1862.
(41) Cleveland, D. W.; Hwo, S.-Y.; Kirschner, M. W. Physical and Chemical Properties of Purified Tau Factor and the Role of Tau in Microtubule Assembly. *Journal of Molecular Biology* **1977**, *116* (2), 227–247. https://doi.org/10.1016/0022-2836(77)90214-5.
(42) Choi, M. C.; Raviv, U.; Miller, H. P.; Gaylord, M. R.; Kiris, E.; Ventimiglia, D.; Needleman, D. J.; Kim, M. W.; Wilson, L.; Feinstein, S. C.; Safinya, C. R. Human Microtubule-Associated-Protein Tau Regulates the Number of Protofilaments in Microtubules: A Synchrotron X-Ray Scattering Study. *Biophysical Journal* **2009**, *97* (2), 519–527. https://doi.org/10.1016/j.bpj.2009.04.047.
(43) Neve, R. L.; Harris, P.; Kosik, K. S.; Kurnit, D. M.; Donlon, T. A. Identification of CDNA Clones for the Human Microtubule-Associated Protein Tau and Chromosomal Localization of the Genes for Tau and Microtubule-Associated Protein 2. *Molecular Brain Research* **1986**, *1* (3), 271–280. https://doi.org/10.1016/0169-328X(86)90033-1.
(44) Andreadis, A.; Brown, W. M.; Kosik, K. S. Structure and Novel Exons of the Human τ Gene. *Biochemistry* **1992**, *31* (43), 10626–10633. https://doi.org/10.1021/bi00158a027.
(45) Gao, Y.-L.; Wang, N.; Sun, F.-R.; Cao, X.-P.; Zhang, W.; Yu, J.-T. Tau in Neurodegenerative Disease. *Annals of Translational Medicine* **2018**, *6* (10). https://doi.org/10.21037/19456.
(46) Avila, J.; Jiménez, J. S.; Sayas, C. L.; Bolós, M.; Zabala, J. C.; Rivas, G.; Hernández, F. Tau Structures. *Frontiers in Aging Neuroscience* **2016**, *8*. https://doi.org/10.3389/fnagi.2016.00262.
(47) Kolarova, M.; García-Sierra, F.; Bartos, A.; Ricny, J.; Ripova, D. Structure and Pathology of Tau Protein in Alzheimer Disease. *Int J Alzheimers Dis* **2012**, *2012*. https://doi.org/10.1155/2012/731526.
(48) Shammas, S. L.; Garcia, G. A.; Kumar, S.; Kjaergaard, M.; Horrocks, M. H.; Shivji, N.; Mandelkow, E.; Knowles, T. P. J.; Mandelkow, E.; Klenerman, D. A Mechanistic Model of Tau Amyloid Aggregation Based on Direct Observation of Oligomers. *Nature Communications* **2015**, *6*, 7025. https://doi.org/10.1038/ncomms8025.

(49) Brandt, R.; Léger, J.; Lee, G. Interaction of Tau with the Neural Plasma Membrane Mediated by Tau's Amino-Terminal Projection Domain. *Journal of Cell Biology* **1995**, *131* (5), 1327–1340. https://doi.org/10.1083/jcb.131.5.1327.
(50) Chen, J.; Kanai, Y.; Cowan, N. J.; Hirokawa, N. Projection Domains of MAP2 and Tau Determine Spacings between Microtubules in Dendrites and Axons. *Nature* **1992**, *360* (6405), 674–677. https://doi.org/10.1038/360674a0.
(51) Lee, G.; Neve, R. L.; Kosik, K. S. The Microtubule Binding Domain of Tau Protein. *Neuron* **1989**, *2* (6), 1615–1624. https://doi.org/10.1016/0896-6273(89)90050-0.
(52) Himmler, A.; Drechsel, D.; Kirschner, M. W.; Martin Jr., D. W. Tau Consists of a Set of Proteins with Repeated C-Terminal Microtubule-Binding Domains and Variable N-Terminal Domains. *Molecular and Cellular Biology* **1989**, *9* (4), 1381–1388. https://doi.org/10.1128/MCB.9.4.1381.
(53) Schweers, O.; Schönbrunn-Hanebeck, E.; Marx, A.; Mandelkow, E. Structural Studies of Tau Protein and Alzheimer Paired Helical Filaments Show No Evidence for Beta-Structure. *J. Biol. Chem.* **1994**, *269* (39), 24290–24297.
(54) Mukrasch, M. D.; Bibow, S.; Korukottu, J.; Jeganathan, S.; Biernat, J.; Griesinger, C.; Mandelkow, E.; Zweckstetter, M. Structural Polymorphism of 441-Residue Tau at Single Residue Resolution. *PLoS Biology* **2009**, *7* (2), e1000034. https://doi.org/10.1371/journal.pbio.1000034.
(55) Jeganathan, S.; von Bergen, M.; Brutlach, H.; Steinhoff, H.-J.; Mandelkow, E. Global Hairpin Folding of Tau in Solution. *Biochemistry* **2006**, *45* (7), 2283–2293. https://doi.org/10.1021/bi0521543.
(56) Sergeant, N.; David, J.-P.; Lefranc, D.; Vermersch, P.; Wattez, A.; Delacourte, A. Different Distribution of Phosphorylated Tau Protein Isoforms in Alzheimer's and Pick's Diseases. *FEBS Letters* **1997**, *412* (3), 578–582. https://doi.org/10.1016/S0014-5793(97)00859-4.
(57) Jeganathan, S.; von Bergen, M.; Mandelkow, E.-M.; Mandelkow, E. The Natively Unfolded Character of Tau and Its Aggregation to Alzheimer-like Paired Helical Filaments. *Biochemistry* **2008**, *47* (40), 10526–10539. https://doi.org/10.1021/bi800783d.
(58) Lippens, G.; Sillen, A.; Smet, C.; Wieruszeski, J.-M.; Leroy, A.; Landrieu, L. B. and I. Studying the Natively Unfolded Neuronal Tau Protein by Solution NMR Spectroscopy http://www.eurekaselect.com/56857/article (accessed Jul 28, 2019).
(59) Gorantla, N. V.; Shkumatov, A. V.; Chinnathambi, S. Conformational Dynamics of Intracellular Tau Protein Revealed by CD and SAXS. In *Tau Protein: Methods and Protocols*; Smet-Nocca, C., Ed.; Methods in Molecular Biology; Springer New York: New York, NY, 2017; pp 3–20. https://doi.org/10.1007/978-1-4939-6598-4_1.
(60) Bergen, M. von; Barghorn, S.; Li, L.; Marx, A.; Biernat, J.; Mandelkow, E.-M.; Mandelkow, E. Mutations of Tau Protein in Frontotemporal Dementia Promote Aggregation of Paired Helical Filaments by Enhancing Local β-Structure. *J. Biol. Chem.* **2001**, *276* (51), 48165–48174. https://doi.org/10.1074/jbc.M105196200.
(61) Dyson, H. J.; Wright, P. E. Intrinsically Unstructured Proteins and Their Functions. *Nature Reviews Molecular Cell Biology* **2005**, *6* (3), 197. https://doi.org/10.1038/nrm1589.
(62) Mylonas, E.; Hascher, A.; Bernadó, P.; Blackledge, M.; Mandelkow, E.; Svergun, D. I. Domain Conformation of Tau Protein Studied by Solution Small-Angle X-Ray Scattering †. *Biochemistry* **2008**, *47* (39), 10345–10353. https://doi.org/10.1021/bi800900d.
(63) Kadavath, H.; Jaremko, M.; Jaremko, Ł.; Biernat, J.; Mandelkow, E.; Zweckstetter, M. Folding of the Tau Protein on Microtubules. *Angew. Chem. Int. Ed.* **2015**, *54* (35), 10347–10351. https://doi.org/10.1002/anie.201501714.

(64) Guo, T.; Noble, W.; Hanger, D. P. Roles of Tau Protein in Health and Disease. *Acta Neuropathol* **2017**, *133* (5), 665–704. https://doi.org/10.1007/s00401-017-1707-9.
(65) Jeganathan, S.; von Bergen, M.; Brutlach, H.; Steinhoff, H.-J.; Mandelkow, E. Global Hairpin Folding of Tau in Solution. *Biochemistry* **2006**, *45* (7), 2283–2293. https://doi.org/10.1021/bi0521543.
(66) Martin, L.; Latypova, X.; Terro, F. Post-Translational Modifications of Tau Protein: Implications for Alzheimer's Disease. *Neurochemistry International* **2011**, *58* (4), 458–471. https://doi.org/10.1016/j.neuint.2010.12.023.
(67) Goedert, M.; Spillantini, M. G.; Potier, M. C.; Ulrich, J.; Crowther, R. A. Cloning and Sequencing of the CDNA Encoding an Isoform of Microtubule-Associated Protein Tau Containing Four Tandem Repeats: Differential Expression of Tau Protein MRNAs in Human Brain. *EMBO J.* **1989**, *8* (2), 393–399.
(68) Bielska, A. A.; Zondlo, N. J. Hyperphosphorylation of Tau Induces Local Polyproline II Helix †. *Biochemistry* **2006**, *45* (17), 5527–5537. https://doi.org/10.1021/bi052662c.
(69) Schwalbe, M.; Kadavath, H.; Biernat, J.; Ozenne, V.; Blackledge, M.; Mandelkow, E.; Zweckstetter, M. Structural Impact of Tau Phosphorylation at Threonine 231. *Structure* **2015**, *23* (8), 1448–1458. https://doi.org/10.1016/j.str.2015.06.002.
(70) Kellogg, E. H.; Hejab, N. M. A.; Poepsel, S.; Downing, K. H.; DiMaio, F.; Nogales, E. Near-Atomic Model of Microtubule-Tau Interactions. *Science* **2018**, *360* (6394), 1242–1246. https://doi.org/10.1126/science.aat1780.
(71) Grundke-Iqbal, I.; Iqbal, K.; Quinlan, M.; Tung, Y. C.; Zaidi, M. S.; Wisniewski, H. M. Microtubule-Associated Protein Tau. A Component of Alzheimer Paired Helical Filaments. *J. Biol. Chem.* **1986**, *261* (13), 6084–6089.
(72) Kosik, K. S.; Joachim, C. L.; Selkoe, D. J. Microtubule-Associated Protein Tau (Tau) Is a Major Antigenic Component of Paired Helical Filaments in Alzheimer Disease. *Proc. Natl. Acad. Sci. U.S.A.* **1986**, *83* (11), 4044–4048. https://doi.org/10.1073/pnas.83.11.4044.
(73) von Bergen, M.; Friedhoff, P.; Biernat, J.; Heberle, J.; Mandelkow, E.-M.; Mandelkow, E. Assembly of Tau Protein into Alzheimer Paired Helical Filaments Depends on a Local Sequence Motif (306VQIVYK311) Forming Beta Structure. *Proceedings of the National Academy of Sciences* **2000**, *97* (10), 5129–5134. https://doi.org/10.1073/pnas.97.10.5129.
(74) Novak, P.; Cehlar, O.; Skrabana, R.; Novak, M. Tau Conformation as a Target for Disease-Modifying Therapy: The Role of Truncation. *JAD* **2018**, *64* (s1), S535–S546. https://doi.org/10.3233/JAD-179942.
(75) Mandelkow, E.-M.; Mandelkow, E. Biochemistry and Cell Biology of Tau Protein in Neurofibrillary Degeneration. *Cold Spring Harbor Perspectives in Medicine* **2012**, *2* (7), a006247–a006247. https://doi.org/10.1101/cshperspect.a006247.
(76) Morris, M.; Maeda, S.; Vossel, K.; Mucke, L. The Many Faces of Tau. *Neuron* **2011**, *70* (3), 410–426. https://doi.org/10.1016/j.neuron.2011.04.009.
(77) Tapia-Rojas, C.; Cabezas-Opazo, F.; Deaton, C. A.; Vergara, E. H.; Johnson, G. V. W.; Quintanilla, R. A. It's All about Tau. *Progress in Neurobiology* **2019**, *175*, 54–76. https://doi.org/10.1016/j.pneurobio.2018.12.005.
(78) Goedert, M.; Jakes, R.; Spillantini, M. G.; Hasegawa, M.; Smith, M. J.; Crowther, R. A. Assembly of Microtubule-Associated Protein Tau into Alzheimer-like Filaments Induced by Sulphated Glycosaminoglycans. *Nature* **1996**, *383* (6600), 550–553. https://doi.org/10.1038/383550a0.
(79) Kampers, T.; Friedhoff, P.; Biernat, J.; Mandelkow, E. M.; Mandelkow, E. RNA Stimulates Aggregation of Microtubule-Associated Protein Tau into Alzheimer-like Paired Helical Filaments. *FEBS Lett.* **1996**, *399* (3), 344–349. https://doi.org/10.1016/s0014-5793(96)01386-5.

(80) Wilson, D. M.; Binder, L. I. Free Fatty Acids Stimulate the Polymerization of Tau and Amyloid Beta Peptides. In Vitro Evidence for a Common Effector of Pathogenesis in Alzheimer's Disease. *Am. J. Pathol.* **1997**, *150* (6), 2181–2195.
(81) Dobson, C. M. Protein Folding and Misfolding. *Nature* **2003**, *426* (6968), 884. https://doi.org/10.1038/nature02261.
(82) Barghorn, S.; Davies, P.; Mandelkow, E. Tau Paired Helical Filaments from Alzheimer's Disease Brain and Assembled in Vitro Are Based on β-Structure in the Core Domain †. *Biochemistry* **2004**, *43* (6), 1694–1703. https://doi.org/10.1021/bi0357006.
(83) García-Sierra, F.; Ghoshal, N.; Quinn, B.; Berry, R. W.; Binder, L. I. Conformational Changes and Truncation of Tau Protein during Tangle Evolution in Alzheimer's Disease. *Journal of Alzheimer's Disease* **2003**, *5* (2), 65–77. https://doi.org/10.3233/JAD-2003-5201.
(84) Chirita, C. N.; Congdon, E. E.; Yin, H.; Kuret, J. Triggers of Full-Length Tau Aggregation: A Role for Partially Folded Intermediates. *Biochemistry* **2005**, *44* (15), 5862–5872. https://doi.org/10.1021/bi0500123.
(85) Sahara, N.; Maeda, S.; Murayama, M.; Suzuki, T.; Dohmae, N.; Yen, S.-H.; Takashima, A. Assembly of Two Distinct Dimers and Higher-Order Oligomers from Full-Length Tau. *European Journal of Neuroscience* **2007**, *25* (10), 3020–3029. https://doi.org/10.1111/j.1460-9568.2007.05555.x.
(86) Mondragón-Rodríguez, S.; Basurto-Islas, G.; Santa-Maria, I.; Mena, R.; Binder, L. I.; Avila, J.; Smith, M. A.; Perry, G.; García-Sierra, F. Cleavage and Conformational Changes of Tau Protein Follow Phosphorylation during Alzheimer's Disease. *International Journal of Experimental Pathology* **2008**, *89* (2), 81–90. https://doi.org/10.1111/j.1365-2613.2007.00568.x.
(87) Lasagna-Reeves, C. A.; Castillo-Carranza, D. L.; Guerrero-Muñoz, M. J.; Jackson, G. R.; Kayed, R. Preparation and Characterization of Neurotoxic Tau Oligomers. *Biochemistry* **2010**, *49* (47), 10039–10041. https://doi.org/10.1021/bi1016233.
(88) Patterson, K. R.; Remmers, C.; Fu, Y.; Brooker, S.; Kanaan, N. M.; Vana, L.; Ward, S.; Reyes, J. F.; Philibert, K.; Glucksman, M. J.; Binder, L. I. Characterization of Prefibrillar Tau Oligomers in Vitro and in Alzheimer Disease. *J. Biol. Chem.* **2011**, *286* (26), 23063–23076. https://doi.org/10.1074/jbc.M111.237974.
(89) Chong, F. P.; Ng, K. Y.; Koh, R. Y.; Chye, S. M. Tau Proteins and Tauopathies in Alzheimer's Disease. *Cellular and Molecular Neurobiology* **2018**, *38* (5), 965–980. https://doi.org/10.1007/s10571-017-0574-1.
(90) LaPointe, N. E.; Morfini, G.; Pigino, G.; Gaisina, I. N.; Kozikowski, A. P.; Binder, L. I.; Brady, S. T. The Amino Terminus of Tau Inhibits Kinesin-Dependent Axonal Transport: Implications for Filament Toxicity. *Journal of Neuroscience Research* **2009**, *87* (2), 440–451. https://doi.org/10.1002/jnr.21850.
(91) Zhu, H.-L.; Fernández, C.; Fan, J.-B.; Chen, J.; Minton, A. P.; Liang, Y. Quantitative Characterization of Heparin Binding to Tau Protein: Implication for Inducer-Mediated Tau Filament Formation. *J. Biol. Chem.* **2010**, *285* (6), 3592–3599. https://doi.org/10.1074/jbc.M109.035691.
(92) Kuret, J.; Chirita, C. N.; Congdon, E. E.; Kannanayakal, T.; Li, G.; Necula, M.; Yin, H.; Zhong, Q. Pathways of Tau Fibrillization. *Biochim. Biophys. Acta* **2005**, *1739* (2–3), 167–178. https://doi.org/10.1016/j.bbadis.2004.06.016.
(93) Carlson, S. W.; Branden, M.; Voss, K.; Sun, Q.; Rankin, C. A.; Gamblin, T. C. A Complex Mechanism for Inducer Mediated Tau Polymerization. *Biochemistry* **2007**, *46* (30), 8838–8849. https://doi.org/10.1021/bi700403a.
(94) Patricia Thomson. Tau Aggregation and Alzheimer's | StressMarq https://www.stressmarq.com/tau-aggregation-and-alzheimers/ (accessed Aug 8, 2019).

(95) Paola Flores-Rodríguez. The Relationship between Truncation and Phosphorylation at the C-Terminus of Tau Protein in the Paired Helical Filaments of Alzheimer's Disease. *Front. Neurosci.* **2015**. https://doi.org/doi: 10.3389/fnins.2015.00033.
(96) Soto, C. Alzheimer's and Prion Disease as Disorders of Protein Conformation: Implications for the Design of Novel Therapeutic Approaches. *Journal of Molecular Medicine* **1999**, *77* (5), 412–418. https://doi.org/10.1007/s001090050371.
(97) Martin, L.; Latypova, X.; Terro, F. Post-Translational Modifications of Tau Protein: Implications for Alzheimer's Disease. *Neurochem. Int.* **2011**, *58* (4), 458–471. https://doi.org/10.1016/j.neuint.2010.12.023.
(98) Rodríguez-Martín, T.; Cuchillo-Ibáñez, I.; Noble, W.; Nyenya, F.; Anderton, B. H.; Hanger, D. P. Tau Phosphorylation Affects Its Axonal Transport and Degradation. *Neurobiology of Aging* **2013**, *34* (9), 2146–2157. https://doi.org/10.1016/j.neurobiolaging.2013.03.015.
(99) Wong, E.; Cuervo, A. M. Integration of Clearance Mechanisms: The Proteasome and Autophagy. *Cold Spring Harb Perspect Biol* **2010**, *2* (12). https://doi.org/10.1101/cshperspect.a006734.
(100) Morishima-Kawashima, M.; Hasegawa, M.; Takio, K.; Suzuki, M.; Titani, K.; Ihara, Y. Ubiquitin Is Conjugated with Amino-Terminally Processed Tau in Paired Helical Filaments. *Neuron* **1993**, *10* (6), 1151–1160. https://doi.org/10.1016/0896-6273(93)90063-W.
(101) Cripps, D.; Thomas, S. N.; Jeng, Y.; Yang, F.; Davies, P.; Yang, A. J. Alzheimer Disease-Specific Conformation of Hyperphosphorylated Paired Helical Filament-Tau Is Polyubiquitinated through Lys-48, Lys-11, and Lys-6 Ubiquitin Conjugation. *J. Biol. Chem.* **2006**, *281* (16), 10825–10838. https://doi.org/10.1074/jbc.M512786200.
(102) Paine, S.; Bedford, L.; Thorpe, J. R.; Mayer, R. J.; Cavey, J. R.; Bajaj, N.; Sheppard, P. W.; Lowe, J.; Layfield, R. Immunoreactivity to Lys63-Linked Polyubiquitin Is a Feature of Neurodegeneration. *Neuroscience Letters* **2009**, *460* (3), 205–208. https://doi.org/10.1016/j.neulet.2009.05.074.
(103) Tan, J. M. M.; Wong, E. S. P.; Kirkpatrick, D. S.; Pletnikova, O.; Ko, H. S.; Tay, S. P.; Ho, M. W. L.; Troncoso, J.; Gygi, S. P.; Lee, M. K.; Dawson, V. L.; Dawson, T. M.; Lim, K. L. Lysine 63-Linked Ubiquitination Promotes the Formation and Autophagic Clearance of Protein Inclusions Associated with Neurodegenerative Diseases. *Hum. Mol. Genet.* **2008**, *17* (3), 431–439. https://doi.org/10.1093/hmg/ddm320.
(104) Shimura, H.; Schwartz, D.; Gygi, S. P.; Kosik, K. S. CHIP-Hsc70 Complex Ubiquitinates Phosphorylated Tau and Enhances Cell Survival. *J. Biol. Chem.* **2004**, *279* (6), 4869–4876. https://doi.org/10.1074/jbc.M305838200.
(105) Petrucelli, L.; Dickson, D.; Kehoe, K.; Taylor, J.; Snyder, H.; Grover, A.; De Lucia, M.; McGowan, E.; Lewis, J.; Prihar, G.; Kim, J.; Dillmann, W. H.; Browne, S. E.; Hall, A.; Voellmy, R.; Tsuboi, Y.; Dawson, T. M.; Wolozin, B.; Hardy, J.; Hutton, M. CHIP and Hsp70 Regulate Tau Ubiquitination, Degradation and Aggregation. *Hum. Mol. Genet.* **2004**, *13* (7), 703–714. https://doi.org/10.1093/hmg/ddh083.
(106) Murata, S.; Minami, Y.; Minami, M.; Chiba, T.; Tanaka, K. CHIP Is a Chaperone-dependent E3 Ligase That Ubiquitylates Unfolded Protein. *EMBO reports* **2001**, *2* (12), 1133–1138. https://doi.org/10.1093/embo-reports/kve246.
(107) Faggiano, S.; Pastore, A. The Challenge of Producing Ubiquitinated Proteins for Structural Studies. *Cells* **2014**, *3* (2), 639–656. https://doi.org/10.3390/cells3020639.
(108) Mali, S. M.; Singh, S. K.; Eid, E.; Brik, A. Ubiquitin Signaling: Chemistry Comes to the Rescue. *Journal of the American Chemical Society* **2017**, *139* (14), 4971–4986. https://doi.org/10.1021/jacs.7b00089.

(109) Abeywardana, T.; Pratt, M. R. Using Chemistry to Investigate the Molecular Consequences of Protein Ubiquitylation. *ChemBioChem* **2014**, *15* (11), 1547–1554. https://doi.org/10.1002/cbic.201402117.
(110) Kim, Y.-J.; Takahashi, R. Role of Polyunsaturated Fatty Acids for Misfolding Protein Aggregations: Implication for Neurodegenerative Diseases. *Ann. N. Y. Acad. Sci.* **2006**, *1086*, 11–20. https://doi.org/10.1196/annals.1377.021.
(111) Fecchio, C.; Palazzi, L.; Polverino de Laureto, P. α-Synuclein and Polyunsaturated Fatty Acids: Molecular Basis of the Interaction and Implication in Neurodegeneration. *Molecules* **2018**, *23* (7). https://doi.org/10.3390/molecules23071531.
(112) Wilson, D. M.; Binder, L. I. Free Fatty Acids Stimulate the Polymerization of Tau and Amyloid Beta Peptides. In Vitro Evidence for a Common Effector of Pathogenesis in Alzheimer's Disease. *Am J Pathol* **1997**, *150* (6), 2181–2195.
(113) King, M. E.; Gamblin, T. C.; Kuret, J.; Binder, L. I. Differential Assembly of Human Tau Isoforms in the Presence of Arachidonic Acid. *Journal of Neurochemistry* **2000**, *74* (4), 1749–1757. https://doi.org/10.1046/j.1471-4159.2000.0741749.x.
(114) Sparr, E.; Linse, S. Lipid-Protein Interactions in Amyloid Formation. *Biochimica et Biophysica Acta (BBA) - Proteins and Proteomics* **2019**, *1867* (5), 455–457. https://doi.org/10.1016/j.bbapap.2019.03.006.
(115) Georgieva, E. R.; Xiao, S.; Borbat, P. P.; Freed, J. H.; Eliezer, D. Tau Binds to Lipid Membrane Surfaces via Short Amphipathic Helices Located in Its Microtubule-Binding Repeats. *Biophys J* **2014**, *107* (6), 1441–1452. https://doi.org/10.1016/j.bpj.2014.07.046.
(116) Elbaum-Garfinkle, S.; Ramlall, T.; Rhoades, E. The Role of the Lipid Bilayer in Tau Aggregation. *Biophys J* **2010**, *98* (11), 2722–2730. https://doi.org/10.1016/j.bpj.2010.03.013.
(117) Brandt, R. Interaction of Tau with the Neural Plasma Membrane Mediated by Tau's Amino-Terminal Projection Domain. *The Journal of Cell Biology* **1995**, *131* (5), 1327–1340. https://doi.org/10.1083/jcb.131.5.1327.
(118) Farah, C. A.; Perreault, S.; Liazoghli, D.; Desjardins, M.; Anton, A.; Lauzon, M.; Paiement, J.; Leclerc, N. Tau Interacts with Golgi Membranes and Mediates Their Association with Microtubules. *Cell Motil. Cytoskeleton* **2006**, *63* (11), 710–724. https://doi.org/10.1002/cm.20157.
(119) Patil, S.; Chan, C. Palmitic and Stearic Fatty Acids Induce Alzheimer-like Hyperphosphorylation of Tau in Primary Rat Cortical Neurons. *Neurosci. Lett.* **2005**, *384* (3), 288–293. https://doi.org/10.1016/j.neulet.2005.05.003.
(120) Kitajka, K.; Puskás, L. G.; Zvara, A.; Hackler, L.; Barceló-Coblijn, G.; Yeo, Y. K.; Farkas, T. The Role of N-3 Polyunsaturated Fatty Acids in Brain: Modulation of Rat Brain Gene Expression by Dietary n-3 Fatty Acids. *Proc. Natl. Acad. Sci. U.S.A.* **2002**, *99* (5), 2619–2624. https://doi.org/10.1073/pnas.042698699.
(121) Broersen, K.; van den Brink, D.; Fraser, G.; Goedert, M.; Davletov, B. Alpha-Synuclein Adopts an Alpha-Helical Conformation in the Presence of Polyunsaturated Fatty Acids to Hinder Micelle Formation. *Biochemistry* **2006**, *45* (51), 15610–15616. https://doi.org/10.1021/bi0617431.
(122) De Franceschi, G.; Frare, E.; Pivato, M.; Relini, A.; Penco, A.; Greggio, E.; Bubacco, L.; Fontana, A.; de Laureto, P. P. Structural and Morphological Characterization of Aggregated Species of α-Synuclein Induced by Docosahexaenoic Acid. *J. Biol. Chem.* **2011**, *286* (25), 22262–22274. https://doi.org/10.1074/jbc.M110.202937.
(123) Gray, E. G.; Paula-Barbosa, M.; Roher, A. Alzheimer's Disease: Paired Helical Filaments and Cytomembranes. *Neuropathol. Appl. Neurobiol.* **1987**, *13* (2), 91–110.
(124) Goux, W. J.; Rodriguez, S.; Sparkman, D. R. Analysis of the Core Components of Alzheimer Paired Helical Filaments. A Gas Chromatography/Mass Spectrometry

Characterization of Fatty Acids, Carbohydrates and Long-Chain Bases. *FEBS Lett.* **1995**, *366* (1), 81–85. https://doi.org/10.1016/0014-5793(95)00486-s.
(125) Anu Mary Ealia, S.; Saravanakumar, M. P. A Review on the Classification, Characterisation, Synthesis of Nanoparticles and Their Application. *IOP Conference Series: Materials Science and Engineering* **2017**, *263*, 032019. https://doi.org/10.1088/1757-899X/263/3/032019.
(126) Nel, A. E.; Mädler, L.; Velegol, D.; Xia, T.; Hoek, E. M. V.; Somasundaran, P.; Klaessig, F.; Castranova, V.; Thompson, M. Understanding Biophysicochemical Interactions at the Nano–Bio Interface. *Nature Materials* **2009**, *8* (7), 543–557. https://doi.org/10.1038/nmat2442.
(127) Nicolini, C.; Bezerra, T.; Pechkova, E. Protein Nanotechnology for the New Design and Development of Biocrystals and Biosensors. *Nanomedicine* **2012**, *7* (8), 1117–1120. https://doi.org/10.2217/nnm.12.84.
(128) Berry, C. C. Chapter 6 - Applications of Inorganic Nanoparticles for Biotechnology. In *Frontiers of Nanoscience*; de la Fuente, J. M., Grazu, V., Eds.; Nanobiotechnology; Elsevier, 2012; Vol. 4, pp 159–180. https://doi.org/10.1016/B978-0-12-415769-9.00006-6.
(129) Laurent, S.; Forge, D.; Port, M.; Roch, A.; Robic, C.; Vander Elst, L.; Muller, R. N. Magnetic Iron Oxide Nanoparticles: Synthesis, Stabilization, Vectorization, Physicochemical Characterizations, and Biological Applications. *Chem. Rev.* **2010**, *110* (4), 2574–2574. https://doi.org/10.1021/cr900197g.
(130) Khan, I.; Saeed, K.; Khan, I. Nanoparticles: Properties, Applications and Toxicities. *Arabian Journal of Chemistry* **2017**. https://doi.org/10.1016/j.arabjc.2017.05.011.
(131) Cho, E. J.; Holback, H.; Liu, K. C.; Abouelmagd, S. A.; Park, J.; Yeo, Y. Nanoparticle Characterization: State of the Art, Challenges, and Emerging Technologies. *Mol. Pharm.* **2013**, *10* (6), 2093–2110. https://doi.org/10.1021/mp300697h.
(132) Shin, W.-K.; Cho, J.; Kannan, A. G.; Lee, Y.-S.; Kim, D.-W. Cross-Linked Composite Gel Polymer Electrolyte Using Mesoporous Methacrylate-Functionalized SiO_2 Nanoparticles for Lithium-Ion Polymer Batteries. *Scientific Reports* **2016**, *6*, 26332. https://doi.org/10.1038/srep26332.
(133) Liberman, A.; Mendez, N.; Trogler, W. C.; Kummel, A. C. Synthesis and Surface Functionalization of Silica Nanoparticles for Nanomedicine. *Surface Science Reports* **2014**, *69* (2), 132–158. https://doi.org/10.1016/j.surfrep.2014.07.001.
(134) Lynch, I.; Dawson, K. A. Protein-Nanoparticle Interactions. *Nano Today* **2008**, *3* (1), 40–47. https://doi.org/10.1016/S1748-0132(08)70014-8.
(135) Daniel, M.-C.; Astruc, D. Gold Nanoparticles: Assembly, Supramolecular Chemistry, Quantum-Size-Related Properties, and Applications toward Biology, Catalysis, and Nanotechnology. *Chem. Rev.* **2004**, *104* (1), 293–346. https://doi.org/10.1021/cr030698+.
(136) Storhoff, J. J.; Elghanian, R.; Mucic, R. C.; Mirkin, C. A.; Letsinger, R. L. One-Pot Colorimetric Differentiation of Polynucleotides with Single Base Imperfections Using Gold Nanoparticle Probes. *Journal of the American Chemical Society* **1998**, *120* (9), 1959–1964. https://doi.org/10.1021/ja972332i.
(137) He, L.; Musick, M. D.; Nicewarner, S. R.; Salinas, F. G.; Benkovic, S. J.; Natan, M. J.; Keating, C. D. Colloidal Au-Enhanced Surface Plasmon Resonance for Ultrasensitive Detection of DNA Hybridization. *J. Am. Chem. Soc.* **2000**, *122* (38), 9071–9077. https://doi.org/10.1021/ja001215b.
(138) De Roe, C.; Courtoy, P. J.; Baudhuin, P. A Model of Protein-Colloidal Gold Interactions. *J. Histochem. Cytochem.* **1987**, *35* (11), 1191–1198. https://doi.org/10.1177/35.11.3655323.
(139) Wang, A.; Vo, T.; Le, V.; Fitzkee, N. C. Using Hydrogen–Deuterium Exchange to Monitor Protein Structure in the Presence of Gold Nanoparticles. *J. Phys. Chem. B* **2014**, *118* (49), 14148–14156. https://doi.org/10.1021/jp506506p.

(140) Klein, J. Probing the Interactions of Proteins and Nanoparticles. *Proceedings of the National Academy of Sciences of the United States of America* **2007**, *104* (7), 2029. https://doi.org/10.1073/pnas.0611610104.
(141) Palmal, S.; Maity, A. R.; Singh, B. K.; Basu, S.; Jana, N. R.; Jana, N. R. Inhibition of Amyloid Fibril Growth and Dissolution of Amyloid Fibrils by Curcumin–Gold Nanoparticles. *Chemistry – A European Journal* **2014**, *20* (20), 6184–6191. https://doi.org/10.1002/chem.201400079.
(142) Brambilla, D.; Le Droumaguet, B.; Nicolas, J.; Hashemi, S. H.; Wu, L.-P.; Moghimi, S. M.; Couvreur, P.; Andrieux, K. Nanotechnologies for Alzheimer's Disease: Diagnosis, Therapy, and Safety Issues. *Nanomedicine* **2011**, *7* (5), 521–540. https://doi.org/10.1016/j.nano.2011.03.008.
(143) Vácha, R.; Linse, S.; Lund, M. Surface Effects on Aggregation Kinetics of Amyloidogenic Peptides. *J. Am. Chem. Soc.* **2014**, *136* (33), 11776–11782. https://doi.org/10.1021/ja505502e.
(144) Ma, W.; Saccardo, A.; Roccatano, D.; Aboagye-Mensah, D.; Alkaseem, M.; Jewkes, M.; Nezza, F. D.; Baron, M.; Soloviev, M.; Ferrari, E. Modular Assembly of Proteins on Nanoparticles. *Nat Commun* **2018**, *9* (1), 1–9. https://doi.org/10.1038/s41467-018-03931-4.
(145) Assfalg, M.; Ragona, L.; Pagano, K.; D'Onofrio, M.; Zanzoni, S.; Tomaselli, S.; Molinari, H. The Study of Transient Protein–Nanoparticle Interactions by Solution NMR Spectroscopy. *Biochimica et Biophysica Acta (BBA) - Proteins and Proteomics* **2016**, *1864* (1), 102–114. https://doi.org/10.1016/j.bbapap.2015.04.024.
(146) Saptarshi, S. R.; Duschl, A.; Lopata, A. L. Interaction of Nanoparticles with Proteins: Relation to Bio-Reactivity of the Nanoparticle. *Journal of Nanobiotechnology* **2013**, *11* (1), 26. https://doi.org/10.1186/1477-3155-11-26.
(147) Mu, Q.; Jiang, G.; Chen, L.; Zhou, H.; Fourches, D.; Tropsha, A.; Yan, B. Chemical Basis of Interactions between Engineered Nanoparticles and Biological Systems. *Chem. Rev.* **2014**, *114* (15), 7740–7781. https://doi.org/10.1021/cr400295a.
(148) Laera, S.; Ceccone, G.; Rossi, F.; Gilliland, D.; Hussain, R.; Siligardi, G.; Calzolai, L. Measuring Protein Structure and Stability of Protein-Nanoparticle Systems with Synchrotron Radiation Circular Dichroism. *Nano Lett.* **2011**, *11* (10), 4480–4484. https://doi.org/10.1021/nl202909s.
(149) Zimbone, M.; Calcagno, L.; Messina, G.; Baeri, P.; Compagnini, G. Dynamic Light Scattering and UV–Vis Spectroscopy of Gold Nanoparticles Solution. *Materials Letters* **2011**, *65* (19), 2906–2909. https://doi.org/10.1016/j.matlet.2011.06.054.
(150) Huang, R.; Lau, B. L. T. Biomolecule-Nanoparticle Interactions: Elucidation of the Thermodynamics by Isothermal Titration Calorimetry. *Biochim. Biophys. Acta* **2016**, *1860* (5), 945–956. https://doi.org/10.1016/j.bbagen.2016.01.027.
(151) Hens, Z.; Martins, J. A Solution NMR Toolbox for Characterizing the Surface Chemistry of Colloidal Nanocrystals. *CHEMISTRY OF MATERIALS* **2013**, *25* (8), 1211–1221. http://dx.doi.org/10.1021/cm303361s.
(152) Chatterjee, A.; Kumar, A.; Chugh, J.; Srivastava, S.; Bhavesh, N. S.; Hosur, R. V. NMR of Unfolded Proteins. *Journal of Chemical Sciences* **2005**, *117* (1), 3–21. https://doi.org/10.1007/BF02704356.
(153) Dyson, H. J.; Wright, P. E. Unfolded Proteins and Protein Folding Studied by NMR. *Chem. Rev.* **2004**, *104* (8), 3607–3622. https://doi.org/10.1021/cr030403s.
(154) Qi, S.; Li, Z.; Schulze-Gahmen, U.; Stjepanovic, G.; Zhou, Q.; Hurley, J. H. Structural Basis for ELL2 and AFF4 Activation of HIV-1 Proviral Transcription. *Nat Commun* **2017**, *8*. https://doi.org/10.1038/ncomms14076.
(155) Prestel, A.; Bugge, K.; Staby, L.; Hendus-Altenburger, R.; Kragelund, B. B. Chapter Eight - Characterization of Dynamic IDP Complexes by NMR Spectroscopy. In *Methods in Enzymology*; Rhoades, E., Ed.; Intrinsically Disordered Proteins;

Academic Press, 2018; Vol. 611, pp 193–226. https://doi.org/10.1016/bs.mie.2018.08.026.
(156) Mao, A. H.; Crick, S. L.; Vitalis, A.; Chicoine, C. L.; Pappu, R. V. Net Charge per Residue Modulates Conformational Ensembles of Intrinsically Disordered Proteins. *PNAS* **2010**, *107* (18), 8183–8188. https://doi.org/10.1073/pnas.0911107107.
(157) Wicky, B. I. M.; Shammas, S. L.; Clarke, J. Affinity of IDPs to Their Targets Is Modulated by Ion-Specific Changes in Kinetics and Residual Structure. *PNAS* **2017**, *114* (37), 9882–9887. https://doi.org/10.1073/pnas.1705105114.
(158) Getz, E. B.; Xiao, M.; Chakrabarty, T.; Cooke, R.; Selvin, P. R. A Comparison between the Sulfhydryl Reductants Tris(2-Carboxyethyl)Phosphine and Dithiothreitol for Use in Protein Biochemistry. *Analytical Biochemistry* **1999**, *273* (1), 73–80. https://doi.org/10.1006/abio.1999.4203.
(159) Lucas, L. H.; Larive, C. K. Measuring Ligand-Protein Binding Using NMR Diffusion Experiments. *Concepts in Magnetic Resonance* **2004**, *20A* (1), 24–41. https://doi.org/10.1002/cmr.a.10094.
(160) Danielsson, J.; Jarvet, J.; Damberg, P.; Gräslund, A. Translational Diffusion Measured by PFG-NMR on Full Length and Fragments of the Alzheimer Aβ(1–40) Peptide. Determination of Hydrodynamic Radii of Random Coil Peptides of Varying Length. *Magnetic Resonance in Chemistry* **2002**, *40* (13), S89–S97. https://doi.org/10.1002/mrc.1132.
(161) Tillett, M. L.; Horsfield, M. A.; Lian, L.-Y.; Norwood, T. J. Protein-Ligand Interactions Measured by 15N-Filtered Diffusion Experiments. *J Biomol NMR* **1999**, *13* (3), 223–232. https://doi.org/10.1023/A:1008301324954.
(162) Fawzi, N. L.; Ying, J.; Torchia, D. A.; Clore, G. M. Probing Exchange Kinetics and Atomic Resolution Dynamics in High-Molecular-Weight Complexes Using Dark-State Exchange Saturation Transfer NMR Spectroscopy. *Nat Protoc* **2012**, *7* (8), 1523–1533. https://doi.org/10.1038/nprot.2012.077.
(163) Stetz, M. A.; Caro, J. A.; Kotaru, S.; Yao, X.; Marques, B. S.; Valentine, K. G.; Wand, A. J. Characterization of Internal Protein Dynamics and Conformational Entropy by NMR Relaxation. *Meth. Enzymol.* **2019**, *615*, 237–284. https://doi.org/10.1016/bs.mie.2018.09.010.
(164) Fawzi, N. L.; Ying, J.; Ghirlando, R.; Torchia, D. A.; Clore, G. M. Atomic-Resolution Dynamics on the Surface of Amyloid-β Protofibrils Probed by Solution NMR. *Nature* **2011**, *480* (7376), 268–272. https://doi.org/10.1038/nature10577.
(165) Post, C. B. Exchange-Transferred NOE Spectroscopy and Bound Ligand Structure Determination. *Curr. Opin. Struct. Biol.* **2003**, *13* (5), 581–588. https://doi.org/10.1016/j.sbi.2003.09.012.
(166) Bodner, C. R.; Dobson, C. M.; Bax, A. Multiple Tight Phospholipid-Binding Modes of Alpha-Synuclein Revealed by Solution NMR Spectroscopy. *J. Mol. Biol.* **2009**, *390* (4), 775–790. https://doi.org/10.1016/j.jmb.2009.05.066.
(167) Gustke, N.; Trinczek, B.; Biernat, J.; Mandelkow, E.-M.; Mandelkow, E. Domains of Tau Protein and Interactions with Microtubules. *Biochemistry* **1994**, *33* (32), 9511–9522. https://doi.org/10.1021/bi00198a017.
(168) Barré, P.; Eliezer, D. Structural Transitions in Tau K18 on Micelle Binding Suggest a Hierarchy in the Efficacy of Individual Microtubule-Binding Repeats in Filament Nucleation. *Protein Sci.* **2013**, *22* (8), 1037–1048. https://doi.org/10.1002/pro.2290.
(169) Nečas, D.; Klapetek, P. Gwyddion: An Open-Source Software for SPM Data Analysis. *Open Physics* **2011**, *10* (1), 181–188. https://doi.org/10.2478/s11534-011-0096-2.
(170) Jangholi, A.; Ashrafi-Kooshk, M. R.; Arab, S. S.; Riazi, G.; Mokhtari, F.; Poorebrahim, M.; Mahdiuni, H.; Kurganov, B. I.; Moosavi-Movahedi, A. A.; Khodarahmi, R. Appraisal of Role of the Polyanionic Inducer Length on Amyloid Formation by 412-Residue 1N4R Tau Protein: A Comparative Study. *Archives of*

Biochemistry and Biophysics **2016**, *609*, 1–19. https://doi.org/10.1016/j.abb.2016.09.004.
(171) Wilson, D. M.; Binder, L. I. Free Fatty Acids Stimulate the Polymerization of Tau and Amyloid Beta Peptides. In Vitro Evidence for a Common Effector of Pathogenesis in Alzheimer's Disease. *Am J Pathol* **1997**, *150* (6), 2181–2195.
(172) Miller, A. J.; Roman, B.; Norstrom, E. A Method for Easily Customizable Gradient Gel Electrophoresis. *Analytical Biochemistry* **2016**, *509*, 12–14. https://doi.org/10.1016/j.ab.2016.07.003.
(173) Lee, W.; Tonelli, M.; Markley, J. L. NMRFAM-SPARKY: Enhanced Software for Biomolecular NMR Spectroscopy. *Bioinformatics* **2015**, *31* (8), 1325–1327. https://doi.org/10.1093/bioinformatics/btu830.